

Investigations on Ultrafast Fiber-based Optical Gates

Vorgelegt von
Vincent Marembert

Von der Fakultät IV (Elektrotechnik und Informatik)
der Technischen Universität Berlin
zur Verleihung des akademischen Grades
Doktor der Ingenieurwissenschaft
Dr.-Ing.

Promotionsausschuss:
Vorsitzender: Pr. Dr.-Ing. Ernst Obermeier
Berichter: Pr. Dr.-Ing. Klaus Petermann
Berichter: Pr. Dr. rer. nat. Hans-Georg Weber

Tag der wissenschaftlichen Aussprache: 26. Juni 2006

Berlin 2006
D 83

Abstract

This work presents investigations carried out on two optical gates based on Dispersion-Shifted Highly Nonlinear Fibers (DS-HNLFs).

In the Nonlinear Optical Loop Mirror (NOLM) and in the so-called Kerr gate, based on the Kerr effect, the phase of a data pulse is modulated by a control pulse through Cross-Phase Modulation (XPM). The induced phase shift is converted into an amplitude modulation by using an interferometric setup. As nonlinear effects are extremely fast in optical fibers, the NOLM and the Kerr gate are candidates of choice for all-optical signal processing in Time-Division Multiplexing (TDM) systems.

The efficiency of such an optical gate can be evaluated by measuring the phase shift induced by the control signal, or by directly measuring the so-called switching window of the gate, which represents the evolution of the transmittance of the gate over the time. Both measurements are carried out in this work, and various DS-HNLFs were used. The influence of experimental parameters such as the fibers parameters and the data and control signals properties is discussed. In accordance with theoretical expectations, the NOLM proved to work more efficiently than the Kerr gate, as with the NOLM, a lower control power is required to reach a given phase shift or a given switching windows than with the Kerr gate.

Finally, both gates were used in high bit-rates TDM experiments. Operated under the same conditions, the NOLM and the Kerr gates could demultiplex a 320 Gbit/s TDM data signal to 40 Gbit/s with low penalties. The NOLM was also used to demultiplex a 640 Gbit/s signal, while the Kerr gate took advantage of its different principle of operation in an Add-Drop Multiplexing (ADM) experiment with a data rate up to 320 Gbit/s.

Used in combination with DS-HNLFs, the NOLM and the Kerr gate offer the potential for high-speed optical signal processing with simple, commercially available fiber components.

Zusammenfassung

In dieser Arbeit wurden zwei optische Schalter basierend auf Dispersion-verschobener Hoch-Nichtlinearer Faser (Dispersion-Shifted Highly Nonlinear Fibers) untersucht. In dem Nonlinear Optical Loop Mirror (NOLM) und in dem Kerr Schalter wird die Phase eines optischen Datenpulses durch Kreuzphasenmodulation (XPM) moduliert. XPM wird von einem zusammen mit dem Datenpuls propagierenden Steuerpuls induziert. Die Phasenänderung kann in eine Amplitudenänderung umgewandelt werden, wenn XPM in einem interferometrischen Aufbau ausgenutzt wird. Da die Geschwindigkeit des XPM-Effektes in der Größenordnung von einigen Femtosekunden liegt, eignen sich der NOLM und der Kerr Schalter für die rein optische Hoch-Geschwindigkeit Signalverarbeitung in Optical Time Division Multiplexing (OTDM) Netzwerken.

Die Phasenänderung wurde für beide Schalter gemessen, sowie das Schaltfenster, das den Verlauf des Transmittance über die Zeit darstellt. Der Einfluss von Parametern wie die Fasereigenschaften, und die Steuer- sowie Datenpuls-Eigenschaften (Wellenlängen, optische Leistungen) wurden experimentell untersucht. Den theoretischen Erwartungen entsprechend, erwies sich der NOLM als ein effektiverer Schalter im Vergleich zum Kerr Schalter, da eine gewisse Phasenänderung bzw. ein gewisses Schaltfenster mit weniger Steuerpulsleistung erreicht wird mit dem NOLM als mit dem Kerr Schalter.

Basierend auf diesen Untersuchungen wurden beide Schalter in OTDM-Anwendungen eingesetzt. Betrieben unter gleichen Bedingungen konnten der NOLM und der Kerr Schalter ein 320 Gbit/s Datensignal auf 40 Gbit/s demultiplexen, mit einer geringen Penalty. Die NOLM wurde benutzt, um ein 640 Gbit/s Datensignal zu demultiplexen. Aufgrund seiner Anordnung, der Kerr Schalter konnte in einem Add-Drop Multiplexing (ADM) Experiment mit Datenraten bis 320 Gbit/s benutzt werden.

Der NOLM und der Kerr Schalter, die in dieser Arbeit untersucht werden, basieren auf kommerziell erhältlichen optischen Komponente und eignen sich für die rein optische Hoch-Geschwindigkeit Datenverarbeitung.

Contents

1	Introduction	1
1.1	Optical Gates for High-Speed Signal Processing	1
1.2	Motivation and Objectives of this Work	3
1.3	Outline of this work	4
2	Basics of Fiber-based Switching	6
2.1	Properties of Optical Fibers	6
2.2	Pulse Propagation in Optical Fibers	11
2.3	Cross-Phase Modulation in Fibers and All-Optical Switching . .	16
2.4	Four-Wave Mixing in Fibers and All-Optical Switching	17
2.5	Walk-Off	20
2.6	Pump-Probe Characterization of Optical Switching Devices . . .	21
3	Gates based on Highly Nonlinear Fibers	26
3.1	Nonlinear Optical Loop Mirror (NOLM)	26
3.1.1	Basics of the NOLM Gate	26
3.1.2	Measurements of induced Phase Shift	29
3.1.3	Measurements of Switching Windows	32
3.2	Kerr gate	39
3.2.1	Basics of the Kerr Gate	39
3.2.2	Measurements of induced Phase Shift	42
3.2.3	Measurements of Switching Windows	43
3.2.4	Experimental Setup for Parametric Amplification mea- surement	47
3.3	Bit Error Rate Characterization	50
3.3.1	Experimental Setup	50
3.3.2	Results	51
3.4	Requirements for a demultiplexer up to 640 Gbit/s	54
3.5	Comparison	57
4	Applications in High Speed OTDM-Systems	61
4.1	Demultiplexing 640 Gbaud	61
4.1.1	Experimental Setup	62
4.1.2	Results	65
4.2	Add-Drop Multiplexing at 160 Gbit/s and 320 Gbit/s	69
4.2.1	Experimental Setup	70
4.2.2	Results	74

5 Conclusion	79
Bibliography	81
A Appendix	86
A.1 Fibers used	86
A.2 Optical pulses	87
B List of Symbols and Abbreviations	88
C Publications by the Author	91
D Acknowledgements	95
E Curriculum Vitae	97

List of Figures

1.1	Typical setup of an OTDM system with the base data rate 40 Gbit/s.	2
2.1	Measurement of the DGD for an 850 m long DS-HNF, for a 8 m long SMF and for a 5 m long piece of PMF (Measurement step $\Delta\lambda=1$ nm).	10
2.2	Intensity profile for sech- and Gaussian pulses with FWHM=1.0 ps. The characteristic widths FWHM and T_0 are represented.	11
2.3	SPM-distorted spectra calculated for an unchirped sech-shaped pulse propagating in a nonlinear and non-dispersive fiber. Spectra are labeled by the maximum nonlinear phase shift $\Delta\varphi_{SPM\ Max}$. f_0 is the carrier frequency.	14
2.4	Principle of Four-Wave Mixing.	18
2.5	Calculated evolutions of $\beta_1 L$ (solid line) and of the walk-off $\Delta\tau$ (dashed line) vs. λ and $\lambda_{mid.}$, respectively, with $\lambda_0=1550$ nm, $S(\lambda_0)=0.02$ ps km ⁻¹ nm ⁻² , $L=1$ km (S is considered to be a constant).	21
2.6	a). Experimental setup for the characterization of all-optical gates by pump-probe measurements, b). Characteristics of the switching window.	22
2.7	Principle of switching window measurement.	24
2.8	a). Calculated transmittance characteristics, and b). corresponding switching windows for probe pulse with varying FWHM.	25
3.1	Basic setup for the NOLM.	27
3.2	a) Setup for phase shift measurements and b) Principle for phase shift evaluation.	29
3.3	Phase Shift Measurement for the NOLM (DS-HNLF C was used). Control pulse: FWHM _C =1.5 ps, 10 GHz.	31
3.4	Setup for switching window measurement.	32
3.5	Influence of the control pulse power on the Extinction Ratio for the NOLM Gate (40 GHz control pulse, FWHM=1.0 ps).	33
3.6	a) Spectral overlap resulting from high control power and/or narrow λ -separation, and b) resulting switching window. The NOLM was considered and included DS*HNLF B	34
3.7	Influence of the control pulse power on the FWHM for the NOLM Gate (40 GHz control pulse, FWHM=1.0 ps).	35
3.8	Influence of the phase shift $\Delta\varphi$ on the FWHM of the transmittance of a NOLM/Kerr gate. Walk-off and control pulse broadening were neglected.	36

3.9	Broadening of the control pulse in DS-HNLF B and DS-HNLF C (40 GHz control pulse, FWHM=1.0 ps, $\lambda_C=1532$ nm).	37
3.10	Influence of the control pulse power on the maximum transmittance for the NOLM Gate (40 GHz control pulse, FWHM=1.0 ps).	38
3.11	Setup and operation principle of the Kerr gate.	39
3.12	Phase Shift Measurement for the Kerr gate. DS-HNLF C was utilized. Control pulse: FWHM _C =1.5 ps, 10 GHz	42
3.13	Influence of the control pulse power on the ER for the Kerr gate ((40 GHz control pulse, FWHM=1.0 ps).	43
3.14	Influence of the control pulse power on the FWHM for the Kerr gate (40 GHz control pulse, FWHM=1.0 ps).	44
3.15	Influence of the control pulse power on the maximum transmittance T_{MAX} for the Kerr gate (40 GHz control pulse, FWHM=1.0 ps).	45
3.16	Influence of the probe pulse power on the ER for the Kerr gate (40 GHz control pulse, FWHM=1.0 ps).	46
3.17	Setup for Gain and Phase Shift Measurements.	47
3.18	Spectra of control and probe signals, measured behind the DS-HNLF D, with overlapping pulses trains (dashed line) and with no overlapping (solid line).	48
3.19	XPM-induced Phase Shift and FWM-induced Parametric Amplification measured in a Kerr gate, for DS-HNLF D. Inset: spectrum of probe and control pulses at the output of the DS-HNLF D. Control pulse: $\lambda_C=1560$ nm, FWHM _C =1.6 ps.	49
3.20	Experimental setup used for BER-characterization of the Kerr gate and of the NOLM.	51
3.21	a) BER measurements for 160 Gbit/s and 320 Gbit/s demultiplexing to 40 Gbit/s using the NOLM and DS-HNLF D and b) switching window measured ($\Delta\tau$: time slot for 320 Gbit/s).	52
3.22	a) BER measurements for 160 Gbit/s and 320 Gbit/s demultiplexing to 40 Gbit/s using the Kerr gate and DS-HNLF D and b) switching window measured.	53
3.23	Evaluation of the influence of cross-talk (simulated): a data pulse is demultiplexed by the gate, and two pulses in the neighbouring bit slots are partly transmitted.	55
3.24	a) Fraction of the cross-talk energy in the total energy transmitted after the demux (demultiplexing of 320 Gbit/s to 40 Gbit/s), b) Ratio $P_{Probe}/P_{cross-talk}$ and c) measured (solid line) and simulated (dashed line) switching windows.	56
3.25	Comparison of phase shift measurement in a NOLM and in a Kerr gate. Control pulse: FWHM _C =1.5 ps, 10 GHz. Fiber DS-HNLF C was used.	58
3.26	Maximum transmittance T_{MAX} measured for the NOLM and the Kerr gate with DS-HNLF B. Using a 3 dB coupler (instead of 10 dB) in the Kerr gate would result in an increase of T_{MAX} by 7 dB.	59
4.1	Experimental setup for DQPSK high bitrate experiment	62
4.2	Switching window of the NOLM used for the demultiplexing of 1.28 Tbit/s. The control power sent to the DS-HNLF was <i>approx</i> 15.8 dBm.	64

4.3	BER measurements up to 1.28 Tbit/s, with Data FWHM=1.0 ps and sensitivities for the 32 40 Gbit/s TDM channels.	65
4.4	BER measurements up to 2.56 Tbit/s, with data FWHM=0.8 ps.	67
4.5	Autocorrelation for the data pulse arriving to the demultiplexer, with and without (dashed line) transmission over the 160 km link.	68
4.6	Principle of Add-Drop Multiplexing	69
4.7	Overlook setup for 160/320 Gbit/s ADD-DROP Multiplexing experiment	70
4.8	Add-Drop Multiplexer based on a Kerr gate.	71
4.9	Eye diagrams measured at the DROP (a) and ADD (b) ports of the ADM, at 160 Gbit/s.	73
4.10	Setup for the FWM-based demultiplexer, autocorrelation of the control pulse gating the demultiplexer and switching window.	74
4.11	BER measurements for 160 Gbit/s and 320 Gbit/s, for the DROP operation.	75
4.12	ADD operation at 160 Gbit/s: BER measurement for each 40 Gbit/s channel after the FMW-based demultiplexer.	76
4.13	ADD operation at 160 Gbit/s: switching characteristic T_{ADD} for the ADD operation of the ADM.	77
4.14	Eye diagram showing the extraction of a 40 Gbit/s channel out of a 320 Gbit/s signal.	78
5.1	Comparison of phase shift measurements in fiber-based gates and in SOA based gates [1]	80

List of Tables

2.1	Typical parameters for a SSMF and a DS-HNLF.	13
2.2	Characteristic parameters for nonlinear fibers used in this work. .	14
2.3	Dispersion and Nonlinear lengths for DS-HNLF A, B, C, D, E, F and for a typical control pulse (FWHM=1.0 ps, Average power=15 dBm at 40 GHz, $\lambda_C=1532$ nm).	15
2.4	Dispersion and Nonlinear lengths for DS-HNLF A, B, C, D, E, F and for a typical data pulse (FWHM=0.5 ps, Average power=0 dBm at 40 GHz, $\lambda_D=1556$ nm).	15
2.5	Typical data rate used in this work, and associated bit-slot period and data pulse FWHM.	25
3.1	Results for 160 Gbit/s and 320 Gbit/s demultiplexing to 40 Gbit/s with NOLM and Kerr gate.	52
3.2	Parameters used for phase shift measurements.	58
3.3	Best parameters measured for the switching windows of the NOLM.	60
3.4	Best parameters measured for the switching windows of the Kerr gate (10 dB coupler). The values of T_{MAX} that could be reached in the case of a 3 dB coupler are indicated in ().	60
A.1	Characteristic parameters for fibers used in this work	86
A.2	Parameters of the Super Large Area (SLA) and Inverse Disper- sion (ID) Fibers used for transmissions in Sections 4.2 and 4.1 . .	86

Chapter 1

Introduction

1.1 Optical Gates for High-Speed Signal Processing

Today's telecommunication networks involve electronic as well as optical components. Electronics meet the requirements for bit rates up to 80 Gbit/s, provide compactness and the possibility for monolithic integration at relatively low cost. Still, for higher bit rates, and particularly along transmission links, where data processing should not slow down the data traffic, only optics ensure the necessary bandwidth and speed, leaving out cumbersome Optic-Electronic-Optic conversion. In order to fully exploit the optical bandwidth of the optical fiber (which exceeds 10 THz in the low-loss transmission window), all-optical data processing techniques are required.

In the field of optical telecommunications, *multiplexing* refers to the operation of combining two or more information channels onto a common transmission medium using hardware (multiplexer MUX). The two basic forms of multiplexing are Wavelength-Division Multiplexing and Time-Division Multiplexing.

- Wavelength-Division multiplexing (WDM) is a technology which multiplexes several optical carrier signals on a single optical fiber by using different wavelengths of laser light to carry different signals. Each of several data streams is modulated onto a different part of the light spectrum. WDM systems are already popular with telecommunications companies.
- Optical Time-Division Multiplexing (OTDM) is the means by which multiple digital signals (or analogue signals carrying digital data) can be carried on a single wavelength by interleaving portions of each signal in time, combining data streams by assigning each stream a different time slot in a set.

Both methods shall be combined in optical networks, however this work focuses on Optical Time Division Multiplexing techniques. A typical Optical TDM (OTDM) system is shown in Fig. 1.1. In the example given, eight 40 Gbit/s channels (provided by eight transmitters T_X) are interleaved (multiplexed) into a 320 Gbit/s optical data signal. The signal is transmitted over a fiber link, and

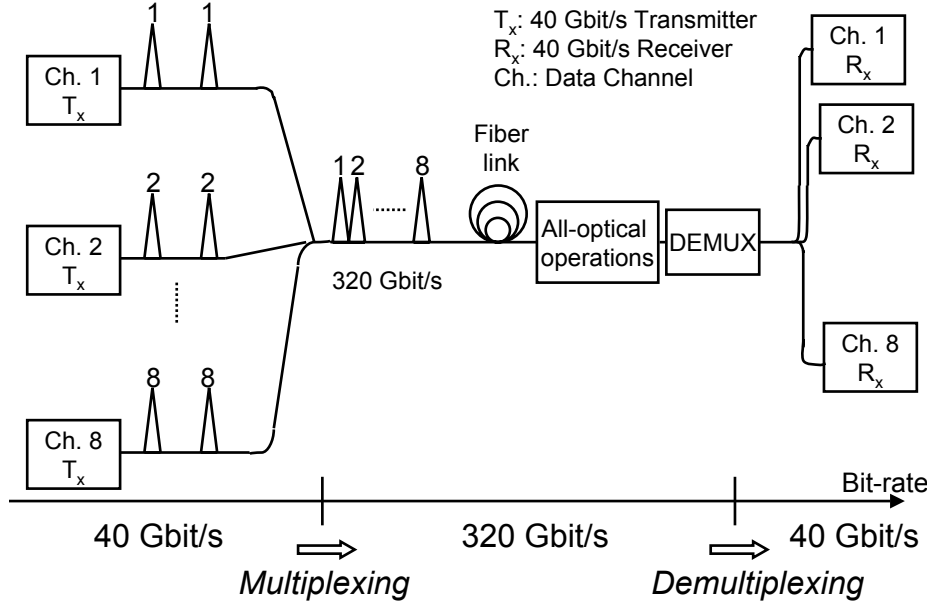


Figure 1.1: Typical setup of an OTDM system with the base data rate 40 Gbit/s.

may experience operations along the optical network, such as wavelength conversion, add-drop multiplexing (ADM) or regeneration [1]. After transmission, the high bit rate signal is sent to a demultiplexer (DEMUX). In the DEMUX, each TDM channel is extracted out of the high bit rate signal. The reduction of the bit rate allows the detection and the electrical processing of the data channels. TDM implies the use of short pulses (the Full Width at Half Maximum FWHM of the data pulse should be shorter than $1/3$ of the bit period) at the Return-to-Zero (RZ) format [2].

The development of technologies enabling TDM bit rates above 160 Gbit/s is driven by the constant demand for capacity. Moreover, high bit rate systems, combining WDM and OTDM, tend to become cheaper than systems based on lower bit rates, due to the smaller amount of wavelengths needed, and thus due to the lower number of expensive components needed by the high bit rate system to allow the same capacity. This argument encouraged the upgrade to 10 Gbit/s and 40 Gbit/s systems, which are today state of the art. The work carried out for the development of 160 Gbit/s systems led also to an improvement of the performance for 40 Gbit/s systems, allowing longer transmission distance and enhanced reliability.

However the increase of the data bit rate has to be followed by an upgrade of the components used in the transmission systems. For the demultiplexing of 160 Gbit/s TDM signals, gates based on Electroabsorption Modulators (EAMs) or SOAs have become state of the art. But an upgrade of these solutions for higher bit rates is difficult.

Today's base rate for optical communication systems is 10 Gbit/s or 40 Gbit/s. As the base rate may be increased in the future, the demultiplexer should be able to be gated by control signals with a higher repetition rate (80 GHz, 160 GHz). Such a gate suitable for signal processing above 160 Gbit/s should not be subject to pattern effects.

The demultiplexer needed before the electronic receiver, as well as the operations carried out on the high bit rate data signals involve logic functions such as *AND* gates, which have to be implemented optically, as a conversion of the optical data signal into the electrical domain would result in a decrease of the transmission speed. In an all-optical gate, the transmission of a *data* signal is controlled (gated) by another optical signal, referred to as the *control* signal.

When Cross-Phase Modulation (XPM) is used, a strong control signal induces a local refractive index change, leading to a modulation of the phase of the data signal. The induced phase shift can be converted into an amplitude change for the data signal if an interferometric setup is used. XPM-based gates have been realized using nonlinear media such as Semiconductor Optical Amplifiers (SOAs) [3], and optical fibers [1]. For DEMUX operations, the operation speed of SOAs limits the application of these components to high speed data signals of 160 Gbit/s. A consequence of the slow recovery time of SOAs is illustrated by pattern effects occurring when the SOA-based gate is driven by control signals at a repetition rate higher than 40 GHz. The slow recovery time is due to the resonant-nature of the nonlinearities in SOAs. In the optical fiber, the nonlinearities are much lower than in SOAs, but long fibers can also be used, as the attenuation of fibers is low. However, the nonlinear effects in fibers are much faster than in SOAs (in the order of a few femtoseconds [1]). Consequently, interferometric gates based on optical fibers do not suffer the same bandwidth limitations of SOAs and the advent of Highly Nonlinear Fibers offers new possibilities for high-speed optical signal processing, permitting to exploit the ultra-fast nonlinear effect without high-power optical amplifier or long fibers.

1.2 Motivation and Objectives of this Work

A much higher processing speed can be reached in fiber-based gates than in SOA-based gates. In a pioneering experiment realized by Nakazawa et al. in 1998 [4], the demultiplexing of a TDM single channel 640 Gbit/s data signal was demonstrated with the Nonlinear Optical Loop Mirror (NOLM, [5]). In this experiment, the setup used for the demultiplexer comprised a Dispersion Flattened Fiber (DFF, with a length of 450 m) made of 9 shorter pieces of DFF. By using a combination of these carefully selected DFF, walk-off free operation was achieved in the NOLM, and the broadening of control and data pulses in the fiber loop was reduced.

In the present work, DS-HNLFs are for the first time systematically investigated for optical signal processing up to 640 Gbit/s. The NOLM and the so-called Kerr gate, based on polarization rotation induced through XPM [6], were investigated experimentally in a much simpler configuration than in the ex-

periment described in [4]. One single DS-HNLF was used as nonlinear medium, the walk-off remained low, and demultiplexing of 640 Gbit/s was also demonstrated.

Fiber-based optical gates are well known for applications as an OTDM-demultiplexer up to 640 Gbit/s [7]. A drawback of conventional fibers is the low nonlinear parameter $\gamma \approx 1 \text{ W}^{-1} \text{ km}^{-1}$, which implies the use of either long fibers or high control powers to enable efficient gating. The fiber length sets a limit for the efficiency of the gate, as dispersive and nonlinear effects influence the shapes and spectra of data and control pulses propagating over the fiber. The development of dispersion-shifted dispersion-flattened highly nonlinear fiber (DS-HNLF) made these gates again attractive for OTDM-demultiplexing. The DS-HNLFs have much higher γ values (e.g. $\gamma > 10 \text{ W}^{-1} \text{ km}^{-1}$), which enables optical gates with a shorter fiber length at moderate control powers. Both gates, the NOLM [8] and the Kerr gate [9] have shown their potential in applications such as OTDM-demultiplexing, add-drop multiplexing or optical sampling [10]. The performance of the gates depends on the properties of the HNLF used (length L , nonlinear parameter γ , zero-dispersion wavelength λ_0), and on operation parameters such as the optical power and temporal width of the control pulses [11] as well as the wavelength allocation of the control and data signals.

Another advantage of the Kerr gate, as will be shown in Section 4.2, is that this arrangement makes the device suitable for all-optical add-drop operations over 160 Gbit/s.

The objective of the present work is to investigate experimentally two interferometric gates based on HNLFs (the NOLM and the Kerr gate), focussing on their application for TDM demultiplexing at bit rates over 160 Gbit/s. In particular:

- Insight is provided on the operation principles of the gates, and on the particularities of fiber-based switches.
- The influence of the common parameters (e.g. properties of the fibers, power and FWHM of the control pulse) is discussed on the basis of experimental results.
- A comparison of both gates is made and high bit rate experiments where each gate was used are presented (demultiplexing and Add-Drop Multiplexing).

1.3 Outline of this work

Chapter 2 provides the basics needed for a theoretical understanding of the propagation of optical waves in optical fibers. Insight into dispersive and nonlinear properties of fibers is delivered, and attention will be paid to the influence of these phenomena in the context of optical switching.

Chapter 3 presents experimental investigations carried out on the NOLM gate and on the Kerr gate. Both gates are based on Dispersion Shifted Highly Nonlinear Fibers (DS-HNLF), and various fibers were utilized. The impact of parameters such as the fibers properties, the data and control signals properties

(wavelengths, powers) will be discussed considering the switching characteristics and the XPM-induced phase shift evaluated for each gate.

The NOLM and the Kerr gate were utilized in high bit rate experiments, as will be shown in Chapter 4. In particular, the NOLM was used to demultiplex a 640 Gbaud data signal (1 baud=1 Symbol/second). An Add-Drop Multiplexing experiment involving the Kerr gate is also presented.

Chapter 2

Basics of Fiber-based Switching

2.1 Properties of Optical Fibers

The development of optical fibers has been driven by the reduction of their intrinsic loss and by the appearance of the Erbium Doped Fiber Amplifier (EDFA), allowing an optical signal to be transmitted in a waveguide over several thousands of kilometers [12].

Optical fibers are made of silica glass (SiO_2), of which the refractive index is 1.44 at $1.5 \mu\text{m}$. Dopants such as GeO_2 , P_2O_5 respectively B_2O_3 , SiF_4 allow to raise respectively lower the refractive index of pure silica glass.

The material the fiber is made of, as well as the form of the fiber waveguide both influence the dispersive properties of the fiber. Material dispersion can be changed only slightly by the dopants, on the other hand the waveguide dispersion can be adjusted by using appropriate refractive index profiles of the fiber.

In the field of optical telecommunications, the commonly used fibers support the propagation of only one mode for the optical field, due to their reduced core size (core radius smaller than $5 \mu\text{m}$). Such fibers are referred to as Single Mode Fibers (SMF). Multi Mode Fibers (MMF) are not considered in this work. The parameters describing the properties of a fiber are discussed in the following.

Attenuation

The attenuation constant α_{dB} , usually given in dB km^{-1} , is minimum around $\lambda=1.5 \mu\text{m}$ (0.2 dB km^{-1}), which is thus the wavelength of prime interest for optical telecommunications. At this wavelength, the losses are mainly dominated by Rayleigh scattering. Assuming that an electro-magnetic wave with the power P_0 was coupled to the input of an optical fiber with an attenuation constant α_{dB} , the power of the wave after propagating over a distance z (to be given in km) is:

$$P(z) = P_0 \exp\left(-\frac{z\alpha_{dB}}{4.343}\right) \quad (2.1)$$

When measured in km^{-1} , the attenuation parameter is given by: $\alpha = \alpha_{dB}/4.343$.

Dispersion

The dispersion parameter D is given in $\text{ps nm}^{-1} \text{ km}^{-1}$.

The so-called zero-dispersion wavelength λ_0 is defined as the wavelength where the dispersion parameter is 0 ($D(\lambda_0)=0$). The dispersion characteristic of an optical fiber is separated into a normal dispersion regime, where $D < 0 \text{ ps nm}^{-1} \text{ km}^{-1}$, and an anomalous dispersion regime ($D > 0$). The dispersion slope parameter S is defined as $S(\lambda) = \frac{\partial D}{\partial \lambda}$. Thus the information on D and S at a given wavelength allows to interpolate the dispersion characteristic of the fiber for the near wavelengths.

Polarization Mode Dispersion

The polarization mode dispersion (PMD) parameter, evaluated in $\text{ps km}^{-1/2}$, gives an information on the birefringence of the fiber. Polarization Mode Dispersion (PMD) is another form of dispersion where two waves at the same wavelength but with different polarization states travel with different group velocities over the fiber. The difference in the group velocities is due a stress of the cylindrical symmetry of the refractive index profile in the fiber, which results in birefringence of the waveguide. PMD causes a differential group delay (DGD) $\Delta\tau_g$ to appear between both polarization modes. At sufficient long fiber lengths, PMD and DGD scale with the square root of the fiber length. Most fibers exhibit birefringence, due to mechanical stresses, asymmetries and random imperfections of the fiber form, often influenced by external factors such as temperature and thus varying over time. PMD leads to a broadening of the optical pulses, setting a limitation for the maximum transmission distance.

For a fiber of length L , the probability of a given value for the DGD follows a Maxwell probability distribution. For a specified PMD value τ_{PMD} , the average DGD is $\tau_{av}=0.921 \tau_{PMD}$, while the most probable PMD value is $\tau_{most \text{ prob.}}=0.816 \tau_{PMD}$. As suggested by the unit of the PMD parameter ($\text{ps}/\sqrt{\text{km}}$), PMD scales with the square root of the length of the fiber link. This is however only true for long fibers, and for short fiber ($L < 1 \text{ km}$) the DGD will scale with the length. As the PMD of Dispersion-Shifted Highly Non-linear Fiber is low ($\text{PMD} < 0.06 \text{ ps km}^{-1/2}$), and as the lengths of the fibers used was relatively short ($L < 1 \text{ km}$), PMD was not considered to be a limiting parameter throughout this work.

Effective core area

The effective core area A_{eff} is given by:

$$A_{eff} = \frac{\left[\int \int_{-\infty}^{+\infty} |F(x,y)|^2 dx dy \right]^2}{\int \int_{-\infty}^{+\infty} |F(x,y)|^4 dx dy} \quad (2.2)$$

where $F(x,y)$ describes the modal distribution of an optical field in the fiber (see Section 2.2).

If $F(x,y)$ is approximated by a Gaussian shape, the effective core area A_{eff} is given by $A_{eff}=\pi w^2$, where w is the mode field radius. A_{eff} characterizes the confinement of the optical wave inside the fiber core.

Nonlinear parameter

The refractive index of a fiber can be described by:

$$n(\omega, P) = n_{lin.}(\omega) + n_2 \frac{P}{A_{eff}} \quad (2.3)$$

where $n(\omega)_{lin.}$ is the part of the index of refraction not varying with the signal power P .

The nonlinear parameter γ characterizes the nonlinear properties of the fibers, i.e. the nonlinear response of the medium to an intense electro-magnetic field and is given by

$$\gamma = \frac{\omega n_2}{c A_{eff}} \quad (2.4)$$

n_2 is the nonlinear index coefficient of the fiber medium, considered to be a constant over the optical frequency ω (for fused silica, $n_2 = 3.2 \times 10^{-16} \text{ cm}^2/\text{W}$), and c is the velocity of light. n_2 is connected with the third order susceptibility $\chi^{(3)}$ of the fiber as follows:

$$n_2 = \frac{3}{4\epsilon_0 c n_0^2} \chi_{xxxx}^{(3)} \quad (2.5)$$

where ϵ_0 is the vacuum permittivity, and $n_0 = n_{lin.}$ (see Eq. 2.3). $\chi^{(3)}$ is related to the nonlinear polarization \vec{P}_{NL} , which raises as a nonlinear response to an electrical field \vec{E} , as stated in Eq. 2.6:

$$\vec{P}_{NL} = \epsilon_0 \chi^3 : \vec{E} \vec{E} \vec{E} \quad (2.6)$$

The nonlinear effects in the optical fibers are usually low compared with the linear effects. However the nonlinear effects accumulate along the fiber length and may become significant.

Throughout this work several types of fibers were used:

For **Standard SMF** (SSMF), $\lambda_0 = 1.3 \text{ } \mu\text{m}$, where the attenuation is 0.4 dB/km. The dispersion and dispersion slope parameters are $D \approx 17 \text{ ps/km.nm}$ and $S \approx 0.058 \text{ ps/km.nm}^2$ respectively at $\lambda = 1.5 \text{ } \mu\text{m}$, where the fiber losses are minimum. Typical values for γ are $\gamma = 1.6 \text{ W}^{-1} \text{ km}^{-1}$, and $A_{eff} \approx 80 \text{ } \mu\text{m}^2$.

In **Dispersion Shifted Fibers** (DSF), the waveguide dispersion is changed by modifying the refractive index profile of the core, which results in a shift of the zero-dispersion wavelength λ_0 near $1.5 \text{ } \mu\text{m}$. DSF is classified into zero- and nonzero-dispersion-shifted fiber, depending on whether $D \approx 0 \text{ ps nm}^{-1} \text{ km}^{-1}$ at $\lambda = 1.55 \text{ } \mu\text{m}$ or not. A standard value for the dispersion slope parameter of a DSF is $S = 0.085 \text{ ps km}^{-1} \text{ nm}^{-2}$.

Dispersion Compensating Fibers (DCF) allow to compensate both the dispersion and the slope of dispersion of the SSMF at $1.55 \text{ } \mu\text{m}$, with a common dispersion and dispersion parameters of -83 ps/km.nm and $-102.4 \text{ ps km}^{-1} \text{ nm}^{-2}$. However, the loss (0.6 dB km^{-1}) and nonlinearity ($\gamma = 6 \text{ W}^{-1} \text{ km}^{-1}$) of such fibers is high.

For **Highly Nonlinear Fibers** (HNLF), A_{eff} is made smaller to enhance the nonlinearity parameter (typical values are $10 < \gamma < 20 \text{ W}^{-1} \text{ km}^{-1}$), and

dopants (Germanium) are used to further increase nonlinear effects. In **Dispersion-Shifted Highly Nonlinear Fiber** (DS-HNLF), the zero-dispersion of the HNLF is shifted to the standard transmission wavelength around $1.55\ \mu\text{m}$. HNLFs are appropriate fibers when a high nonlinear parameter is needed. The requirements concerning the dispersion characteristics of such fibers is relaxed, as a short length of HNLFs generally provides enough nonlinear response. Recently, photonic crystal fibers (PCF, also known as "holey" or microstructured fibers) have raised attention, offering extremely high nonlinear parameters ($\gamma > 200\ \text{W}^{-1}\ \text{m}^{-1}$). The structure of such special fibers consists of an array of holes (diameter varying from $25\ \text{nm}$ to $50\ \mu\text{m}$) along the fiber length. These novative fibers are now commercially available, but still present losses over $50\ \text{dB km}^{-1}$. Bismuth-doped fibers also present extremely high nonlinearities. γ -values higher than $1000\ \text{W}^{-1}\ \text{km}^{-1}$ have been measured [13] and these fibers are gaining interest also for OTDM applications such as supercontinuum generation [14, 15], pulse compression [16] and demultiplexing [17]. In spite of their high dispersion values, bismuth-doped fibers take advantage of the high nonlinearities and very short length (in the order of a few meters) are usually needed [18]. PCFs and bismuth-doped fibers were not used in this work.

Polarization Maintaining Fibers (PMF) are characterized by their high birefringence, as the refractive index difference between the fast and slow axis is intentionally made high during the fabrication process. When the polarization state of a light wave is sent inside such a fiber parallel with one of its main axis, the polarization will remain unchanged during propagation. A PMF exhibit high PMD ($1.7\ \text{ps km}^{-1}$), as a consequence of its high birefringence. These special fibers are also called High Birefringent fibers, though they will only keep the light polarization unchanged under the conditions mentioned before. The Differential Group Delay was measured for an HNLF, and is presented in Fig. 2.1. The DGD for a SSMF and for a PMF were also plotted, for comparison purpose. As expected, the DGD of a PMF is much higher than that of a SMF or DS-HNLF.

PMD is commonly considered to be significant when the DGD is of the same order of magnitude than the pulse width [19].

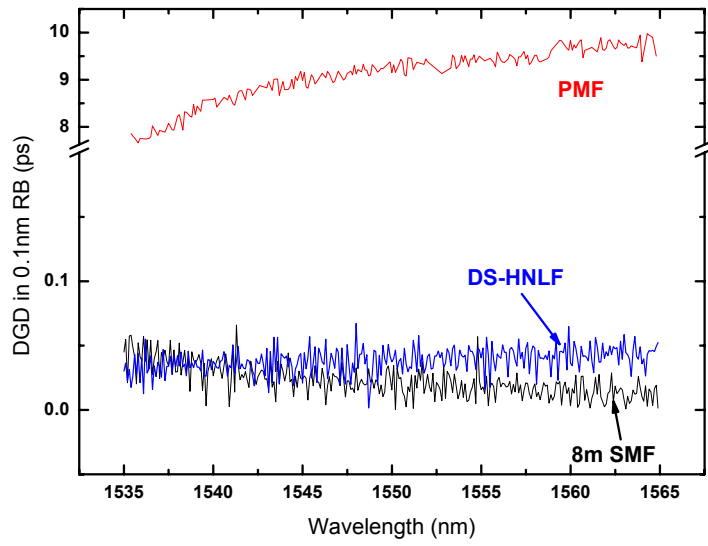


Figure 2.1: Measurement of the DGD for an 850 m long DS-HNF, for a 8 m long SMF and for a 5 m long piece of PMF (Measurement step $\Delta\lambda=1$ nm).

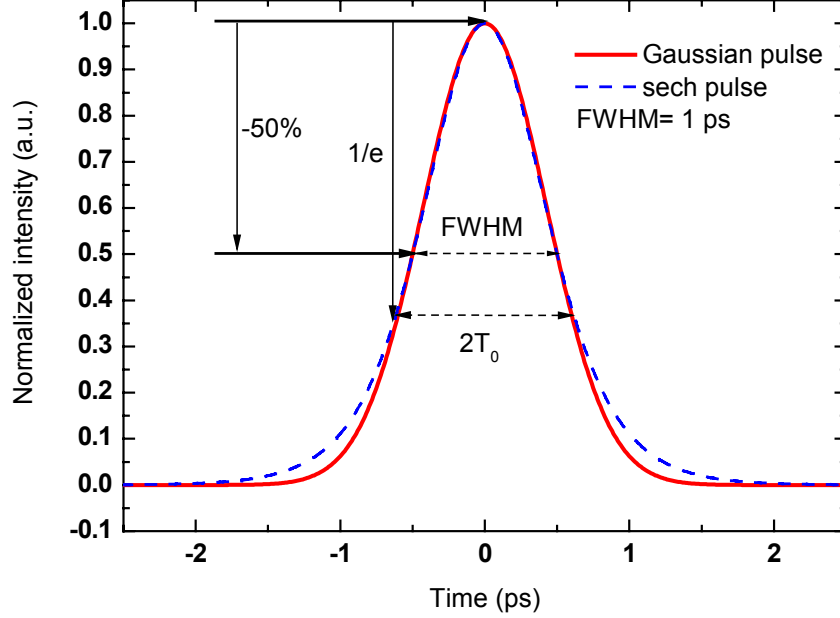


Figure 2.2: Intensity profile for sech- and Gaussian pulses with FWHM=1.0 ps. The characteristic widths FWHM and T_0 are represented.

2.2 Pulse Propagation in Optical Fibers

We consider the propagation of a linearly polarized pulse (polarization vector \vec{e}_x) in the fundamental mode along a monomode fiber (axis z). The optical wave spectrum is assumed to be centered on the wavelength λ , corresponding to the carrier frequency $\omega_0 = \frac{2\pi c}{\lambda}$, and the nonlinear response of the fiber to be instantaneous. The optical pulse is supposed to be wider than 0.1 ps. The fiber is assumed to be non-birefringent, so that \vec{e}_x can be chosen arbitrarily and the polarization state of the optical pulse remains constant.

Under these assumptions, an optical pulse can be represented by the following expression for the electrical field strength $\vec{E}(\vec{r}, t)$:

$$\vec{E}(\vec{r}, t) = \frac{1}{2} \vec{e}_x \{ F(x, y) A(z, t) \exp[i(\beta_0 z - \omega_0 t)] + c.c. \} \quad (2.7)$$

In optical communications, E is conventionally normalized such that $2|\bar{E}|^2 = |A(z, t)|^2 = P$, where P is the optical power and the bar means a time average over the fast oscillations of $|E|^2$.

$F(x, y)$ stands for the modal distribution of the field \vec{E} . $A(z, t)$ describes the slowly varying pulse envelope of the signal, and throughout this work a Gaussian or Sech shape is assumed for the temporal distribution of the optical power. The pulses considered are transform limited.

The intensity profile of a Gaussian pulse and of a sech pulse is proportional to $|A(z, t)|^2$. Both profiles are depicted in Fig. 2.2 for pulses with the same

Full Width at Half Maximum (FWHM, defined as the temporal width of the pulse at the point where its intensity decreased by 50 %). β_0 is the value of the propagation constant of the fiber at the carrier frequency ω_0 (see Eq. 2.9). The half-width at 1/e intensity point T_0 is also sometimes used to characterize the width of an optical pulse.

The basics for understanding the phenomenon of propagation of an optical pulse through an optical fiber are the Maxwell's equations. However in general, one is only interested in the propagation of the envelope $A(z,t)$. The propagation of $A(z,t)$ is determined by the following propagation equation, derived from the Maxwell equations [20] and known as the Nonlinear Schrödinger Equation (NLSE):

$$\frac{\partial A}{\partial z} + \beta_1 \frac{\partial A}{\partial t} + i \frac{\beta_2}{2} \frac{\partial^2 A}{\partial t^2} - \frac{\beta_3}{6} \frac{\partial^3 A}{\partial t^3} + \frac{\alpha}{2} A = i\gamma |A|^2 A \quad (2.8)$$

β_n stands for the value of the n-th derivative of the propagation constant β at the carrier frequency wavelength ($\omega_0 = \frac{2\pi c}{\lambda}$), as given by the expansion of β about the carrier frequency ω_0 :

$$\beta(\omega) = \frac{n_{lin}(\omega)\omega}{c} = \beta_0 + \beta_1(\omega - \omega_0) + \frac{1}{2}\beta_2(\omega - \omega_0)^2 + \frac{1}{6}\beta_3(\omega - \omega_0)^3 + \dots \quad (2.9)$$

$v_g = \frac{1}{\beta_1}$ is the group velocity of the optical wave. β_2 and β_3 represent the second and third order chromatic dispersion at the carrier frequency ω_0 , respectively. Though generally known for one given frequency, as stated in Eq. 2.9, the coefficients $\beta_n = \partial^n \beta / \partial \omega^n$ can be considered as functions of the variable λ , as Eq. 2.9 can be written for any other $\omega \neq \omega_0$.

The dispersion parameters D and S are related to β according to:

$$D = \left(\frac{\partial}{\partial \lambda} \left(\frac{\partial \beta}{\partial \omega} \right) \right)_{\lambda=\lambda_0} = -\frac{2\pi c}{\lambda^2} \beta_2 \quad (2.10)$$

$$S = \frac{\partial D}{\partial \lambda} = \left(\frac{2\pi c}{\lambda^2} \right)^2 \left(\frac{\lambda}{\pi c} \beta_2 + \beta_3 \right) \quad (2.11)$$

Standard values for the dispersion parameters of a SSMF and of a DS-HNLF are presented in Table 2.1. In Eq. 2.8, only the contributions β_n with $n \leq 3$ were considered, as further coefficients have much lower values (see Table 2.1). In most cases (for pulses with FWHM ≥ 1 ps and when the pulse wavelength λ is not close to λ_0), β_3 can also be neglected.

The different terms of the nonlinear differential equation 2.8 represent physical effects, which are divided in linear and nonlinear effects, listed hereunder.

The wavelength dependence of β_1 ($\beta_1 = \partial \beta / \partial \omega$) is responsible for the increase of the time delay between two pulses at different wavelengths sent simultaneously inside a fiber, the so-called walk-off. $\frac{\beta_2}{2} \frac{\partial^2 A}{\partial t^2}$ accounts for Group Velocity Dispersion (GVD) in the fiber.

The terms $\gamma |A|^2 A$ leads to the so-called Self-Phase Modulation (SPM) of the electro-magnetic wave, as well as to Cross-Phase Modulation (XPM) and

	SSMF	DS-HNLF
$A_{eff} (\mu\text{m}^2)$	80	110
D (ps km ⁻¹ nm ⁻¹) at 1550 nm	17	≈ 0
S (ps km ⁻¹ nm ⁻²)	0.058	0.02
β_2 (ps ² km ⁻¹)	-22	≈ 0
β_3 (ps ³ km ⁻¹)	0.13	≈ 0.032
β_4 (ps ⁴ km ⁻¹)	-5.10^{-8}	

Table 2.1: Typical parameters for a SSMF and a DS-HNLF.

Four-Wave Mixing (FWM), as will be shown in Sections 2.3 and 2.4. When propagating inside the fiber, an optical pulse experiences a phase shift dependent on its own intensity. At the maximum of the optical pulse, where the optical power reaches the peak value P_{Peak} , and given that the GVD and attenuation of the fiber can be neglected, the so-called nonlinear phase shift $\Delta\varphi$ is given by:

$$\Delta\varphi_{SPM \text{ Max}} = \gamma P_{Peak} L \quad (2.12)$$

where L is the length, which the pulse has been propagating over.

Combined with GVD, SPM influences the pulse shape, and offers the possibility of creating soliton optical pulses.

The term $\frac{\alpha}{2}A$ stands for the attenuation along the fiber.

As both dispersion and nonlinearity have to be taken into account, it is useful to define the following characteristic lengths.

The Dispersion Length L_D and the Nonlinear Length L_{NL} are defined as

$$L_D = \frac{T_0^2}{|\beta_2|} \quad L_{NL} = \frac{1}{\gamma P_0} \quad (2.13)$$

where T_0 is the half-width at the $\frac{1}{e}$ -intensity point (for a sech pulse, $T_{FWHM} = 1.7627 T_0$, while for a Gaussian pulse $T_{FWHM} = 1.6651 T_0$), and P_0 is the pulse peak power.

Practical meaning of L_D and L_{NL}

Depending on the the ratio $\frac{L_D}{L_{NL}}$, nonlinearity or dispersion can be seen as dominating the pulse change. If the case where $L \gg L_D$ and $L \gg L_{NL}$, none of dispersive and nonlinear effects should be neglected. On the contrary, if the fiber length is much shorter than L_D and L_{NL} , dispersive and nonlinear effects should not affect the pulse shape during propagation.

After propagating over a distance equal to L_D , a chirp-free Gaussian pulse is broadened by a factor $\sqrt{2}$ (a sech pulse would be broadened by a factor 1.61). When neglecting the dispersive effects and the attenuation along the fiber (so that the "effective" fiber length, which is the parameter accounting for dispersive and nonlinear effects, can be considered to be identical with the physical length), the nonlinear length L_{NL} is the distance at which the propagating pulse has accumulated a phase shift of 1 radian. This phase shift is proportional to the product $(P_0 L \gamma)$ and results not only in the general broadening of the pulse

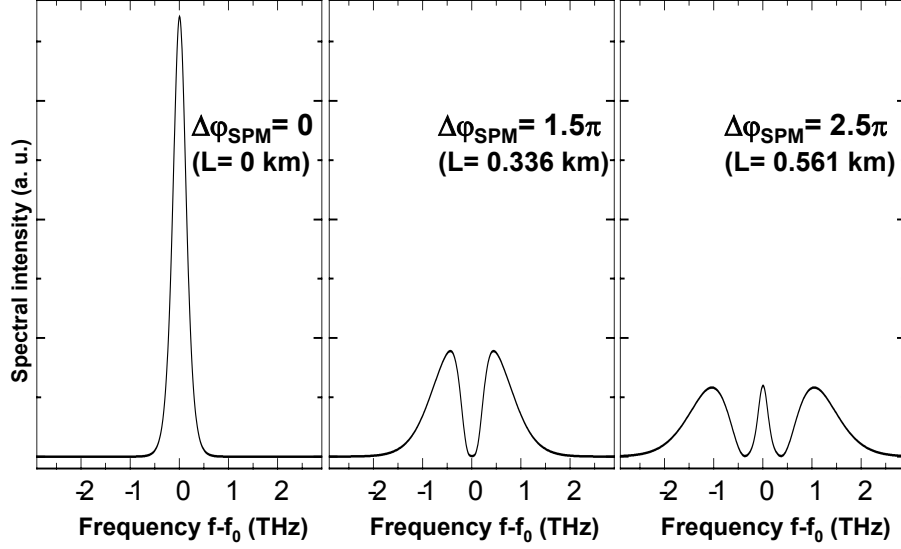


Figure 2.3: SPM-distorted spectra calculated for an unchirped sech-shaped pulse propagating in a nonlinear and non-dispersive fiber. Spectra are labeled by the maximum nonlinear phase shift $\Delta\varphi_{SPM \text{ Max}}$. f_0 is the carrier frequency.

spectrum, but also in the appearance of oscillations on the spectrum, as can be seen in Fig. 2.3, where optical spectra are represented for different values of the accumulated phase shift. The Sech-pulse considered for these calculations had a FWHM of 1.0 ps, and was sent with an average power of 15 dBm (at a repetition rate of 40 GHz) in a fiber with $\gamma = 21 \text{ W}^{-1} \text{ km}^{-1}$, $D = 0 \text{ ps km}^{-1} \text{ nm}^{-1}$, $\alpha_{dB} = 0 \text{ dB km}^{-1}$ (the loss of the fiber was neglected). This phenomenon is due to SPM.

Common parameters for various DS-HNLF used in the following are listed in Table 2.2 herunder:

DS-HNLF	A	B	C	D	E	F
$\gamma \text{ (W}^{-1} \text{ km}^{-1}\text{)}$	21	10	21	21	20	21
$L \text{ (m)}$	100	300	850	46	503	94
$\lambda_0 \text{ (nm)}$	1536.7	1556.0	1550.3	1560.9	1550.0	1549.0
$S \text{ (ps km}^{-1} \text{ nm}^{-2}\text{)}$	0.02	0.02	0.02	0.03	0.02	0.016
Loss (dB)	0.6	1.4	1.6	1.4	1.4	0.8

Table 2.2: Characteristic parameters for nonlinear fibers used in this work.

Care has to be taken concerning the evaluation of γ , as the method used to calculate the nonlinear parameter strongly influences its value.

Orders of magnitude

The following presents characteristic lengths associated with the different DS-HNLFs used throughout this work. The first pulse considered had a FWHM of 1.0 ps (sech shape), a spectrum centered on 1532 nm and was emitted with an average power of 15 dBm at a repetition rate of 40 GHz (corresponding to the properties of a typical control pulse used for gating). The peak power of such a pulse is 0.7 W.

Fiber	Fiber length (km)	L_D (km)	L_{NL} (km)
DS-HNLF A	0.100	2.75	0.07
DS-HNLF B	0.300	0.54	0.14
DS-HNLF C	0.850	0.71	0.07
DS-HNLF D	0.046	0.30	0.07
DS-HNLF E	0.503	0.72	0.07
DS-HNLF F	0.094	0.95	0.07

Table 2.3: Dispersion and Nonlinear lengths for DS-HNLF A, B, C, D, E, F and for a typical control pulse (FWHM=1.0 ps, Average power=15 dBm at 40 GHz, $\lambda_C=1532$ nm).

Nonlinear effects and dispersion will affect this pulse during propagation, as L_D and L_{NL} are of the order of magnitude of the fiber lengths.

When considering a shorter pulse with FWHM=0.5 ps, emitted at 1556 nm with an average power of 0 dBm at 40 GHz (this pulse meets the requirements for a data pulse at a bit rates up to 640 Gbit/s):

Fiber	Fiber length (km)	L_D (km)	L_{NL} (km)
DS-HNLF A	0.100	0.16	1.08
DS-HNLF B	0.300	$\gg 1$	2.27
DS-HNLF C	0.850	0.55	1.08
DS-HNLF D	0.046	0.43	1.08
DS-HNLF E	0.503	0.52	1.13
DS-HNLF F	0.094	0.56	1.08

Table 2.4: Dispersion and Nonlinear lengths for DS-HNLF A, B, C, D, E, F and for a typical data pulse (FWHM=0.5 ps, Average power=0 dBm at 40 GHz, $\lambda_D=1556$ nm).

In this case, nonlinearities should remain low, which is due to the relatively low peak power of the pulse. Still, because of its narrow FWHM, dispersive effects should not be neglected. As the bit-rate becomes higher, the tolerance of transmission systems to the different effects mentioned above (chromatic dispersion, PMD, nonlinearities) becomes smaller.

2.3 Cross-Phase Modulation in Fibers and All-Optical Switching

The nonlinear properties of optical fibers play a dual role in telecommunication systems. Nonlinearities may induce changes in the pulse shape and spectrum, thus limiting the distance over which the signal can be transmitted without loss of the coded information. On the other hand, fiber nonlinearities can be utilized for manipulating the data signal, in devices such as wavelength converters, demultiplexers, or all-optical regenerators.

In the special case of optical gates, two optical waves at different wavelengths travel and interact inside a fiber, in such a way that the transmission of one wave (referred to as the *probe*, or *data* wave) is influenced by the other wave (*control* wave). This can usually be done by using the nonlinear effects of Cross-Phase Modulation (XPM), or by using the phenomenon of Four Wave Mixing (FWM). The interaction of two waves propagating inside a dispersive and nonlinear medium is thus of high interest for optical switching applications, and is presented in the following.

In the following, we will focus on XPM in optical fibers, and the phenomenon of FWM will be described separately.

The equations governing the propagation of the probe wave (at the wavelength $\lambda_P = \frac{2\pi c}{\omega_P}$, with the slowly varying envelope A_P) and of the control signal ($\lambda_C = \frac{2\pi c}{\omega_C}$, A_C), can be written as [20]:

$$\frac{\partial A_P}{\partial z} + \beta_{1P} \frac{\partial A_P}{\partial t} + i \frac{\beta_{2P}}{2} \frac{\partial^2 A_P}{\partial t^2} + \frac{\alpha}{2} A_P = i\gamma(|A_P|^2 + a|A_C|^2)A_P \quad (2.14)$$

$$\frac{\partial A_C}{\partial z} + \beta_{1C} \frac{\partial A_C}{\partial t} + i \frac{\beta_{2C}}{2} \frac{\partial^2 A_C}{\partial t^2} + \frac{\alpha}{2} A_C = i\gamma|A_C|^2 A_C \quad (2.15)$$

a is a coefficient which value depends on the relative state of polarization of the control and probe waves. For two optical fields interfering with the same linear polarization state, $a=2$, whereas $a=\frac{2}{3}$ if both fields are linearly polarized, but with a relative angle of 90° .

The attenuation and nonlinear parameter of the fiber is assumed to be the same for both wavelengths, which is a good approximation when the wavelengths difference is below 50 nm.

The first equation already shows the coupling between A_P and A_C induced in the nonlinear medium. As will be shown later, this results in the modulation of the phase of the probe signal by the control signal (Cross-Phase Modulation, XPM). Because attention is focused on investigating the all-optical switching of a probe signal, and as for such applications the probe intensity is relatively small compared to this of the control signal, the equation 2.15 could be simplified by neglecting the influence of the probe signal. This approximation is due to the fact that $|A_C|^2 \gg |A_P|^2$ (10 dB difference in the signals peak powers is usual).

In the following, the contribution of the most relevant terms in Eq. 2.14 and Eq. 2.15 are discussed:

By neglecting the fiber loss ($\alpha=0$) and the dispersion (i.e. by setting $\beta_{2P} \approx 0$ and $\beta_{3P} \approx 0$ in Eq. 2.14), and considering the pulse envelope A_P in a reference

frame moving with the pulse at the velocity $1/\beta_1$, the Eq. 2.14 can be simplified to

$$\frac{\partial A_P}{\partial z} = i\gamma(|A_P|^2 + a|A_C|^2)A_P \quad (2.16)$$

The solution for A_P has the form

$$A_P = \sqrt{P_P} \exp[i(\Delta\varphi_{SPM} + \Delta\varphi_{XPM})] \quad (2.17)$$

with

$$\Delta\varphi_{SPM} = \gamma P_P L \quad (2.18)$$

and

$$\Delta\varphi_{XPM} = a\gamma P_C L \quad (2.19)$$

where $P_P = |A_P|^2$, $P_C = |A_C|^2$ and a is a factor depending on the relative polarization states of the probe and control pulses. In the equations 2.18 and 2.19 above, P_C and P_P are time-dependent, as these variables are related to the shape of the pulses in the time-domain.

$\Delta\varphi_{SPM} = \gamma P_P L$ stands for SPM, as seen in Subsection 2.2, whereas $\Delta\varphi_{XPM}$ describes the phase modulation induced by the control wave power on the probe wave. Depending on the value of the factor a in Eq. 2.19, XPM may occur in a more significant manner than SPM in the fiber.

The term $\gamma|A_C|^2 A_P$, appearing only in Eq. 2.14 and accounting for Cross-Phase Modulation (XPM), is of high importance, as this is the physical factor on which the switching operation principle described in this work relies on. As explained in the case of SPM, an optical pulse propagating in a nonlinear medium induces an intensity-dependent refractive index change. In the case of XPM, and considering here the context of an optical gate where a probe pulse and a control pulse at different wavelengths are interfering, the probe optical pulse experiences a phase shift induced by the control pulse. As stated in Eq. 2.14 by the presence of the coefficient a , the strength of XPM depends on the relative polarization state of both pulses.

2.4 Four-Wave Mixing in Fibers and All-Optical Switching

Four-Wave Mixing is another effect resulting from nonlinear processes occurring in an optical fiber. In this work, only the case of partially degenerated FWM is considered. Fig. 2.4 illustrates the principle of FWM in an HNLF. Two optical waves, a control wave and a probe wave (centered at the frequencies ω_C and ω_P , respectively, with $\Delta\omega = \omega_P - \omega_C$), are fed together into the HNLF. Given that the probe and control signals propagate simultaneously and with the same states of polarization inside the fiber and that the phase-matching condition is met (see below, p. 19), new spectral components (FWM-products) appear at the optical frequencies $\omega_P + \Delta\omega$ and $\omega_C - \Delta\omega$. As suggested in Fig. 2.4, the intensity of new wave at the frequency $\omega_C - \Delta\omega$ is larger than the intensity of the wave at $\omega_P + \Delta\omega$, as the control signal power is also larger than the probe signal power. The generation of a new wave through FWM can be used as optical AND logical

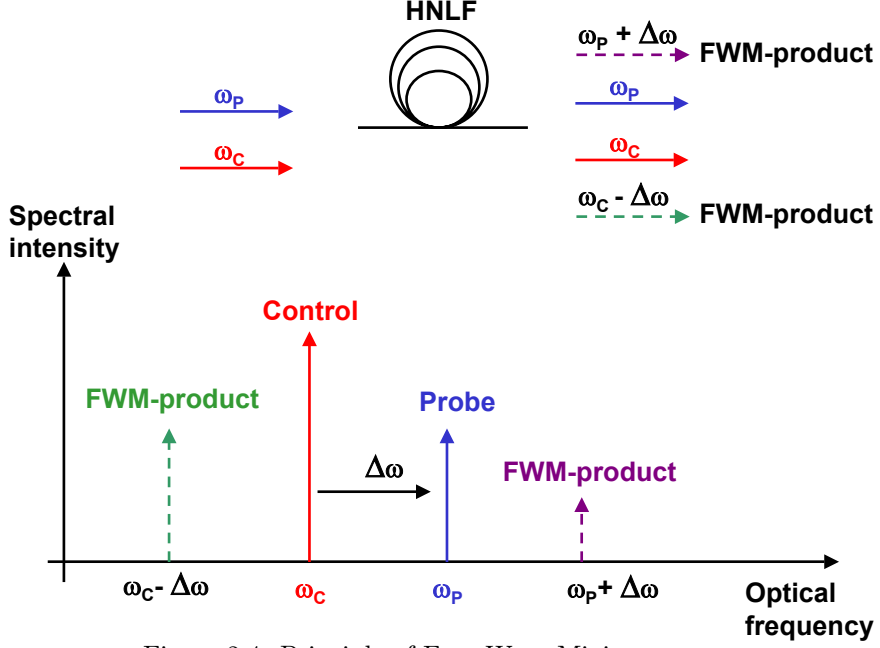


Figure 2.4: Principle of Four-Wave Mixing.

gate between probe and control signals. When control and probe pulses do not overlap in the fiber, no FWM-products can be observed.

To understand the phenomenon of FWM in a fiber, the starting point are the Maxwell-equations with the nonlinear part of the induced polarization:

$$P_{NL} = \epsilon_0 \chi_{xxxx}^3 E_x^T E_x^T E_x^T \quad (2.20)$$

where E_x^T is the total optical field in the fiber. It is assumed that all fields are linearly polarized along the x -axis, because co-polarization is a prerequisite for FWM to occur. For simplicity the index x is omitted in E^T in the following. P_{NL} involves all nonlinear interactions. In particular, P_{NL} is the source term, for the generation of the new frequency components.

The general treatment of the FWM process starts with the coupled equations of four optical fields, the two input fields with the frequencies ω_P and ω_C , and the two newly generated optical fields with frequencies $\omega_C - \Delta\omega$ and $\omega_P + \Delta\omega$ ($\omega_C < \omega_P$). In the following, only the generation of the frequency component at $\omega_C - \Delta\omega$ is considered, as this is the dominant process in the case where $|A_C|^2 \gg |A_P|^2$.

Consequently, E^T is the sum of 3 fields:

$$E^T = \frac{1}{2} \sum_{j=1}^3 A_j F_j(x, y) \exp[ik_j z - i\omega_j t] + c.c. \quad (2.21)$$

with $\omega_1 = \omega_C$, $\omega_2 = \omega_P$, $\omega_3 = \omega_{FWM} = \omega_C - \Delta\omega$, $A_1 = A_C$, $A_2 = A_P$, $A_3 = A_{FWM}$, and $k_j = n\omega_j/c$. For simplicity, all modal distributions $F_j(x, y)$

are assumed to be independent of j .

Replacing this expression for E^T in the induced nonlinear polarization P_{NL} (Eq. 2.20), one obtains P_{NL} as the sum of several frequency terms

$$P_{NL} = \widetilde{P}_{NL}(\omega_P)\exp(-i\omega_P t) + \widetilde{P}_{NL}(\omega_C)\exp(-i\omega_C t) + \widetilde{P}_{NL}(\omega_{FWM})\exp(-i\omega_{FWM} t) + c.c. \quad (2.22)$$

The terms with $\omega_S = \omega_1, \omega_2, \omega_3$ describe the effects of SPM and XPM, as explained in Section 2.2 and Section 2.3. The terms with frequencies $\omega = \omega_C + \omega_P + \omega_{FWM}, 3\omega_C, 3\omega_P, 3\omega_{FWM}, 2\omega_C + \omega_P, 2\omega_C + \omega_{FWM} \dots$ describe the effects of sum frequency generation, in particular third harmonics generation ($\omega = 3\omega_C, 3\omega_P, 3\omega_{FWM}$). Finally, the terms with $\omega = \omega_C + \omega_P - \omega_{FWM}, \omega_C + \omega_{FWM} - \omega_P, \omega_P + \omega_{FWM} - \omega_C, 2\omega_C - \omega_P, 2\omega_C - \omega_{FWM}, 2\omega_P - \omega_C, 2\omega_P - \omega_{FWM} \dots$ describe the effects of FWM.

The generation of the FWM-component at $\omega_C - \Delta\omega$ is based on the term

$$\widetilde{P}_{NL}(\omega_{FWM}) = \frac{3}{8}\chi_{xxxx}^3 A_C^2 A_P^* F^2(x, y) F^*(x, y) \exp[i(2k_C - k_P)z] \quad (2.23)$$

with $\omega_{FWM} = 2\omega_C - \omega_P = \omega_C - \Delta\omega$. The frequency condition is written as:

$$2\omega_C - \omega_P - \omega_{FWM} = 0 \quad (2.24)$$

In quantum-mechanical terms, this condition means that two photons at the control frequency ω_C are annihilated and that simultaneously a photon at the frequency ω_P and a photon at the frequency $\omega_{FWM} = \omega_C - \Delta\omega$ are created. Consequently, the generation of the new FWM-component at $\omega_C - \Delta\omega$ is associated with the amplification (parametric gain) of the optical field at ω_P . However, the term $\widetilde{P}_{NL}(\omega_{FWM})$ in Eq. 2.23 is only efficient in generating the new optical wave

$$E_{FWM} = \frac{1}{2}A_{FWM}F(x, y)\exp[ik_{FWM}z - i\omega_{FWM}t] + c.c. \quad (2.25)$$

if E_S and $P_{NL}(\omega_{FWM})$ in Eq. 2.22 have the same phase, i.e. if the wave-vector mismatch Δk obeys the relation

$$\Delta k = k_P + k_{FWM} - 2k_C = 0 \quad (2.26)$$

The requirement $\Delta k = 0$ is referred to as the phase matching condition.

Parametric gain

The parametric gain experienced by the optical field at $\omega_2 = \omega_P$ after propagating along the length z is obtained by explicitly evaluating the three coupled wave equations. For CW-signals, one obtains the gain $G = \exp(gz)$ with:

$$g = \sqrt{(2\gamma P_C)^2 - \frac{1}{4}(\Delta k + 2\gamma P_C)^2} \quad (2.27)$$

where P_C is the optical power of the control signal [20]. The parametric gain is only defined when $-6\gamma P_C \leq \Delta k \leq 2\gamma P_C$, as this condition ensures that $(2\gamma P_C)^2 - \frac{1}{4}(\Delta k + 2\gamma P_C)^2 \geq 0$ in Eq. 2.27.

For a fiber of length L , the maximum gain $G_{MAX} = \exp(2\gamma P_C L)$ is obtained for $\Delta k = -2\gamma P_C$. The shift of the gain peak from $\Delta k = 0$ is due to the contribution of SPM and XPM to the phase mismatch. Although high gain values can be reached for CW-signals, the parametric gain remain low when the control signal consists of pulses, and in this case the Eq. 2.27 is not valid for g .

2.5 Walk-Off

The phenomenon referred to as Walk-off results from the wavelength dependence of the group velocity $v_g = 1/\beta_1$. The probe and the control waves experience different group velocities (as $\beta_{1P} \neq \beta_{1C}$ in general), thus two pulses entering a fiber of length L at the same time will be separated by a delay $\Delta\tau = L |\beta_{1C} - \beta_{1P}|$ when leaving the fiber of length L . Walk-off may set a limit for the efficiency of switching but can be reduced, by setting the probe and control wavelengths symmetric around the λ_0 ($D(\lambda_0)=0$ ps nm⁻¹ km⁻¹) of the fiber [21].

The walk-off can be evaluated as a function of the fiber parameters and of the properties of the probe and control signals (wavelength allocation), as presented in the following. The dispersion slope parameter S of the fiber is supposed to be known at the given wavelength λ' ($S(\lambda') = S_{\lambda'}$), as well as the dispersion parameter at λ' ($D(\lambda') = D_{\lambda'}$).

We also suppose that S is not dependent on the wavelength (i.e. S is a constant over λ equal to $S_{\lambda'}$) over a narrow wavelength domain centered on λ' . The dispersion parameter D is then $D(\lambda) = D_{\lambda'} + S_{\lambda'}(\lambda - \lambda')$. As $D(\lambda) = \frac{\partial\beta_1}{\partial\lambda}$, one obtains:

$$\beta_1(\lambda) = \frac{S_{\lambda'}}{2} \lambda^2 + (D_{\lambda'} - S_{\lambda'} \lambda')\lambda + K \quad (2.28)$$

where K is an integration constant. β_1 shows a parabolic dependence on the wavelength, with a minimum at λ_0 .

Two optical waves are considered at the wavelengths

$$\lambda_P = \lambda_{mid.} + \frac{\Delta\lambda}{2} \quad \lambda_C = \lambda_{mid.} - \frac{\Delta\lambda}{2} \quad (2.29)$$

The wavelength separation between both waves is $\Delta\lambda$, and $\lambda_{mid.}$ is the "middle" wavelength, situated between the wavelengths of the two waves, as $\lambda_{mid.} = (\lambda_P + \lambda_C)/2$.

The walk-off $\Delta\tau$ between the waves is proportional to the difference $|\beta_1(\lambda_P) - \beta_1(\lambda_C)|$, which is given by:

$$\frac{\Delta\tau}{L} = \Delta\lambda |\{D_{\lambda'} + S_{\lambda'} (\lambda_{mid.} - \lambda')\}| \quad (2.30)$$

Consequently, a solution to cancel the walk-off in the case where S is taken to be constant is to set $\lambda_{mid.} = \lambda' - \frac{D_{\lambda'}}{S_{\lambda'}} = \lambda_0$. $\beta_1 L$ and the walk-off $\Delta\tau$ were evaluated as function of λ and $\lambda_{mid.}$, respectively, and were plotted in Fig. 2.5. The integration constant K in Eq. 2.28 was chosen such that $\beta_1(\lambda_0) = 0$. The parameters of the fiber considered are recapitulated in the figure caption.

The wavelength separation for the two waves considered was taken to be 15 nm. As can be seen in Fig. 2.5, and as stated in Eq. 2.30, the slope of the curve evaluating the walk-off in Fig. 2.5 (dashed line) is proportional to $\Delta\lambda$ and to S . As the parameter S is usually low for a DS-HNLF, the walk-off remains

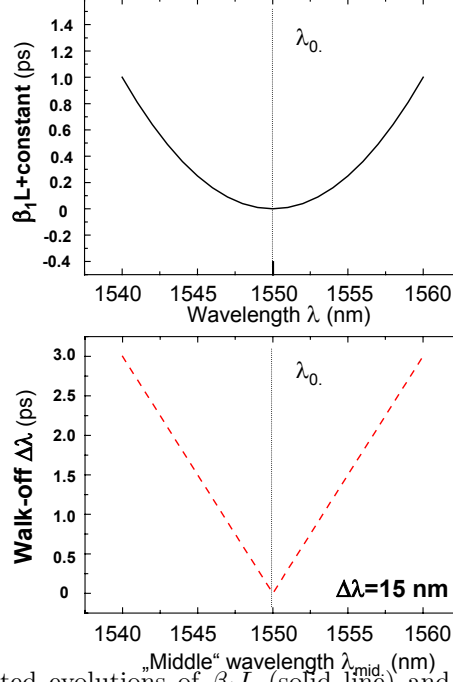


Figure 2.5: Calculated evolutions of $\beta_1 L$ (solid line) and of the walk-off $\Delta\tau$ (dashed line) vs. λ and $\lambda_{mid.}$, respectively, with $\lambda_0=1550$ nm, $S(\lambda_0)=0.02$ ps $\text{km}^{-1} \text{ nm}^{-2}$, $L=1$ km (S is considered to be a constant).

moderate for common values of $\Delta\lambda$ and L ($\Delta\lambda < 20$ nm, $L < 1$ km). For the fiber considered above, and with $\Delta\lambda = 15$ nm, a walk-off value of 1.5 ps was calculated for $\lambda_{mid.} = \lambda_0 + 5$ nm.

2.6 Pump-Probe Characterization of Optical Switching Devices

In this work, two techniques are used to characterize optical gates. One method uses BER-measurements of a probe signal before and after passage through the optical gate. This technique is referred to as Bit Error Rate (BER) measurement and will be used the demultiplexing experiments discussed in Chapter 3, as well as in Chapter 4.

The other method is based on pump-probe measurements of the transmittance T of the optical gate, defined as

$$T = \frac{P_{out}}{P_{in}} \quad (2.31)$$

where P_{in} and P_{out} are the probe optical powers at the input and output of the gate, respectively.

The method of pump-probe measurement is described in the following.

The transmittance T of the gate is defined as the measurement of the light

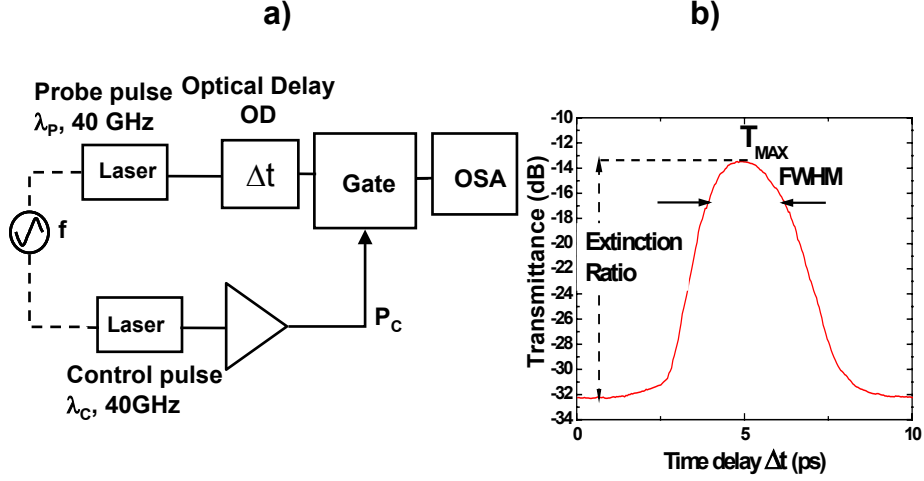


Figure 2.6: a). Experimental setup for the characterization of all-optical gates by pump-probe measurements, b). Characteristics of the switching window.

fraction that passes through the gate. The value of the transmittance is comprised between 0 (no transmission) and 1 (full transmission). It is often evaluated in dB, using the relation $T_{dB} = 10 \log(T)$. In the ideal case, the control signal changes the transmittance T for the probe signal at a given time instantaneously from $T = 0$ to $T = 1$ and after a time interval τ back from $T = 1$ to $T = 0$. The switching window is the dependence of T versus time. Fig. 2.6 a) depicts a pump-probe measurement setup, which is often used to measure switching windows. The investigated switch is represented by a black box with inputs for the pump and probe signals and an output for the switched probe signal.

The pump and probe signals are Return-to-Zero (RZ) pulse trains with a repetition frequency of 40 GHz for example, a given pulse width and the wavelengths λ_C and λ_P , respectively. Semiconductor Mode-Locked Lasers, Fibers Lasers, as well as Solid-State Lasers have been used throughout this work. Both pulse trains are coupled into the switch with well defined polarization and with a relative time delay Δt , which is controlled by a variable optical delay-line (OD). The pulse width of the probe signal limits the temporal resolution of the measurement, while the pulse width of the pump signal determines in general the width and the amplitude of the switching window itself. The transmitted probe signal is detected by an optical spectrum analyzer (OSA) or by an optical power meter versus the time delay Δt between the pump and probe pulses. The switching window is thus evaluated as the convolution of the transmittance of the gate with a probe pulse. Fig. 2.6 b) is an example of the measurement of a

switching window. The switching window considered in this work is the result of the convolution product of the transmittance of the gate with a probe pulse. As the FWHM of the probe pulse influences the FWHM of the convolution product, care has to be taken when discussing on the width of the switching windows.

The extinction ratio (ER), the width (FWHM) of the switching window and the maximum transmittance T_{MAX} are the parameters used to characterize a switching window.

- The extinction ratio is defined as the ratio of detected probe power for maximum transmittance to the detected probe power of the minimum transmittance. This is a measurement of the available switching contrast between the state where the gate is transmitting as much as possible of the probe signal, and the state where the gate is attenuating the probe signal as much as possible.
- The FWHM of the switching windows gives an information on the width of the windows at the level where the transmittance decreased by 3 dB (50 %) from its maximum value.
- The transmittance at maximum of the switching window T_{MAX} is another parameter of interest, as it gives an information on the minimum attenuation of the gate. In a system experiment, the gate should work with losses as low as possible, as it would otherwise cause the Optical Signal-to-Noise Ratio (OSNR) to decrease if the gate is followed by an EDFA, or even attenuate the probe signal power below the sensitivity level of the receiver.

The quantities ER , $FWHM$ and T_{MAX} of the switching windows can be used to characterize and compare different switching configurations. The time resolution of the pump-probe measurement depends on the step used to vary Δt , and of the unwanted temporal drift occurring between signals emitted by pulse sources.

For OTDM-demultiplexing of 640 Gbit/s data signals, a high ER (about 15 dB or higher), a FWHM shorter than 1.7 ps and a high maximum transmittance (ensuring that the transmitted signal power meets the sensitivity requirements of the system) are required, as was asserted in numerous experiments.

Limitation of pump-probe measurements

As shown in Fig. 2.7, the pump-probe measurement of the switching characteristic of an optical gate relies on the sampling of the transmittance by an optical probe pulse. The switching window measured as presented in this Section thus corresponds to the convolution product of the "real" switching window (the transmittance) with the sampling (probe) pulse. In particular, the resolution of this measurement method is determined by the width of the probe pulse, as well as by the step Δt used when varying the delay between control and probe. For a fiber-based interferometric gate, the transmittance is related to the phase

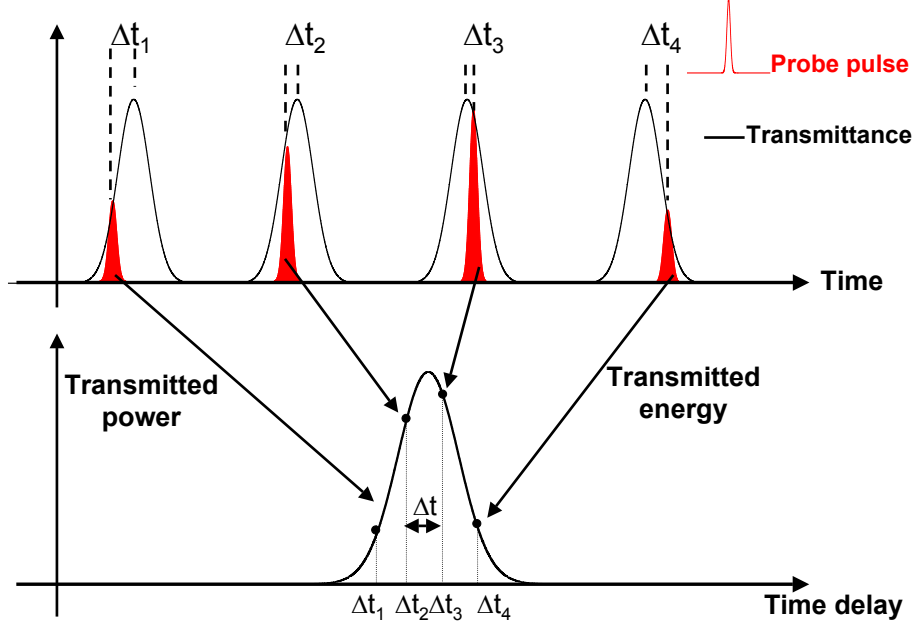


Figure 2.7: Principle of switching window measurement.

shift $\Delta\varphi$ induced through XPM in the fiber. As the relation linking T and $\Delta\varphi$ is periodic in $\Delta\varphi$ ($T = \sin^2(\Delta\varphi/2)$, as will be demonstrated later in Chapter 3), a value of $\Delta\varphi$ above π will result in a decrease of T . This will lead to a switching window presenting extrema (i.e. more than one local maximum and one local minimum), which can also happen when the control pulse presents more than one local maximum. The convolution product might occult the rapidly varying structures for such a resulting transmittance characteristic if the probe pulse is not short enough to resolve them.

Fig. 2.8 a) shows the calculated transmittance for a fiber based gate, where the control pulse power was willingly set high, which led to a decrease of the transmittance even before the peak power of the control pulse was reached. Consequently, the transmittance presents several local extrema. Still, when sampled (convoluted) with a 0.8 ps (FWHM) probe pulse, the impairments can not be seen on the switching windows (see Fig. 2.8 b)). Only when sampling with a shorter pulse ($\text{FWHM} = 0.5 \text{ ps}$), the ripple structure of the transmittance can be better resolved.

Table 2.5 presents data bit rates and the associated bit-slot periods, as well as the recommended pulse widths to be used when generating these signals [22], [23]. The data signal was assumed to be single polarized. Throughout this work, switching window investigations were carried out with probe pulse FWHM narrower than the control pulse FWHM, as for most experiments a short data pulse width was required for increasing the data bit-rate through time-division multiplexing.

However, as will be shown in Chapter 3, the phase shift $\Delta\varphi$ induced in the

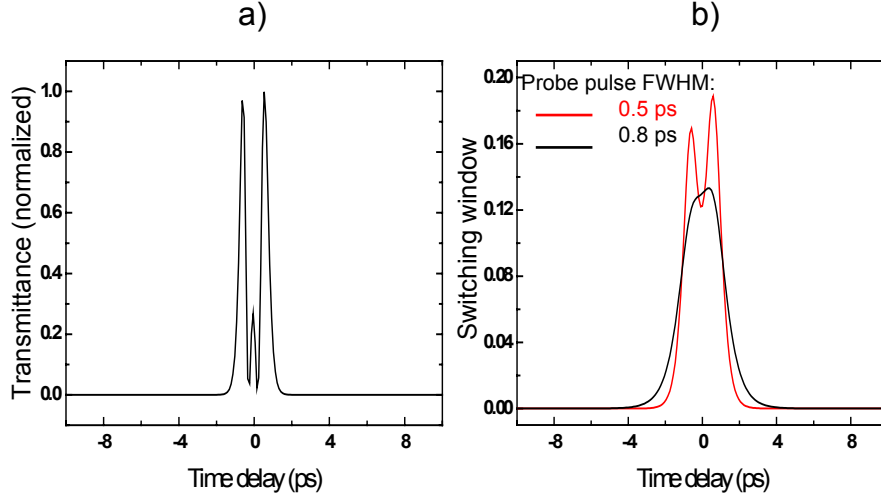


Figure 2.8: a). Calculated transmittance characteristics, and b). corresponding switching windows for probe pulse with varying FWHM.

	40 Gbit/s	160 Gbit/s	320 Gbit/s	640 Gbit/s
Bit-slot period (ps)	25	6.25	3.125	1.5625
Required data pulse FWHM	8.3 ps	2.1 ps	1.0 ps	0.52 ps

Table 2.5: Typical data rate used in this work, and associated bit-slot period and data pulse FWHM.

DS-HNLF included in the gate did not exceeded π . Consequently, a decrease of the resulting transmittance T due to high values of $\Delta\varphi$ is unlikely to occur. Other impairments such as the instability of the time position of data and control pulse, which might be due to a malfunctioning optical delay line (OD in Fig. 2.6), may also cause the switching window to present irregularities. Nevertheless, proper care was accorded to the measurement setups, so that the switching windows measurement could be considered to reflect the true switching characteristic of the optical gates.

Chapter 3

Gates based on Highly Nonlinear Fibers

To convert the phase change into an amplitude change, which is to be detected by a receiver, the nonlinear medium is incorporated into an interferometric scheme.

The Sagnac Interferometer, which prefigured the setup for the Nonlinear Optical Loop Mirror (NOLM), was first investigated in the 1960's, originally for applications as a gyroscope [24]. The interest for the NOLM grew in the field of optical telecommunications when the gate was used to modulate a CW wave, which transmission was controlled by a control pulse signal. Later, the NOLM imposed itself as a demultiplexer for Terabit OTDM signals [25], [26]. The Kerr gate (also called Kerr shutter) gained attention in a comparable experiment [6].

3.1 Nonlinear Optical Loop Mirror (NOLM)

3.1.1 Basics of the NOLM Gate

The NOLM gate is based on the Sagnac Interferometer [27, 28], where an optical fiber is incorporated as nonlinear medium.

The setup is shown in Fig. 3.1. The NOLM basically comprises a first optical 3 dB coupler ("A" in Fig. 3.1) splitting the input probe signal, another optical coupler ("B") used to insert the control signal in the loop and a loop made of optical fiber. Polarization controllers (PC) are included, so that the control and probe polarization states in the loop can be adjusted independently. At the output of the NOLM, an optical bandpass (OBF) blocks the control signal wavelength.

The passive losses of a NOLM include the loss of the 3 dB couplers used to couple the control and probe signal into the fiber loop, the loss of the filter, and the losses due to fiber splices and other components built in the loop (PC, HNLF). The length of the fiber loop is usually in the order of 1 km when a piece of HNLF is included, while lengths longer than 5 km are needed when the loop comprises a fiber with low nonlinearity (SMF).

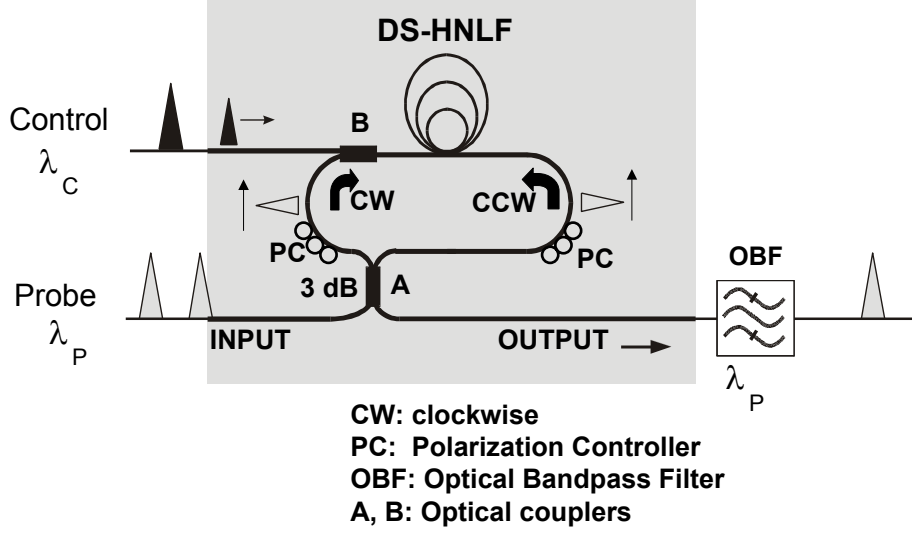


Figure 3.1: Basic setup for the NOLM.

Operating principle of the NOLM

The operation principle of the NOLM is explained in the following (the optical waves are assumed to maintain their polarization states throughout propagation, allowing a scalar approach).

The probe optical wave is represented by the electrical field strength E_{in} at the input of the NOLM. E_{in} is split at the input coupler, resulting in two waves $E_{CW} = E_{in}/\sqrt{2}$ and $E_{CCW} = (E_{in}/\sqrt{2})e^{i\frac{\pi}{2}}$, propagating clockwise (CW) and counter-clockwise (CCW) in the loop. The crossing of the 3 dB coupler also induces a relative phase shift of $\frac{\pi}{2}$ for one of the two waves exclusively, namely for E_{CCW} . When neglecting the birefringence of the fiber in the loop (which is a good approximation when the loop consists of pieces of SMF and HNLF), both waves experience the same phase shift φ (induced by dispersion and non-linearity in the fiber loop) during transmission over the loop, and recombine at the coupler, where E_{CCW} once again experiences a $\frac{\pi}{2}$ phase shift, leading to a destructive recombination, as

$$E_{out} = \frac{1}{\sqrt{2}} \frac{1}{\sqrt{2}} E_{in} e^{i\varphi_{CW}} + \frac{1}{\sqrt{2}} \frac{1}{\sqrt{2}} E_{in} e^{i\frac{\pi}{2}} e^{i\frac{\pi}{2}} e^{i\varphi_{CCW}} \quad (3.1)$$

If $\varphi_{CCW} = \varphi_{CW}$, $E_{out} = 0$. Consequently, no signal is transmitted to the output of the NOLM, and E_{in} is reflected to the input. In the practical case, the birefringence of the fiber can not be neglected, due to bends and stresses in the setup. However, the phase shift difference raising between CW and CCW propagating signals in the fiber loop can be compensated by adjusting the polarization states for both signals. This can be done by using the PCs in the fiber

loop. The residual phase shift difference $\Delta\varphi_0$, that may be not compensated by using the PCs, was always extremely small throughout the investigations, as stated by the very good extinction (> 40 dB) that was reached with the NOLM.

Consider the case where a control pulse is fed into the HNLF together with a clockwise propagating probe signal. The control pulse will induce a nonlinear phase shift φ_{XPM} on the probe signal, due to XPM, and this phase shift depends on the power of the control pulse. As φ_{XPM} represents the relative phase shift difference between the clockwise and counter-clockwise propagating pulses in the fiber loop, we denote $\varphi_{XPM} = \Delta\varphi$ in the following. Consequently:

$$\varphi_{CCW} = \varphi_{CW} + \Delta\varphi \quad (3.2)$$

The counter-clockwise propagating pulse does not experience the same nonlinear phase shift, as it does not propagate simultaneously with a control pulse through the nonlinear medium. This results in a non-destructive interference at the coupler and gives

$$E_{out} = \frac{1}{2}E_{in}e^{i\varphi_{CW}} - \frac{1}{2}E_{in}e^{i\varphi_{CCW}} = \frac{1}{2}E_{in}(1 - e^{i\Delta\varphi})e^{i\varphi_{CW}} \quad (3.3)$$

The coupler splitting the input probe signal was assumed to have exactly the same coupling ratios for bar and cross-coupling. As $(1 - e^{i\Delta\varphi}) = -2ie^{i\frac{\Delta\varphi}{2}}\sin(\frac{\Delta\varphi}{2})$, the transmittance $T = P_{out}/P_{in}$ for the probe signal at the output of the NOLM is given by:

$$T = \sin^2\left(\frac{\Delta\varphi}{2}\right) \quad (3.4)$$

The starting point to obtain the relation linking $\Delta\varphi$ with P_C is the propagation equation Eq. 2.14 with $a=2$, as probe and control pulses propagate copolarized along the fiber.

The relative phase shift difference $\Delta\varphi = \Delta\varphi_{NOLM}$ acquired by the probe pulse propagating clockwise in the loop (simultaneously with a control pulse) and co-polarised with the control pulse is given by:

$$\Delta\varphi_{NOLM} = 2\gamma P_C L \quad (3.5)$$

As control and probe pulses propagate copolarized inside the DS-HNLF, parametric amplification of the clockwise (CW) propagating probe pulse is expected. This was not observed in the experiments carried out. In particular, the amplification of the CW propagating pulse should lead to non-perfect destructive recombination at the input 3 dB coupler of the NOLM (coupler "A" in Fig. 3.1). This is due to the fact that when reaching the 3 dB coupler "A" after propagating through the fiber loop, the CW and CCW propagating signals will have opposite phases (which is equivalent to a phase difference $\Delta\varphi=\pi$), but different amplitudes, as the CW propagating signal experienced parametric amplification.

Still, the NOLM always proved to reach an extinction of the probe signal better than -40 dB, asserting proper destructive interference at coupler "A". The parametric amplification was thus neglected when investigating the NOLM.

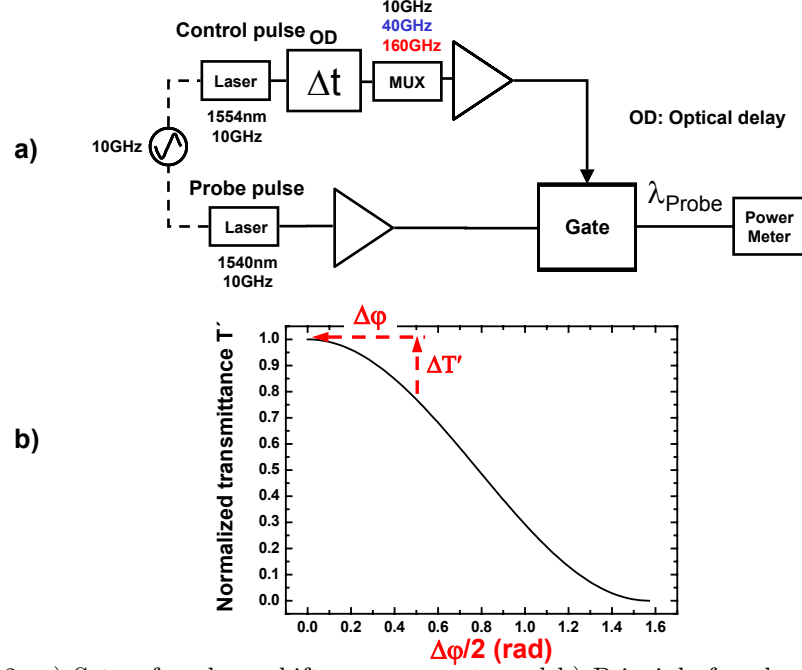


Figure 3.2: a) Setup for phase shift measurements and b) Principle for phase shift evaluation.

3.1.2 Measurements of induced Phase Shift

As stated in Eq. 3.4 and Eq. 3.5, the transmittance of the gate, is determined by the phase shift $\Delta\varphi_{NOLM}$ induced by a control pulse on the probe pulse. The transmittance can be measured directly using pump-probe measurement, and the relative phase shift can also be evaluated.

The setup used to evaluate $\Delta\varphi$ is shown in Fig. 3.2 a). A 10 GHz probe pulse train was emitted by a Tunable Semiconductor Mode-Locked Laser (TSMLL, $FWHM_P=1.6$ ps) at the wavelength 1540 nm, and sent to the gate. The control pulse was emitted by a second TSMLL ($FWHM_C=1.5$ ps), synchronized with the first one, emitting a 10 GHz pulse train at 1554 nm. An optical delay-line allowed to vary the delay between probe and control pulse. The setup included a multiplexer (MUX), so that the repetition rate of the control pulse could be varied up to 160 GHz. An optical bandpass filter (3 nm) blocked the control wavelength at the output of the gate.

The phase shift difference $\Delta\varphi$ was evaluated using the following method. At first, a relative delay of the pulses trains was set, so that control and probe pulses do not overlap. Under this condition the polarization of the probe pulses was adjusted for maximum transmittance by using the polarization controllers (PC) in the loop. This corresponds to the case where the phase difference ($\varphi_{CW} - \varphi_{CCW}$) is adjusted to π (see Eq. 3.1) by influencing the birefringence in the fiber loop using the PCs. Next, the relative delay between both pulse trains and the state of polarization of the control pulses are adjusted to give a minimum in the transmittance of the probe pulses. Under these conditions, the

variation of the transmittance ΔT (measured as the variation of the transmitted power after the gate) is linked to the induced relative phase shift difference by the relation $T' = \cos^2(\frac{\Delta\varphi}{2})$, and $T' = 1 - T$ (the relation is plotted in Fig. 3.2 b). Thus the dependence of $\Delta\varphi$ on the power of the control pulse can be derived by measuring the transmittance T' as a function of the control pulse power. This method has the advantage of being more accurate for measuring higher phase shifts than the method where the transmittance is set on minimum (in this latter method of measuring $\Delta\varphi$, T would be given by $T = \sin^2(\frac{\Delta\varphi}{2})$).

The control pulse power was varied, and the optical power was measured using a power meter. The repetition rate of the control pulses was also varied, so that the relative phase shift could be measured for a control pulse repetition rate of 10 GHz, 40 GHz and 160 GHz. For each measurement, the polarization of control and probe signals was optimized. The results can be seen in Fig. 3.3, where the phase shift $\Delta\varphi$ is represented as a function of the control pulse energy. The control pulse energy does not depend on the repetition rate of the signal, and was thus chosen as the varying parameter. Pulse peak power and corresponding average power (denoted Avg. power) were also mentioned for a few pulse energies in Fig. 3.3, and for the repetition rate 10 GHz exclusively. An increase of the repetition rate implies an increase of the average power of the signal if the energy per pulse has to remain unchanged. The maximum output power of optical amplifiers sets a limit for the pulse energy at high repetition rates. As expected, the fiber-based interferometer showed no patterning, contrary to what could be shown with SOA-based interferometric gates, where the slow recovery times led to a strong dependence of the switching characteristics of the control pulse repetition rate [29]. For the NOLM, a given control pulse energy leads to the same $\Delta\varphi$ for 10 GHz, 40 GHz and 160 GHz repetition rates. The three measurements, for repetition rates of 10 GHz, 40 GHz and 160 GHz for the control pulses, showed the same behaviour at low control powers. In particular, the phase shift depends linearly on the control peak power, in accordance with the Eq. 3.5.

A collapse of the phase shift was observed at high control power, which is not in agreement with Eq. 3.5. This is attributed to the broadening of the control pulse at high power, leading to a decrease of its peak power and also to spectral overlap of control and probe pulse. The broadening of the control pulse depends on the dispersive properties of the fibers at λ_C and leads to a decreasing efficiency of the switching process for high powers of the control pulses. The spectral broadening makes this measurement method less accurate for high control powers, as part of the optical power measured at λ_P will consist of control pulses energy. The control pulse considered in this part had $FWHM_C = 1.5$ ps, and is broader than the typical control pulse as considered in Table 2.3 (p. 15). Still, as the repetition rate is now 10 GHz, and assuming that the average control power remains around 15 dBm, higher peak power causes the nonlinear length L_{NL} to decrease.

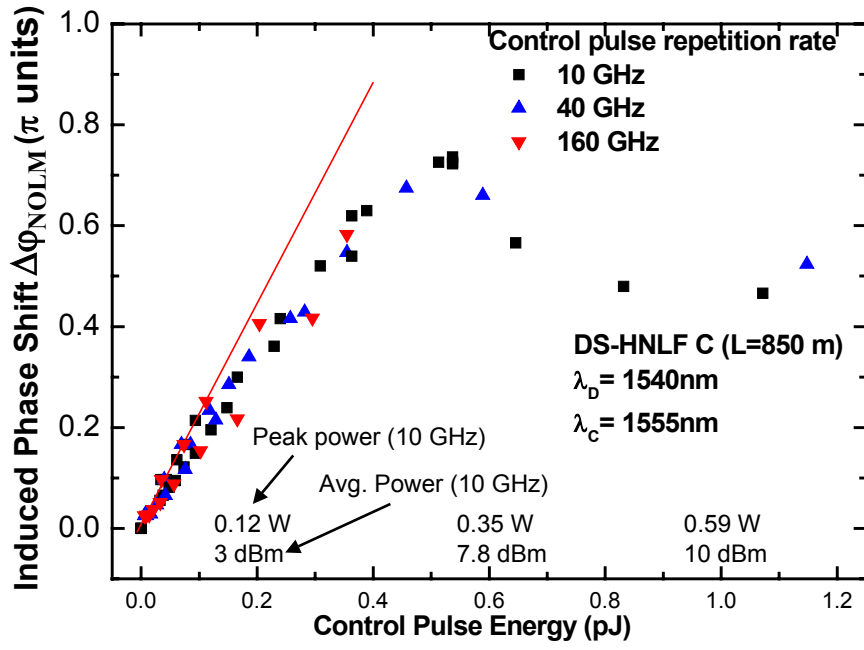


Figure 3.3: Phase Shift Measurement for the NOLM (DS-HNLF C was used). Control pulse: $\text{FWHM}_C=1.5$ ps, 10 GHz.

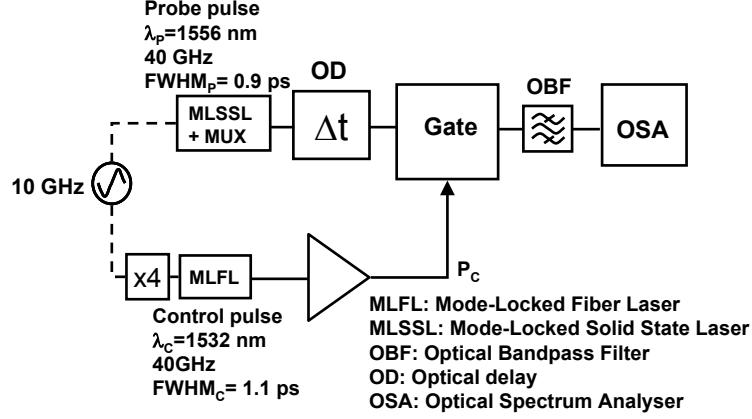


Figure 3.4: Setup for switching window measurement.

3.1.3 Measurements of Switching Windows

The setup used for switching window measurements is shown in Fig. 3.4. The 40 GHz probe signal ($\lambda_D=1556$ nm, $FWHM=0.9$ ps) was provided by a 10 GHz mode locked solid-state laser (MLSSL), followed by a passive delay line pulse multiplier ($\times 4$). The 40 GHz control signal ($\lambda_C=1532$ nm, $FWHM=1.1$ ps) was provided by a mode locked fiber laser (MLFL). A 6 nm optical band-pass filter was used after the gate to separate the probe signal. Switching windows were measured and characterized using the criteria presented in Section 2.6: Extinction Ratio ER , Full Width at Half Maximum $FWHM$, and maximum transmittance T_{MAX} . The three DS-HNLF A, B and C presented in Section 2.2 (see Table 2.2) were tested as nonlinear medium in the gate: DS-HNLF A ($L=100$ m, $\lambda_0=1537$ nm), DS-HNLF B ($L=300$ m, $\lambda_0=1556$ nm) and DS-HNLF C ($L=850$ m, $\lambda_0=1550$ nm). An important operation parameter, which influences all three evaluation criteria given above, is the average control pulse power P_C , which was also varied in our experiments. The wavelength allocation of the control and probe signal was kept constant during all experiments, as well as the probe pulse $FWHM_P$.

Influence of the control pulse power on the Extinction Ratio

Fig. 3.5 shows the extinction ratio of the switching windows as a function of the average control pulse power for the NOLM, measured for DS-HNLF A, DS-HNLF B, and DS-HNLF C. The polarization states of control and probe signals in the NOLM were adjusted for minimum transmittance of the probe pulse in

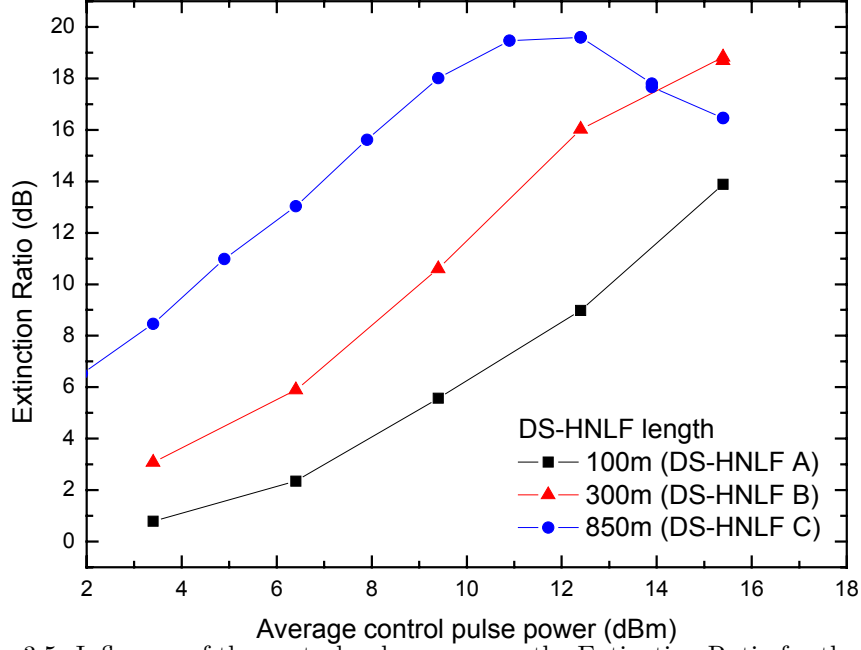


Figure 3.5: Influence of the control pulse power on the Extinction Ratio for the NOLM Gate (40 GHz control pulse, FWHM=1.0 ps).

absence of a control pulse, as explained in 3.1.1.

As expected, the ER is increasing with increasing control pulse power and longer fiber length. This is due to the higher nonlinear phase shift $\Delta\varphi$ obtained for longer fibers and to higher control powers, which leads to a higher switched output power and thus a higher ER. With the 100 m and 300 m long DS-HNLF (DS-HNLF A and B, respectively), no saturation behavior could be observed up to the maximum available control pulse power. A decrease of the ER is observed for high control pulse powers when using the 850 m fiber (DS-HNLF C). The saturation effects and the decrease of the ER are mainly due to spectral cross talk from the control pulse, as can be seen in Fig. 3.6.

Fig. 3.6a) presents the spectrum of probe (right) and control signal (left, showing also SPM-induced spectral broadening on the top of the spectrum) for increasing control pulse powers, measured in 0.5 nm resolution bandwidth (RB). As the control power increases, the spectrum of the pulse broadens and a larger amount of the control spectrum overlaps with the probe spectrum, limiting the minimum level where the probe power can be attenuated in the absence of control pulse. Fig. 3.6b) shows two switching windows measured for two different control powers: the solid line represents the measurement carried out for $P_C = 10.9$ dBm (at a repetition rate of 40 GHz, and FWHM=1.0 ps), while the dashed curve stands for the same measurement, but with a higher control power ($P_C = 15.4$ dBm). The overlap of control and probe spectra clearly results in an increase of the transmittance, even when both pulses trains do not overlap in the fiber. This leads to a decrease of the ER for the switching window.

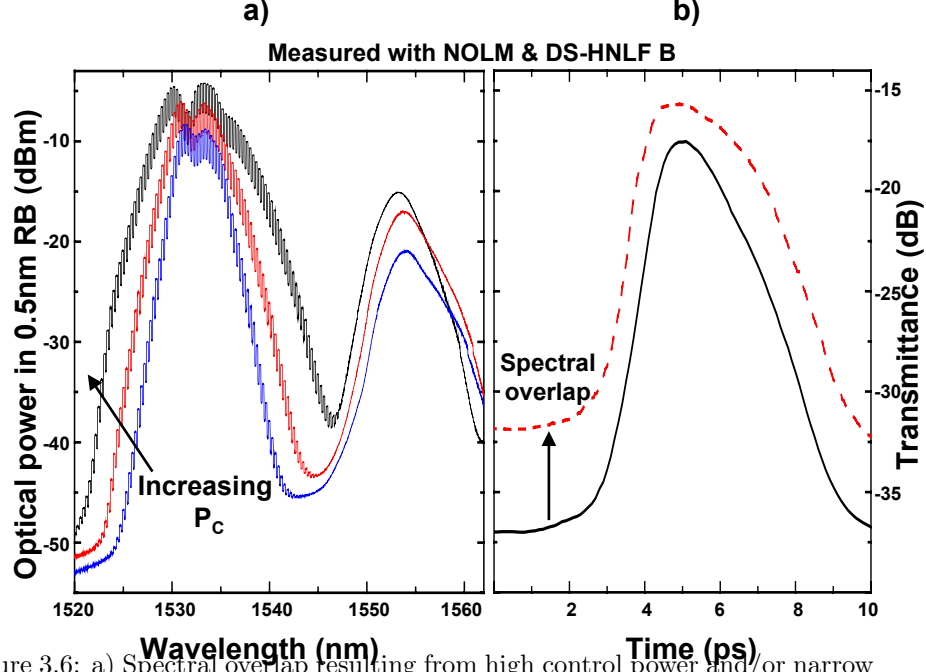


Figure 3.6: a) Spectral overlap resulting from high control power and/or narrow λ -separation, and b) resulting switching window. The NOLM was considered and included DS*HNLF B

Influence of the control pulse power on the FWHM of the switching window

Fig. 3.7 shows the FWHM of the switching windows as a function of the control pulse power for the NOLM.

Switching windows with an $ER \leq 8$ dB were not used for the FWHM evaluation as in these cases the measured optical power after the gate was strongly influenced by the ASE noise within the 6 nm filter bandwidth of the gate. The shortest switching windows measured in our experiments were about 1.7 ps, though a 1.0 ps control pulse was used to gate the NOLM. The FWHM increases with increasing P_c . This broadening effect has mainly two reasons. First, the switching windows in interferometric gates generally broaden with increasing XPM-induced relative phase shift, due to the nonlinear phase-to-amplitude transfer function in the interferometer ($T = \sin^2(\Delta\varphi/2)$). To illustrate this, the following calculations were carried out.

A sech pulse with a FWHM=1 ps was simulated, and is assumed to propagate inside a fiber of length L and of nonlinear parameter γ . The phase shift induced through XPM by the pulse was calculated as $\Delta\varphi = a\gamma LP$, a being a factor standing for the effectivity of the gate (for a NOLM, $a = 2$, as seen in Subsection 3.1.1). For the calculations, the product $(a\gamma L)$ was set to 1 W^{-1} , so that the relative phase shift is practically equal to the power P of the pulse. In particular, the maximum value of $\Delta\varphi$ ($\Delta\varphi_{MAX}$) is given by the value of the peak power of the sech pulse.

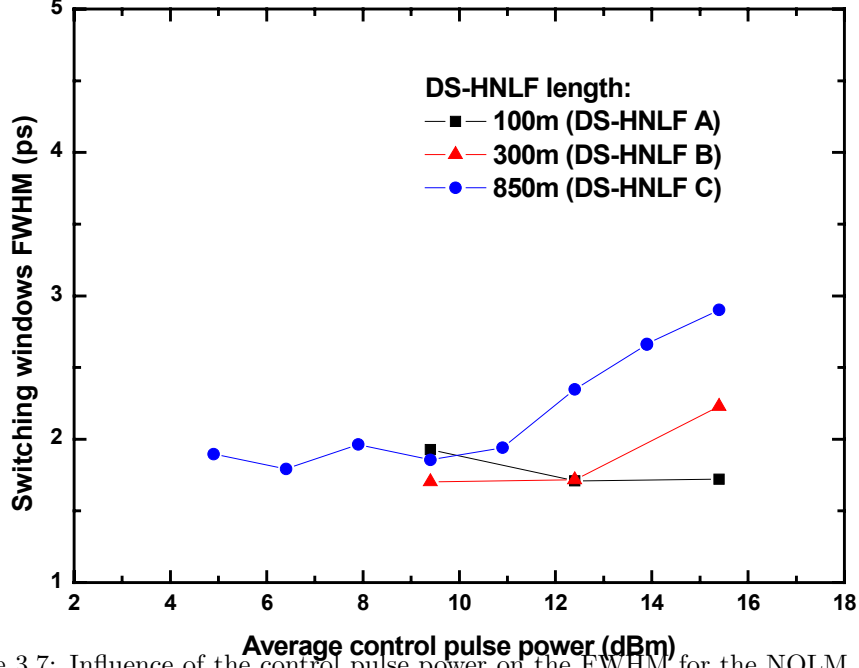


Figure 3.7: Influence of the control pulse power on the FWHM for the NOLM Gate (40 GHz control pulse, FWHM=1.0 ps).

The simulated results are depicted in Fig. 3.8. For three values of the pulse peak power (corresponding to a maximum phase shift $\Delta\varphi_{MAX}$ of 0.4π , 0.8π and π), the intensity profile of the sech pulse was calculated (solid curve), which also exactly matches the induced $\Delta\varphi$. The evolution of the transmittance of the NOLM was calculated using the relation $T = \sin^2 \frac{\Delta\varphi}{2}$. In this ideal case, the walk-off and the broadening of the control pulse was neglected. The FWHM of the switching windows were 0.71 ps, 0.85 ps and 0.98 ps, corresponding to the maximum phase shifts $\Delta\varphi_{MAX}$ of 0.4π , 0.8π , and π , respectively (experimentally, values higher than 0.7π could be measured). An increase of $\Delta\varphi$ results in a broadening of the transmittance of the gate, as well as in a change of the shape of T , as Eq. 3.5 is not linear in $\Delta\varphi$.

Second, the FWHM of the control pulses increase in the DS-HNLF due to the interplay between nonlinear spectral broadening and dispersion, if the wavelength of the control pulses is in the normal dispersion regime. This temporal broadening of the control pulse causes a broadening of the switching window. The broadening of the control pulse can be seen in Fig. 3.9, where the FWHM of the control pulses measured at the DS-HNLF output is plotted as a function of the average control pulse power for the fibers B and C. The broadening effect is stronger for the fiber C because of the longer length of this fiber. Dispersive effects are responsible for pulse changes in the fiber, in particular for the control pulse, and scale with the length of the DS-HNLF used. For this reason, and in the case where the power budget ensures that $\Delta\varphi$ will enable good switching efficiency ($\Delta\varphi \geq 0.6\pi$), a DS-HNLF with a short length should be preferred.

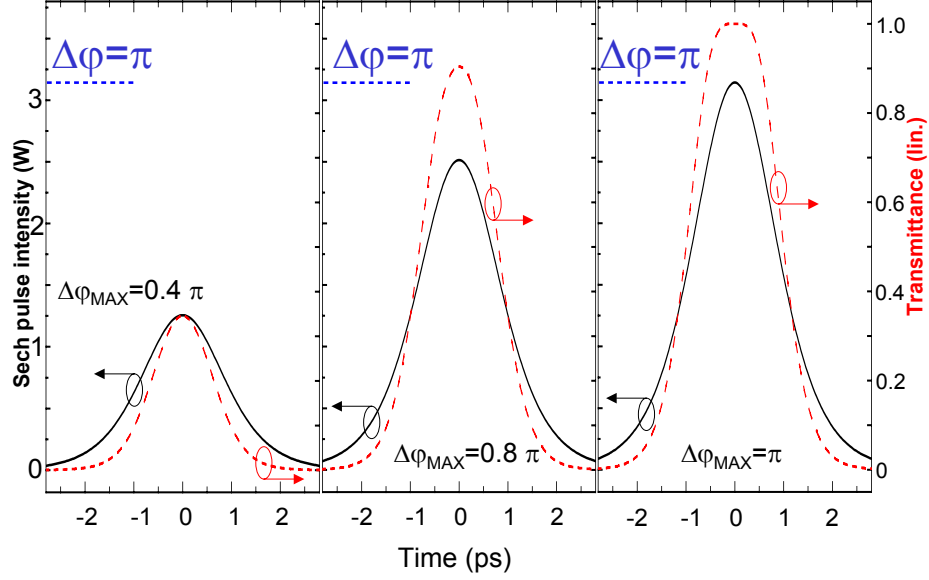


Figure 3.8: Influence of the phase shift $\Delta\varphi$ on the FWHM of the transmittance of a NOLM/Kerr gate. Walk-off and control pulse broadening were neglected.

Influence of the control pulse power on the maximum transmittance T_{MAX}

Another important parameter for the gate is the transmittance at the maximum of the switching window T_{MAX} . T_{MAX} depends on the passive losses of the gate (depending on the quality of splices and the loss of optical components used) and on the switching losses, which result from a nonperfect switching process (for example an insufficient phase change in the nonlinear medium).

The maximum transmittance for the NOLM is shown in Fig. 3.10 as a function of the average control pulse power for fibers A, B and C. As indicated in the figure, the passive loss is 12.0 dB for the NOLM, including the 6 nm band pass filter. Figure 3.10 shows that the maximum transmittance is increasing with increasing control pulse power. This is due to the increasing induced phase shift $\Delta\varphi$, which leads to a reduction of the switching losses. For an ideal phase difference of π in the interferometer, the switching losses would be reduced to zero. As expected, using the shortest DS-HNLF led to the lowest transmittance for the switching windows (-20.4 dB was measured at the maximum of the switching window, when sending the maximum available control power). When gating the NOLM Gate with the optimal control power (with a maximum available power of 15.4 dBm), the maximum transmittance -20.4 dB, -13.5 dB and -15.6 dB for the DS-HNLF lengths of 100 m, 300 m and 850 m, respectively.

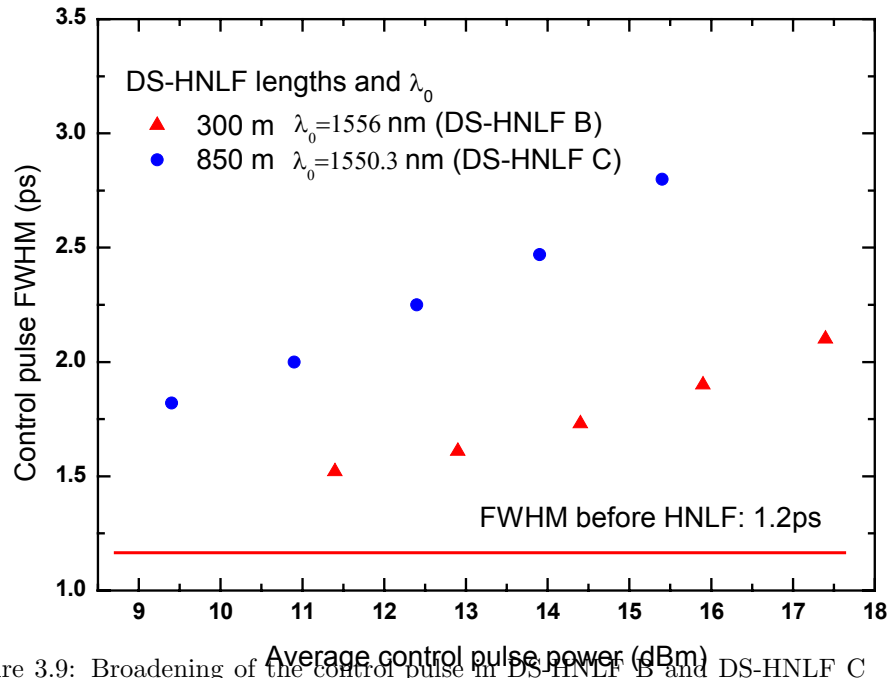


Figure 3.9: Broadening of the control pulse in DS-HNLF B and DS-HNLF C (40 GHz control pulse, FWHM=1.0 ps, $\lambda_C=1532$ nm).

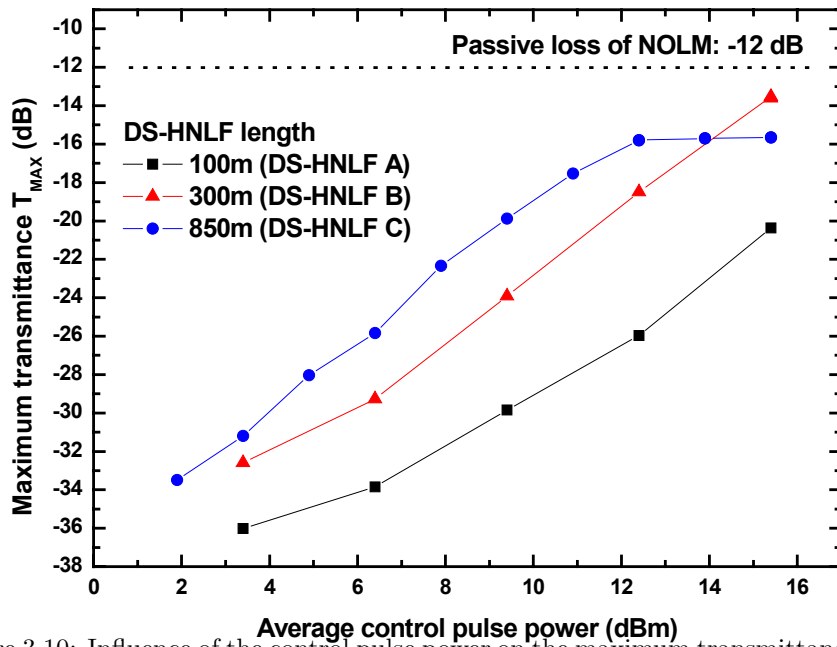


Figure 3.10: Influence of the control pulse power on the maximum transmittance for the NOLM Gate (40 GHz control pulse, FWHM=1.0 ps).

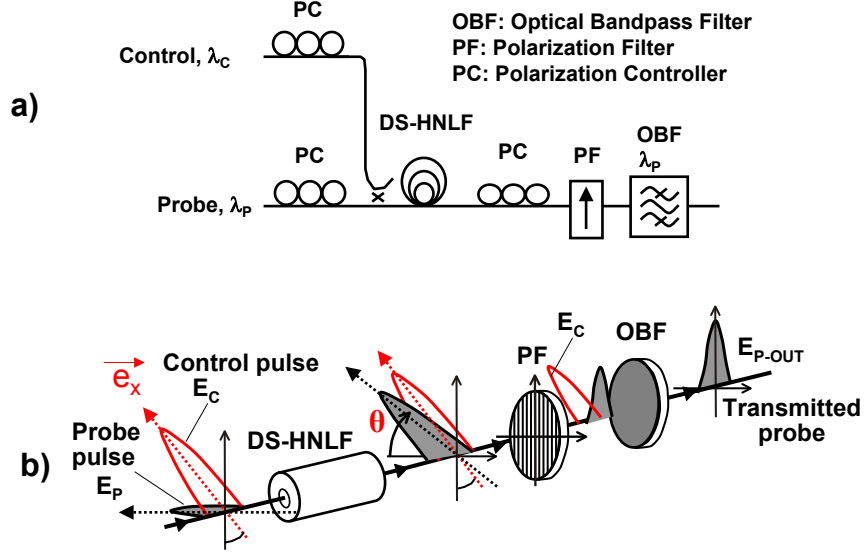


Figure 3.11: Setup and operation principle of the Kerr gate.

3.2 Kerr gate

3.2.1 Basics of the Kerr Gate

The setup for the Kerr gate investigated in this work is shown in Fig. 3.11 a), while the operating principle is depicted in Fig. 3.11 b).

The Kerr gate consists of an optical coupler, a HNLF (DS-HNLF are mostly used), and a polarization filter. The coupler enables the coupling of two optical waves into the DS-HNLF. Throughout this work, a 3 dB or a 10 dB coupler was used, which influences the passive loss of the gate, as well as the maximum control power that could be sent to the DS-HNLF. As the optical waves are generally emitted at different frequencies, an optical bandpass filter (OBF) is included after the polarization filter (PF) to block the control signal. Polarization controllers allow separate polarization adjustment for both signals.

The general operation of the Kerr gate as an OTDM-demultiplexer is as follows. The state of polarization of the probe signal at λ_D is adjusted to minimum light transmission through the polarizer in the absence of the control pulses (or when probe and control pulses do not overlap inside the DS-HNLF). When a control pulse at λ_C , polarized linearly along the direction defined by a unit vector \vec{e}_x , is sent simultaneously with a probe pulse into the DS-HNLF, the control pulse will induce through XPM a phase change for the probe signal $\varphi_{XPM} = a\gamma P_C L$ (see Section 2.3), where $a = 2$ ($\varphi_{XPM}^{\parallel} = 2\gamma P_C L$) for the polarization component of the probe signal parallel to \vec{e}_x , and $a = \frac{2}{3}$ ($\varphi_{XPM}^{\perp} = \frac{2}{3}\gamma P_C L$) for the polarization component of the probe signal orthogonal to \vec{e}_x .

Thus both components experience a relative phase change:

$$\Delta\varphi_{Kerr} = \varphi_{XPM}^{//} - \varphi_{XPM}^{\perp} = \frac{4}{3}\gamma P_C L \quad (3.6)$$

This relative phase change of both components of the probe signal causes a change of the polarization of the probe signal, which is consequently partly transmitted through the polarization filter.

The state of polarization of the control signal and the delay between both pulses is adjusted to cause maximum light transmission of the probe signal through the polarizer. This is expected to correspond to overlapping control and probe pulses in time in the Kerr gate and to a linear state of polarization of the control signal with an angle of 45° with respect to the state of polarization of the probe signal. The formula described by Eq. 3.6 does not take into account the parametric amplification, which can influence one of the polarization component of the probe pulse more than the other. In the following, the influence of the parametric gain on the transmittance T for a Kerr gate is discussed.

Considering the geometry assumed in Subsection 3.2.1, the amplitude A_P of the probe electrical field E_P is decomposed in the two orthogonal components

$$\vec{A}_P = A_x \vec{e}_x + A_y \vec{e}_y \quad (3.7)$$

where A_x and A_y obey the NLSE given in Eq. 2.14 (p. 16) for the probe signal. Consequently:

$$A_x(L) = A_x(0) \exp(gL + i2\gamma P_C L + i\varphi(L)) \quad (3.8)$$

and

$$A_y(L) = A_y(0) \exp(i\frac{2}{3}\gamma P_C L + i\varphi(L)) \quad (3.9)$$

where the x-component A_x is parallel to the linearly polarized control signal and experiences the XPM induced phase change $2\gamma P_C L$ as well as the FWM induced parametric gain $\exp(gL)$ (see Section 2.4). The y-component A_y experiences the XPM induced phase change $\frac{2}{3}\gamma P_C L$ and no parametric gain. Both components are assumed to have the same linear phase change $\varphi(L)$, as the DS-HNLF is low birefringent. $A_x(0)$ and $A_y(0)$ are the two components at the input of the fiber of length L .

The optical power after the polarization filter at the input of the fiber is:

$$P_{out} = \left| \vec{A}_P(L) \cdot \vec{p}^* \right|^2 \quad (3.10)$$

where \vec{p} represents the polarization vector (according to the Jones Formalism) of the polarization filter, with $|\vec{p}|^2 = 1$ and $\vec{p} = p_x \vec{e}_x + p_y \vec{e}_y$.

According to the principle of operation described in Subsection 3.2.1, and assuming that the DS-HNLF is not birefringent, $\vec{A}_P(0)$ and \vec{p} satisfy $\vec{A}_P(0) \cdot \vec{p} = 0$. For a birefringent fiber, $\vec{A}_P(0) \cdot \vec{p} \neq 0$ in general as the polarization of the \vec{A}_P is expected to vary during propagation.

The equation $\vec{A}_P(0) \cdot \vec{p} = 0$ gives:

$$p_x = \frac{A_y(0)}{\sqrt{P_{in}}} \quad p_y = \frac{-A_x(0)}{\sqrt{P_{in}}} \quad \text{with } P_{in} = |A_x(0)|^2 + |A_y(0)|^2 \quad (3.11)$$

By using these relations, one obtains the following equation for $\vec{A_P}(L) \cdot \vec{p}$:

$$\vec{A_P}(L) \cdot \vec{p} = \frac{1}{\sqrt{P_{in}}} \{A_x(L)A_y(0) - A_y(L)A_x(0)\} \quad (3.12)$$

$$\vec{A_P}(L) \cdot \vec{p} = \frac{A_x(0)A_y(0)}{\sqrt{P_{in}}} \exp \left[+i\frac{2}{3}\gamma P_C L \right] \exp [+i\varphi(L)] \left\{ \exp \left[gL + i\frac{4}{3}\gamma P_C L \right] - 1 \right\} \quad (3.13)$$

The phase shift $\varphi(L)$ accumulated by A_x and A_y when propagating along the fiber of length L , and the nonlinear phase shift $\frac{2}{3}\gamma P_C L$ in Eq. 3.2.1 disappear in the expression of the transmitted power:

$$P_{out} = \left| \vec{A_P}(L) \cdot \vec{p} \right|^2 = \frac{|A_x(0)|^2 |A_y(0)|^2}{P_{in}} |G \exp(i\Delta\varphi_{Kerr}) - 1|^2 \quad (3.14)$$

where the parametric gain G for the intensity after the length L is given by

$$G = \exp(gL) \quad (3.15)$$

and $\Delta\varphi_{Kerr} = \frac{4}{3}\gamma P_C L$. g is defined in Eq. 2.27 (see p. 19).

$$P_{out} = \frac{|A_x(0)|^2 |A_y(0)|^2}{P_{in}} \{G^2 + 1 - 2G \cos(\Delta\varphi_{Kerr})\} \quad (3.16)$$

We write $|A_x(0)|^2 = P_{in} \cos^2 \theta$ and $|A_y(0)|^2 = P_{in} \sin^2 \theta$, where θ is the angle between $\vec{A_P}$ and \vec{e}_x . When using the relations $\cos^2 \theta \sin^2 \theta = \frac{1}{4} \sin^2(2\theta)$ and $\cos(\Delta\varphi_{Kerr}) = 1 - 2 \sin^2(\Delta\varphi_{Kerr}/2)$, the transmittance $T = P_{out}/P_{in}$ is given by

$$T = \frac{\sin^2(2\theta)}{4} \left\{ (G - 1)^2 + 4G \sin^2 \frac{\Delta\varphi_{Kerr}}{2} \right\} \quad (3.17)$$

By setting $G \approx 1$ (which means that very low parametric amplification occurs, as observed experimentally), and as $\theta = \pi/4$ (according with the principle of operation of the Kerr gate), one obtains the following relation linking T , $\Delta\varphi_{Kerr}$ and P_C for the Kerr gate:

$$T = \sin^2 \left(\frac{\Delta\varphi_{Kerr}}{2} \right) \quad (3.18)$$

with

$$\Delta\varphi_{Kerr} = \frac{4}{3}\gamma P_C L \quad (3.19)$$

Case of elliptic polarization states for Probe and Control signals.

In a real case, the polarization states of control and probe pulses will not remain linear in the DS-HNLF included in the Kerr gate, due to stresses and bends of the fiber. The elliptic polarization state of the probe signal is influenced through XPM induced by the control signal, which, in the general case, is also elliptically

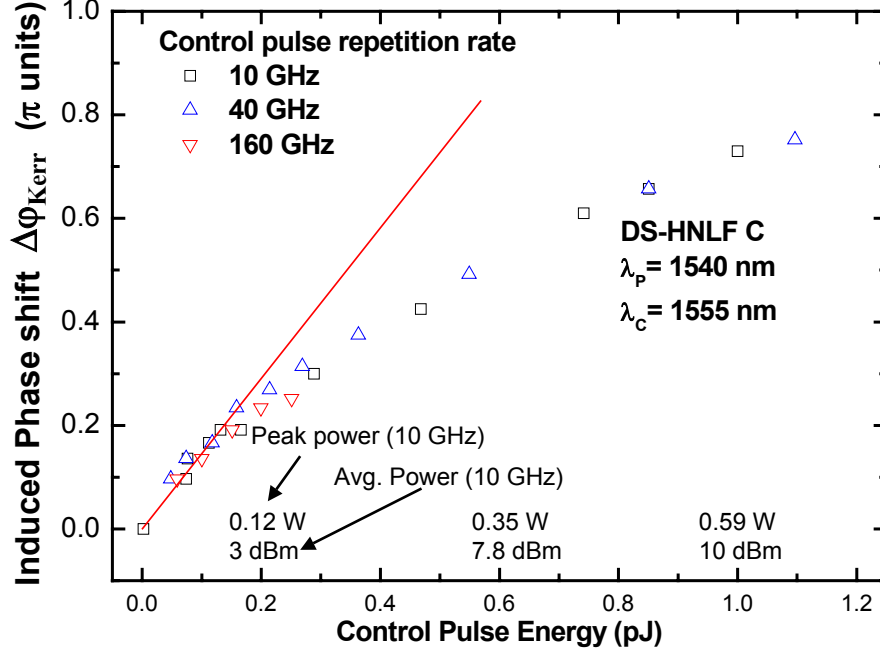


Figure 3.12: Phase Shift Measurement for the Kerr gate. DS-HNLF C was utilized. Control pulse: $\text{FWHM}_C=1.5$ ps, 10 GHz

polarized. In this case, the attenuation of the probe signal in the absence of a control signal should be done by sending the probe signal parallel with one of the two effective main axis of the DS-HNLF, and by aligning the characteristic direction of the polarization filter with the other polarization axis. Then, the polarization of the control signal should be adjusted to maximize XPM, which results in an increase of the probe power at the output of the gate.

The polarization of the control signal may also be conserved if the control signal is linearly polarized at the input of the DS-HNLF and propagates parallel with an effective main axis of the fiber. In this case, the polarization of the probe signal, which shall be polarized with an angle of 45° with respect to the control signal, will rapidly change along the DS-HNLF length. This can be explained by considering that the probe signal will propagate between the two effective main axis of the DS-HNLF.

In both cases, the changes of polarization of control and/or probe signals will cause the characteristic parameters (ER , T_{MAX}) of the gate to be lower than expected in the case of a non-birefringent fiber.

3.2.2 Measurements of induced Phase Shift

The phase shift was measured using the same experimental setup as described in Fig. 3.2, and the results are presented in Fig. 3.12.

Similarly to the case of a NOLM, a given control pulse energy induces the

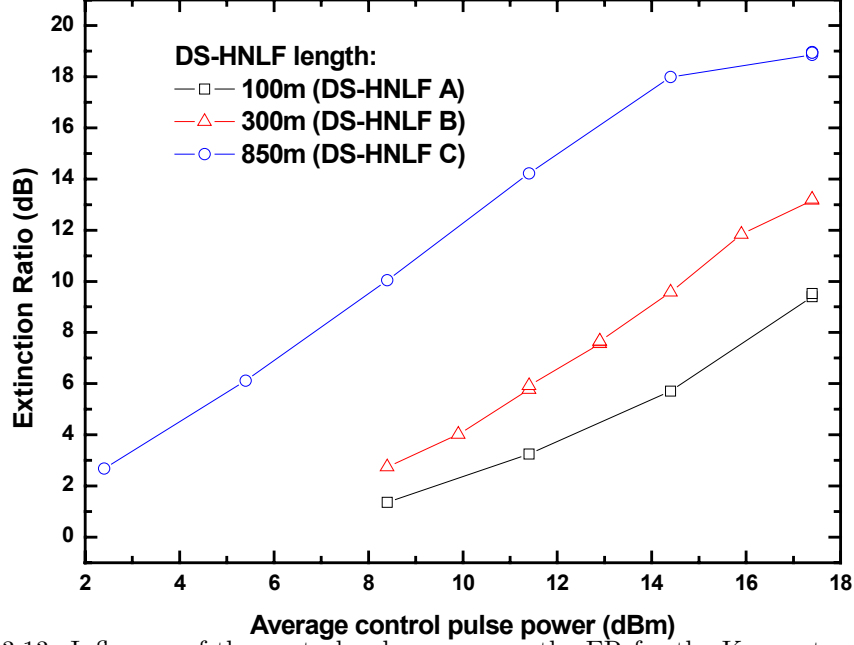


Figure 3.13: Influence of the control pulse power on the ER for the Kerr gate ((40 GHz control pulse, FWHM=1.0 ps).

same value for the phase shift, independently of the repetition rate of the control signal. As suggested by the straight line in Fig. 3.12, a linear dependence of $\Delta\varphi_{Kerr}$ on P_C was observed only for low control pulse power, as expected from Eq. 3.19. As the control power further increases, $\Delta\varphi_{Kerr}$ does not linearly follow P_C . This is attributed to a change in the control pulse shape, leading to a decrease of the peak power. This assumption was verified also when investigating switching windows, as presented for the NOLM in Subsection 3.1.3. Moreover, spectral overlap of the control pulse spectrum with the probe spectrum affects the measurement of the probe power. The relation $T = \sin^2(\Delta\varphi/2)$ is not valid when a significant part of the control power is responsible for a change of the transmittance T .

3.2.3 Measurements of Switching Windows

The switching characteristic of the Kerr gate (comprising a 10 dB coupler, so that the probe and control signal experienced 10 dB and 0.46 dB attenuation, respectively) was investigated using the setup presented in Fig. 3.4, and the DS-HNLF A, B and C were used for these investigations (probe pulses: $\lambda_P=1555$ nm, $FWHM_P=0.8$ ps / control pulses: $\lambda_C=1535$ nm, $FWHM_C=1.0$ ps).

Influence of the control pulse power on the Extinction Ratio

As can be seen in Fig. 3.13, the ER of the switching windows of the Kerr gate showed a linear dependence on the control pulse power. No decrease of

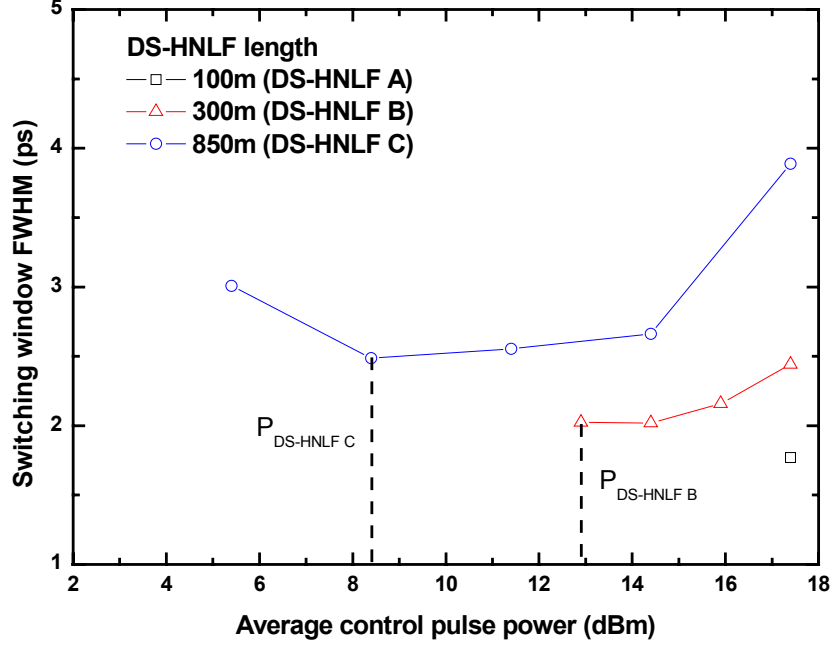


Figure 3.14: Influence of the control pulse power on the FWHM for the Kerr gate (40 GHz control pulse, FWHM=1.0 ps).

the ER could be observed until the maximum available control pulse power (approximately 17 dBm at 40 GHz) was reached. This shows that contrary to what was observed with the NOLM, the optimal efficiency of the Kerr gate was not reached, even when using the longest DS-HNLF (DS-HNLF C), which should provide the greatest phase shift in the interferometric gate. In this case, the increase of the control power, which was required to reach optimum switching efficiency, led to the SPM-induced broadening of the control pulse. For a constant repetition rate, this results in a decrease of the induced phase shift in the interferometer, and to a lower ER for the switching window. With the DS-HNLF C ($L=850$ m), a maximum ER of 18.8 dB was measured for the Kerr gate.

Influence of the control pulse power on the FWHM

Fig. 3.14 shows the evolution of the FWHM of the switching windows as a function of the control pulse power. DS-HNLF A did not allow sufficient switching for the Kerr gate, due to its short length (100 m): even when using the maximum available power, the ER of the resulting switching window was not higher than 8 dB, and the results could not be used for FWHM evaluation (see remark in p. 34). On the contrary, when using the 300 m (respectively 850 m) long fiber, an optimum control pulse power of approx. 12.9 dBm (resp. 8.4 dBm) could be measured, enabling the shortest available switching windows for each of the DS-HNLF. The differences in the absolute FWHM measured can be explained by the different dispersive properties of the three DS-HNLF, leading

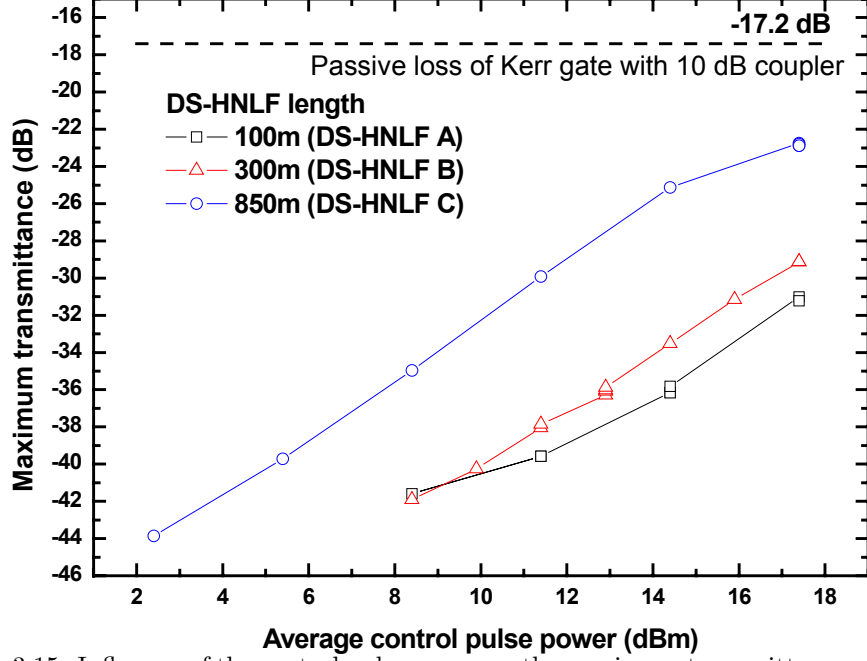


Figure 3.15: Influence of the control pulse power on the maximum transmittance T_{MAX} for the Kerr gate (40 GHz control pulse, FWHM=1.0 ps).

to different control pulse broadening in the nonlinear medium. On Fig. 3.14, an optimum value of $P_{DS-HNLF C} = 8.4$ dBm was measured for the Kerr gate comprising DS-HNLF C. This value of P_C led to the shortest available switching window, with an ER=10.0 dB. When using DS-HNLF B in the gate, the optimum value for P_B was $P_{DS-HNLF B} = 14.4$ dBm, which led to the shortest available switching window (FWHM=2.0 ps) with ER=9.6 dB. Comparable switching windows were measured, corresponding to comparable values for $\Delta\varphi_{Kerr}$. The linear relation giving the phase shift $\Delta\varphi_{Kerr} = (4/3)\gamma P_C L$ is the physical quantity determining the switching window properties. In the present case, and when considering a given value for $\Delta\varphi_{Kerr}$, the increase of the length by a factor 2.8 ($L_{DS-HNLF C}/L_{DS-HNLF B}$) is expected to correspond to a decrease of the required control power by 4.5 dB. The difference measured was $P_{DS-HNLF B} - P_{DS-HNLF C} = 5.5$ dB.

Influence of the control pulse power on T_{MAX}

Fig. 3.15 shows the evolution of the maximum transmittance T_{MAX} of the gate as a function of the control power. The passive losses for the Kerr gate were 17.2 dB (including the losses of the band pass filter). This high value for the passive losses is partly due to the 10 dB coupler that was used to couple probe and control pulses into the HNLF, causing a 7 dB higher passive loss than in the case of a 3 dB coupler. This drawback still was balanced by the advantage of sending a higher control power to the gate, which enhanced the switching efficiency (higher $\Delta\varphi$). As expected, the longest DS-HNLF enabled the highest

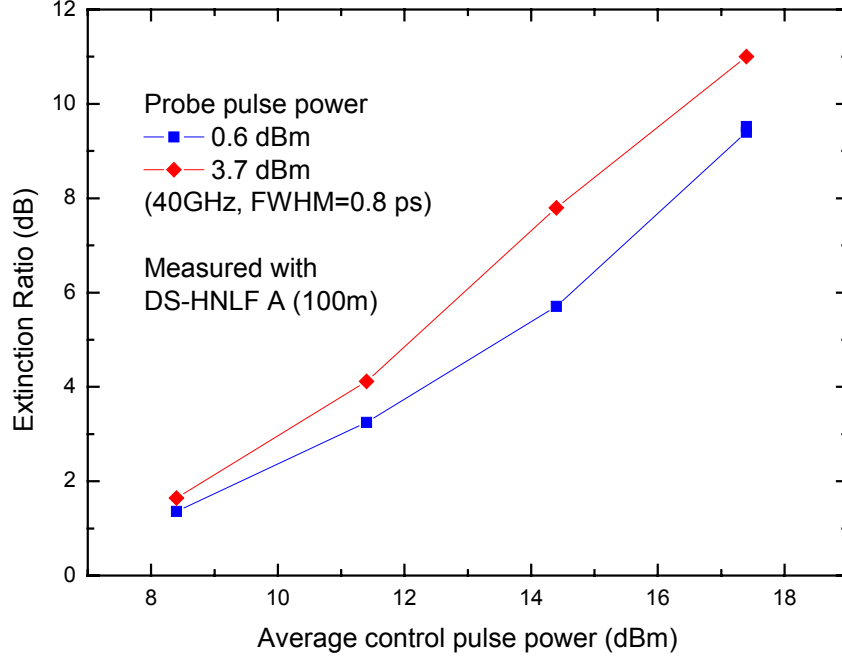


Figure 3.16: Influence of the probe pulse power on the ER for the Kerr gate (40 GHz control pulse, FWHM=1.0 ps).

transmittance for the switching windows. When gating the Kerr gate with a control power of 14.4 dBm (evaluated at the input of DS-HNLF), the maximum transmittance when using the 100 m, 300 m, respectively the 850 m long DS-HNLF were -35.8 dB, -33.5 dB, -25.1 dB.

Influence of the probe pulse power

The probe power was increased by 3 dB, and switching windows were measured again. The results are shown in Fig. 3.16. The probe power increase resulted in an improvement of the ER by approx. 2 dB. This confirms that the ER of the gates (NOLM and Kerr gate) is limited by the ASE. This can be explained by considering that the extinction of the probe signal that can be reached using a standard polarization filter is better than 40 dB. This high extinction is also made possible by the high degree of polarization (DOP) of the probe pulses. After having been emitted by lasers, optical pulses went through a number of EDFA which rarely exceeded 5 units, and the DOP remained high. If the DOP of the probe signal had been severely affected, a high extinction of the probe signal after the polarization filter would not have been possible. The OSNR of the probe signal before the gate was also in the order of 40 dB. When the polarization of the probe signal was set such that the signal was canceled in absence of a control pulse, the measured transmitted power was mainly ASE power, which consequently limits the ER. A higher probe power sent to the gate allows to overcome this limitation.

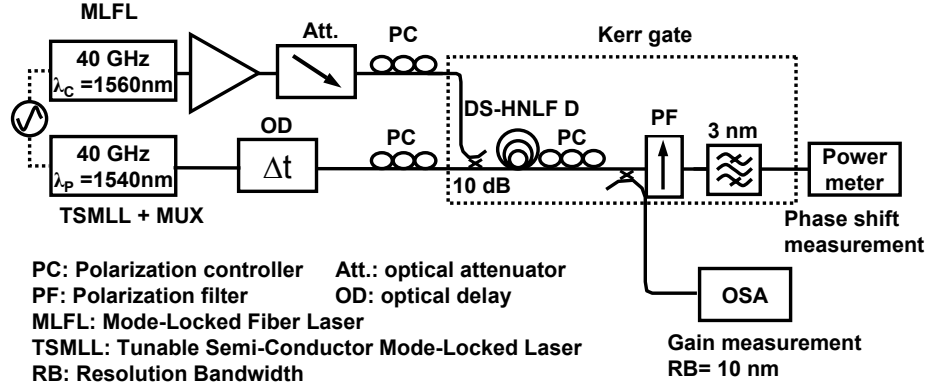


Figure 3.17: Setup for Gain and Phase Shift Measurements.

3.2.4 Experimental Setup for Parametric Amplification measurement

Fig. 3.17 shows the experimental setup used for simultaneous phase shift and gain measurements in a Kerr gate. The 40 GHz probe signal ($\lambda_P = 1540$ nm, $\text{FWHM}_P = 2.0$ ps) was provided by a 10 GHz tunable semiconductor mode-locked laser (TSMLL), of which the pulse train was multiplexed to 40 GHz by a phase-stable multiplier. The 40 GHz control signal ($\lambda_C = 1560$ nm, $\text{FWHM}_C = 1.6$ ps at the input to the DS-HNLF) was provided by a mode-locked fiber laser (MLFL). An optical delay line was used to adjust the relative delay of control and probe pulses in the switch. The control pulses were fed via the high-power arm of a 10 dB-coupler into DS-HNLF D ($L = 46$ m, $\gamma = 21$ W⁻¹ km⁻¹, $\lambda_0 = 1560.9$ nm, see Table 2.2 p. 14). The state of polarization of both signals could be adjusted appropriately by polarization controllers (PC). Behind the fiber was a polarization filter (PF) and an optical filter (the practical realization of the filter consisted of two cascaded optical bandpass filters) blocking the light of the control pulses. A powermeter and an optical spectrum analyzer were used for the measurements.

As stated in Eq. 3.17, the transmittance T is influenced by the parametric amplification occurring in the DS-HNLF because of parametric processes, so that the gain due to parametric amplification has to be taken into account (neglecting other nonlinear interactions) when evaluating $\Delta\varphi$. The gain due to parametric amplification was measured using an optical spectrum analyser (OSA, see Fig. 3.17) with a resolution bandwidth (RB) of 10 nm. Spectra were taken before the PF for different control pulse powers in a state where probe and

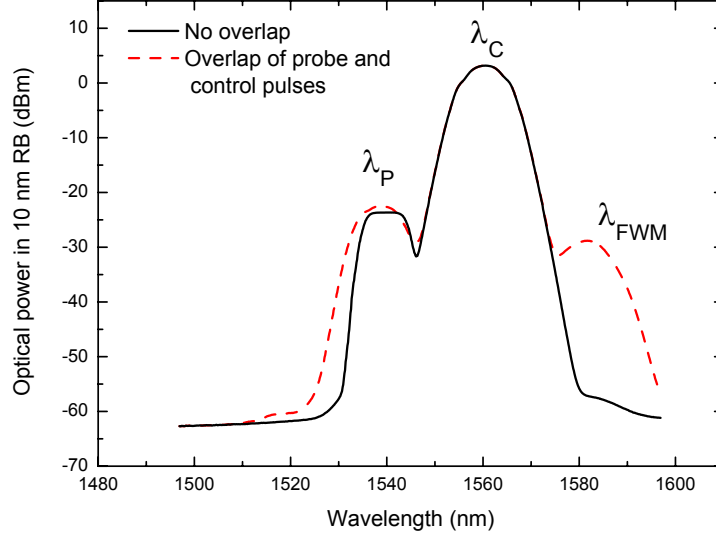


Figure 3.18: Spectra of control and probe signals, measured behind the DS-HNLF D, with overlapping pulses trains (dashed line) and with no overlapping (solid line).

control pulses overlap in the DS-HNLF, and in a state where they do not overlap. An example for such spectra is shown in Fig. 3.18. The generated FWM-product can be clearly observed, in accordance with the principle of FWM presented in Fig. 2.4. No depletion of the control wave was observed.

The gain is then defined as the power ratio between both measured spectra at the probe wavelength. Fig. 3.19 shows the phase shift and the gain measured versus the control power. Due to the low value obtained for the parametric amplification in this measurement, the measured gain values (a maximum gain of 1.3 dB was measured, see Fig. 3.19) were not taken into account for the evaluation of the phase shift. The states of polarization of the probe and the control signal were not changed between the phase shift measurements and the measurements of the parametric gain. Thus, the relative angle between the probe and control polarization states could be assumed to be 45° , maximizing the switching performance of the Kerr gate at cost of the parametric amplification. A saturation of the phase shift was observed at high control power. However, at a high control power, we measured also a broadening of the spectrum of the control pulses due to Self Phase Modulation in the DS-HNLF (see inset in Fig. 3.19, showing the output spectrum of the DS-HNLF for high control powers) and pulse distortions in the time domain. This might lead to a decreasing efficiency of the switching process for high powers of the control pulses.

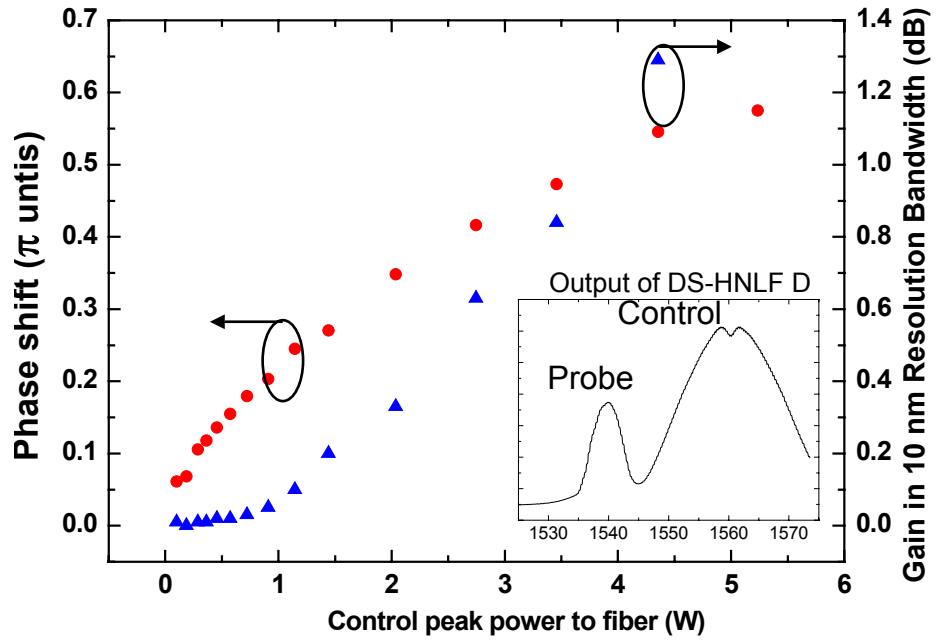


Figure 3.19: XPM-induced Phase Shift and FWM-induced Parametric Amplification measured in a Kerr gate, for DS-HNLF D. Inset: spectrum of probe and control pulses at the output of the DS-HNLF D. Control pulse: $\lambda_C=1560$ nm, $\text{FWHM}_C=1.6$ ps.

3.3 Bit Error Rate Characterization

The Kerr gate (built with a 10 dB coupler before the DS-HNLF, so that the control signal went through the low attenuation arm of the coupler, thus maximizing the available control power at the input of the DS-HNLF) and the NOLM were tested as demultiplexers for a single-wavelength, single polarization 320 Gbit/s data signal. The modulation format was Differential Phase-Shift Keying (DPSK, [30, 31]) at 40 Gbit/s, which had no influence on the performances of the gates. The modulation format of the 320 Gbit/s data signal was not DPSK, as the phase relation between adjacent pulses is randomized in the fiber-based multiplexer. Still, proper DPSK modulation format was recovered after the demultiplexer, as a single 40 Gbit/s channel was extracted. The quality of operation was evaluated using bit-error rate (BER) measurements [32], [33]. As presented in Section 3.1 and Section 3.2, each gate is expected to show a switching window with different properties (ER , $FWHM$, T_{MAX}), which influence on the BER is discussed in the following.

3.3.1 Experimental Setup

Fig. 3.20 shows the experimental setup used for a demultiplexing experiment where both the Kerr gate and the NOLM were tested.

The 40 Gbit/s DPSK transmitter comprised a 40 GHz optical pulse source (40 GHz mode-locked fiber laser MLFL), a pulse compression stage and a phase modulator driven by a pattern generator to provide a 40 Gbit/s DPSK data signal. The optical source provided 1.9 ps (FWHM) pulses at 1540 nm. The pulses were compressed to 900 fs (FWHM_P) in DS-HNLF F (see Table.2.2, p. 14). After DPSK modulation, the data signal was fed into a fibre delay line multiplexer (MUX) providing a multiplexed single-polarization 160 Gbit/s or 320 Gbit/s RZ-DPSK data signal. Due to the insufficient phase stability of the MLFL used in the transmitter, the comparison of the NOLM and of the Kerr gate on the basis of BER-measurement was limited to 320 Gbit/s.

For both demultiplexers, the 40 GHz control signal ($\lambda_C=1561$ nm, $FWHM_C=1.5$ ps at the input to the DS-HNLF) was provided by a second MLFL with low jitter. The fiber included in the demultiplexers used in this Section was DS-HNLF D (Table. 2.2, p. 14). This fiber was chosen due to its zero-dispersion wavelength $\lambda_0=1560.9$ nm close to λ_C , which ensured low control pulse broadening. Due to the short length of the DS-HNLF ($L=46$ m), high control power was needed to gate the demultiplexers, and dispersive effects were expected to remain low. Two cascaded optical bandpass filters (5 nm and 3 nm) were used to filter the control pulses in the gates.

The 40 Gbit/s DPSK receiver comprised an optical pre-amplifier, an optical filter (2.6 nm), a DPSK-demodulator and a balanced photoreceiver. The BER was measured by a 40 Gbit/s BER-tester (BERT), and was investigated as function of the 40 Gbit/s receiver input power. An optical attenuator was included before the receiver.

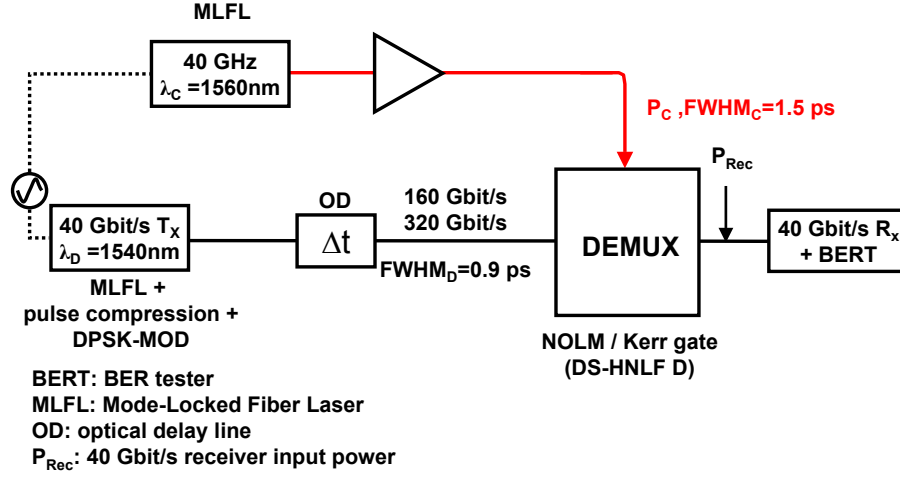


Figure 3.20: Experimental setup used for BER-characterization of the Kerr gate and of the NOLM.

3.3.2 Results

The BER measured for the NOLM when demultiplexing 160 Gbit/s and 320 Gbit/s is depicted in Fig. 3.21 a). Penalties of 1.1 dB and 2.0 dB were observed for the demultiplexing of 160 Gbit/s and 320 Gbit/s, respectively. The switching window was measured (Fig 3.21 b)) and showed a high T_{MAX} (-8.1 dB), and a high ER (23.8 dB). The passive loss of the gate was lower than in Section 3.1, as a different filter was used to filter the control pulses, and due to reduced insertion loss in the NOLM. The maximum control power available was used to gate the demultiplexers, and the switching windows presented in this section correspond to an operation point of the gates optimized after BER.

Fig. 3.22 shows the results for the Kerr gate. The penalties for the demultiplexing of 160 Gbit/s and 320 Gbit/s were 0.9 dB and 1.4 dB respectively. The minor difference in the sensitivities for the measurements of the 40 Gbit/s back-to-back measurements in Fig. 3.21 a) and Fig. 3.22 b) was due to non-perfect adjustment of the DPSK-demodulator. The parameters of the switching window were $ER=24.4$ dB, a $FWHM=1.6$ ps, and $T_{MAX}=-18.7$ dB. In Section 3.1 and Section 3.2, the control pulse was propagating in the anomalous dispersion regime of the DS-HNLF, which caused the pulse to broaden in time domain. In the present experiment, the control pulse propagated in the wavelength domain near λ_0 , and the DS-HNLF was very short. Consequently, the control pulse did not broaden, and enabled a short switching window ($FWHM=1.6$ ps).

The penalties measured in both cases (demux with NOLM and Kerr gate) are very similar, and so were the switching windows. As expected (10 dB coupler

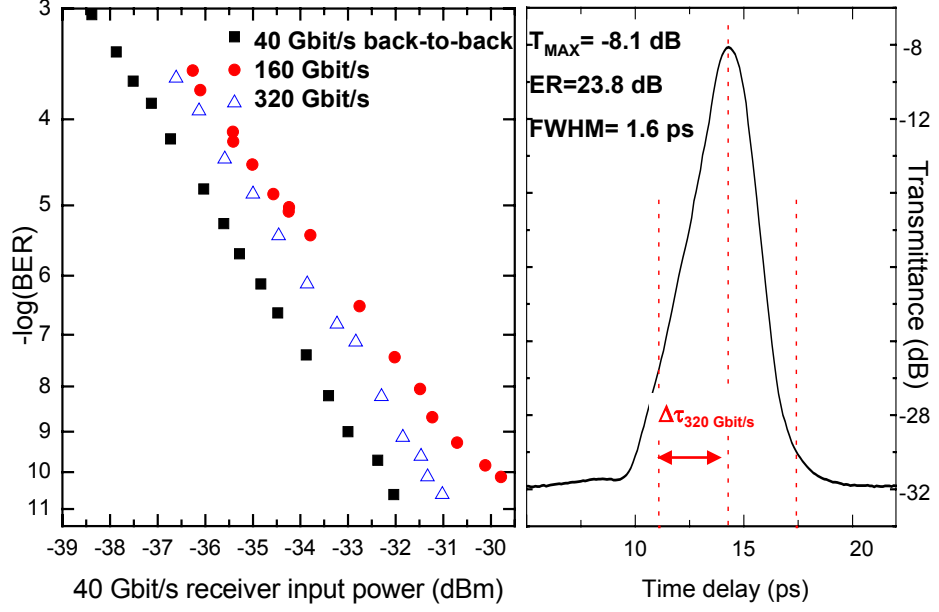


Figure 3.21: a) BER measurements for 160 Gbit/s and 320 Gbit/s demultiplexing to 40 Gbit/s using the NOLM and DS-HNLF D and b) switching window measured ($\Delta\tau$: time slot for 320 Gbit/s).

before the DS-HNLF), the Kerr gate showed higher attenuation due to the 10 dB coupler included before DS-HNLF D. This difference in the T_{MAX} for both gates had no influence on the BER measured, as the data signal power after demultiplexing lied beyond the receiver sensitivity. On the switching windows depicted in Fig. 3.22 b) and Fig. 3.21 b), the positions of the neighbour channels (dotted lines left and right from the maximum of the switching windows) were also plotted. The neighbouring TDM channels were attenuated by more than 18 dB. Table 3.1 presents the ER, FWHM, and T_{MAX} measured for the Kerr gate and the NOLM, as well as the penalties measured when demultiplexing 320 Gbit/s.

	ER (dB)	FWHM (ps)	T_{MAX}	Penalty 160 Gbit/s/320 Gbit/s
NOLM	23.8	1.6	-8.1	1.1 dB / 2 dB
Kerr gate	24.4	1.6	-18.7	0.9 dB / 1.4 dB

Table 3.1: Results for 160 Gbit/s and 320 Gbit/s demultiplexing to 40 Gbit/s with NOLM and Kerr gate.

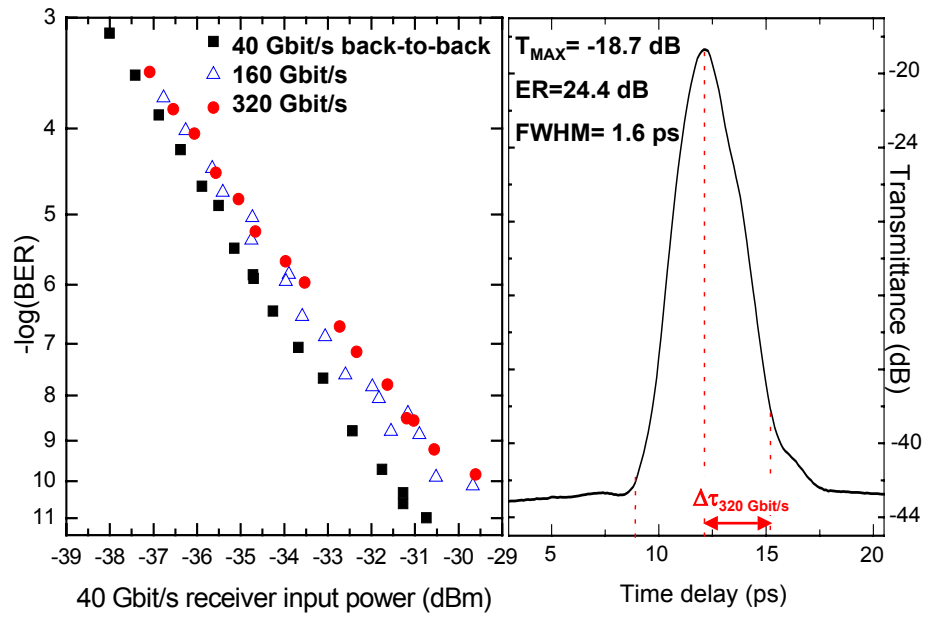


Figure 3.22: a) BER measurements for 160 Gbit/s and 320 Gbit/s demultiplexing to 40 Gbit/s using the Kerr gate and DS-HNLF D and b) switching window measured.

3.4 Requirements for a demultiplexer up to 640 Gbit/s

Pulse sources

The transmittance of a fiber-based optical gate is controlled by a second optical signal (control signal), and the synchronization between the data and control signals should be as stable as possible. According to [34], the timing jitter should not exceed $1/14.1$ of the bit slot $\Delta\tau$ for the considered data rate when the switching window width is approximately $\Delta\tau$. For the symbol rate 640 Gb/s, $\Delta\tau=1.5625$ ps, and the switching windows presented in the present chapter had a FWHM *approx* 1.8 ps. This suggests that the timing jitter of data and control signals should not exceed 110 fs. Higher jitter values will cause an error-floor to occur.

All pulse sources used in this work had jitter values under 150 fs, with the exception of the semiconductor lasers used in Subsections 3.1.2 and 3.2.2. However, these sources were not used for demultiplexing.

Switching window parameters

For an optical gate able to demultiplex a data signal at a bit-rate up to 640 Gbit/s, a short switching window is required, as well as a high extinction ratio. These conditions ensure that a 10 Gbit/s (resp. 40 Gbit/s, depending of the base data rate for the system considered) channel can be properly extracted out of the 64 (resp. 16) multiplexed channels that build a 640 Gbit/s TDM signal. The condition on the FWHM of the switching window is justified in the following. The typical switching window of the NOLM or of the Kerr gate (see Fig. 3.21 a and Fig. 3.22 b) can be approximated by using the characteristic $T=\sin^2(\Delta\varphi/2)$, where $\Delta\varphi$ linearly depends on the intensity profile P_C of a control pulse ($\Delta\varphi = 2\gamma L P_C(t)$, for a fiber of length L and of nonlinear parameter γ). Dispersive effects (control pulse broadening, walk-off) and the attenuation of the DS-HNLF were neglected. A sech pulse was considered for the control pulse, and the FWHM of the switching window could be influenced by varying the FWHM of the control pulse.

Using this simple model, normalized switching windows were calculated for FWHMs varying between 1.2 ps and 3.0 ps. A probe pulse train was also simulated (sech-shape, $\text{FWHM}_P=0.6$ ps), consisting of three pulses. The central pulse is the pulse to be demultiplexed, and two neighbouring pulses account for the influence of cross-talk. The optical power was evaluated at the output of the gate as the product of the switching window with the probe signal, as shown in Fig. 3.23.

As normalized signals were used, the values obtained should not be considered as absolute, but a comparison is allowed. The following ratios were investigated:

- P_{Probe} : the probe signal consisted of a single probe pulse, which enters the switching window at its maximum. In this configuration, the probe pulse is the pulse that would have to be transmitted in a demultiplexing experiment, thus P_{Probe} can be considered as the "useful" power.
- P_{Total} : the probe signal consisted of three probe pulses, separated by a time delay of 3.125 ps (which corresponds to a repetition rate of 320 GHz),

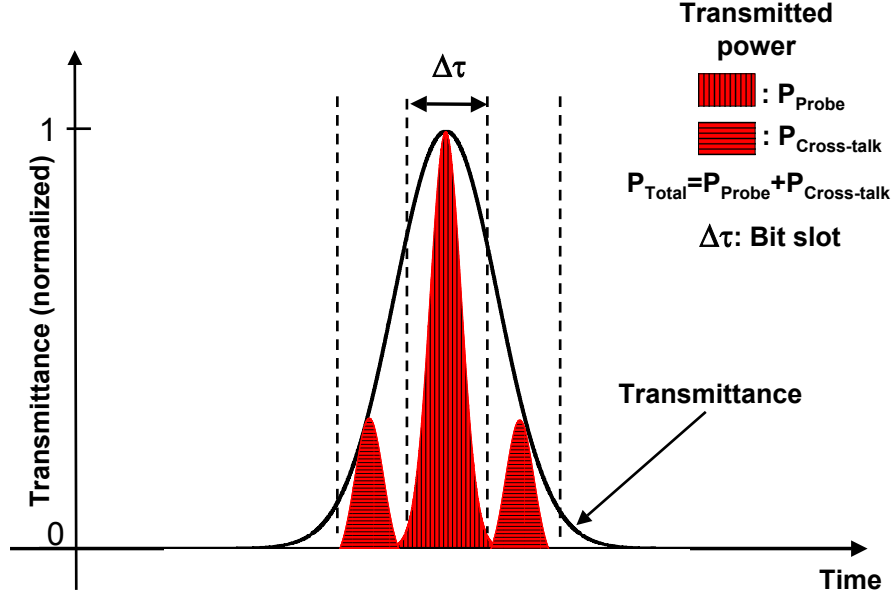


Figure 3.23: Evaluation of the influence of cross-talk (simulated): a data pulse is demultiplexed by the gate, and two pulses in the neighbouring bit slots are partly transmitted.

and centered on the maximum of the switching windows. In this configuration, the middle pulse is supposed to be demultiplexed by the gate, while the two neighbouring pulses (at the left and at the right of the middle pulse) shall be attenuated by the demux. P_{Total} is the power measured after the demux by an optical receiver.

- $P_{cross-talk}$: the probe signal consisted of the two neighbouring pulses only. $P_{cross-talk}$ is an evaluation of the power unintentionally transmitted by the gate, and clearly depends on the width of its switching window.

The fraction of $P_{cross-talk}$ in P_{Total} was evaluated, and the result can be seen in Fig. 3.24 a. For a switching window FWHM of 1.2 ps, the power transmitted by the demux consisted almost exclusively of the middle pulse, as attested by the low value of $P_{cross-talk} / P_{Total}$. The value of the ratio $P_{cross-talk} / P_{Total}$ remains below 1% until the FWHM of the switching window reaches 1.8 ps. The same ratio however strongly raises for switching windows with FWHM > 2.0 ps.

The ratio $P_{cross-talk} / P_{Total}$ clearly influences the results of the demultiplexing operation. The Bit-Error Rate is usually measured as a function of the power coming to the receiver after the demux. By attenuating the signal power right before the receiver, the Optical Signal-to-Noise Ratio (OSNR) is varied. The best case for the BER corresponds to a signal consisting of a high data power and of a low level noise. Due to the non-rectangular shape of its switching window, the fiber-based gate will cause additional noise to be added to the signal.

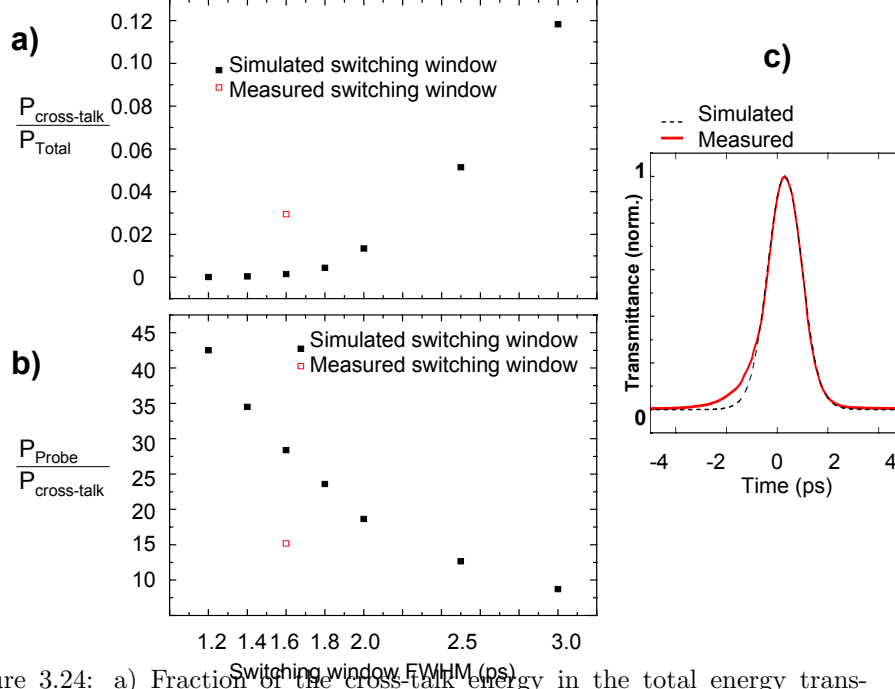


Figure 3.24: a) Fraction of the cross-talk energy in the total energy transmitted after the demux (demultiplexing of 320 Gbit/s to 40 Gbit/s), b) Ratio $P_{\text{Probe}}/P_{\text{cross-talk}}$ and c) measured (solid line) and simulated (dashed line) switching windows.

The ratio $P_{\text{Probe}}/P_{\text{cross-talk}}$ is a parameter describing how strong the OSNR of the signal coming to the demux will be affected by the non-perfect extinction of the neighbouring TDM channels. The evolution of $P_{\text{Probe}}/P_{\text{cross-talk}}$ over the FWHM of the switching window can be seen in Fig. 3.24 b. However, due to its different distribution, the influence of the power resulting of the partly transmitted two neighbouring pulses is not directly comparable with ASE-noise, usually considered when evaluating the OSNR, and evaluating the OSNR-degradation induced by cross-talk is difficult.

These results could be obtained by using a simple model for the switching window. Still, for low values of P_C , the experimentally measured switching window shows a slight difference, which however proved to influence significantly the amount of noise added to the signal. The red dot in Fig. 3.24 a and Fig. 3.24 b account for the values of $P_{\text{Probe}}/P_{\text{cross-talk}}$ and $P_{\text{cross-talk}}/P_{\text{Total}}$ in the case where a measured switching window was considered to evaluate P_{Probe} , $P_{\text{cross-talk}}$, and P_{Total} (see Fig. 3.24 c)).

Consequently, a gate aiming to demultiplex data rates over 320 Gbit/s should be characterized by a switching window with FWHM < 1.8 ps.

In another attempt to specify the optimum switching window FWHM, the OTDM receiver is compared with an ETDM receiver [35, 36], and an equivalent electrical receiver is proposed for the OTDM receiver. A switching window

with a ER higher than > 18 dB and a FWHM narrower than half of the bit slot appear to be optimal, which confirms the value proposed in the present Section (FWHM < 1.8 ps when demultiplexing 320 Gbit/s).

3.5 Comparison

Both gates investigated in this work fulfill the requirements for an all-optical demultiplexer aiming to process data bit-rates up to 640 Gbit/s. Still, differences in performances and ways of operating should be discerned between the NOLM and the Kerr gate.

Walk-off

Throughout this work, the condition $(\lambda_D + \lambda_C)/2 = \lambda_0$, which ensures that no walk-off occurs during propagation of data and control pulses, could not be met, at the wavelengths of the available pulse sources could not be detuned. Moreover, other constraints imposed by the experimental context make such a condition difficult to satisfy. In a transmission experiment, λ_D will be chosen so that the dispersion of the fiber spans is optimally compensated. The choice of λ_D and λ_C may also be influenced by the bandwidth of available optical amplifiers.

Walk-off affects both gates in the same manner, as suggested by the expression given for $\Delta\tau$ in Eq. 2.30, and should limit the phase shift that can be reached in the gates, as walk-off reduces the interaction length of control and data pulses. Reducing the walk-off implies the data and control wavelength to be set symmetrically around λ_0 . Consequently, $D \neq 0$ at the control wavelength, and the control pulse will experience dispersive effects (eventually combined with nonlinear effects, as suggested by L_D and L_{NL} in Table 2.3. High bit-rates require the control pulse to have a short FWHM, and the pulse shape should not change inside the DS-HNLF. For this reason, a short DS-HNLF ($L < 500$ m) should be preferred to reduce both the influences of walk-off and dispersive effects.

In the case of DS-HNLF B and DS-HNLF C, the walk-off parameter was in the same order of magnitude, due to the relative position of control and data wavelength compared with λ_0 (the *middle* wavelength - see Section 2.5 - was approx. 1544 nm for this experiment, and is to be compared with the λ_0 of DS-HNLF A and DS-HNLF B, which are 1556.0 nm and 1550.3 nm, respectively). As DS-HNLF B is almost three times longer than DS-HNLF A, a three times higher walk-off value is expected. Still the advantage of using DS-HNLF B was shown. Walk-off did not prove to be a limiting parameter for the NOLM or the Kerr gate. The control pulse power, and the pulse changes (in the time and spectral domains), due to second order dispersion and nonlinear effects, are parameters of greater importance.

Phase shift measurement in a NOLM and in a Kerr gate

Fig. 3.25 shows the phase shift measurements for the NOLM and for the Kerr gate, carried out with the parameters recapitulated in the following Table:

	Repetition rate (GHz)	Wavelength (nm)	FWHM (ps)
Data pulses	10	1540	1.6
Control pulses	10,40,160	1555	1.5

Table 3.2: Parameters used for phase shift measurements.

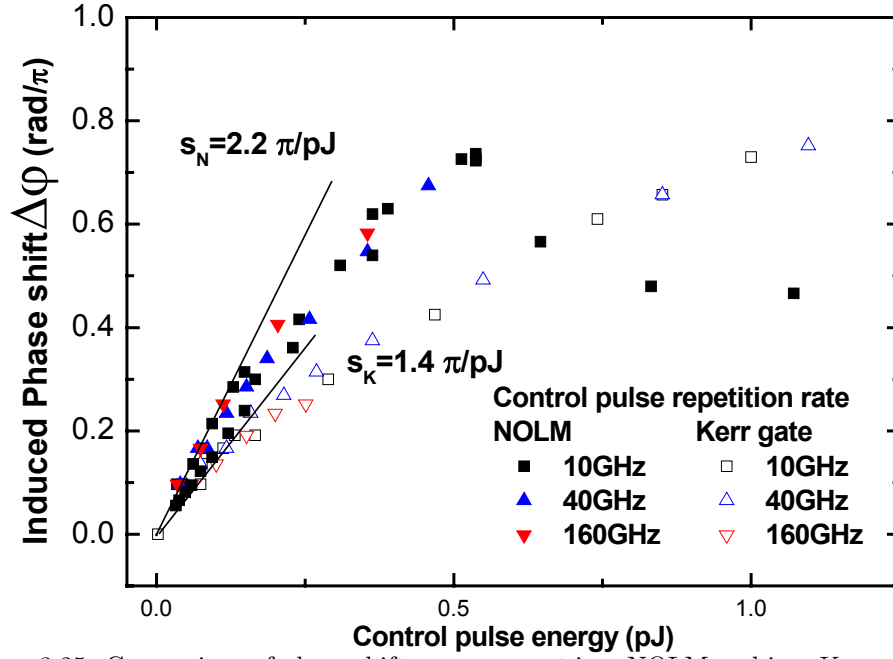


Figure 3.25: Comparison of phase shift measurement in a NOLM and in a Kerr gate. Control pulse: $\text{FWHM}_C = 1.5$ ps, 10 GHz. Fiber DS-HNLF C was used.

Clearly, the phase shift reached in the NOLM for a given control pulse power is higher than in the Kerr gate, and a factor 1.5 is expected between the slope of both curves, as suggested by Eq. 3.5 and Eq. 3.19. The slopes S_N and S_K of the characteristic $\Delta\phi = f(\text{Control pulse energy})$ at low control pulse energy were evaluated considering the experimental results for the NOLM and the Kerr gate, respectively, and are reported in Fig. 3.25. The ratio of these coefficient was $S_N/S_K \approx 1.57$, showing a good agreement with theoretical results. Though the same maximal phase shift was reached in both gates, the NOLM works thus more efficiently than the Kerr gate, which is a crucial advantage when the available control power is limited, and/or when high control power would lead to control pulse broadening.

Measurements of switching windows

Concerning the switching window characterizing both gates, a minimum FWHM value of 1.7 ps could be reached for each of the three investigated fibers, by adjusting the control power. Shorter widths can be reached for the switching

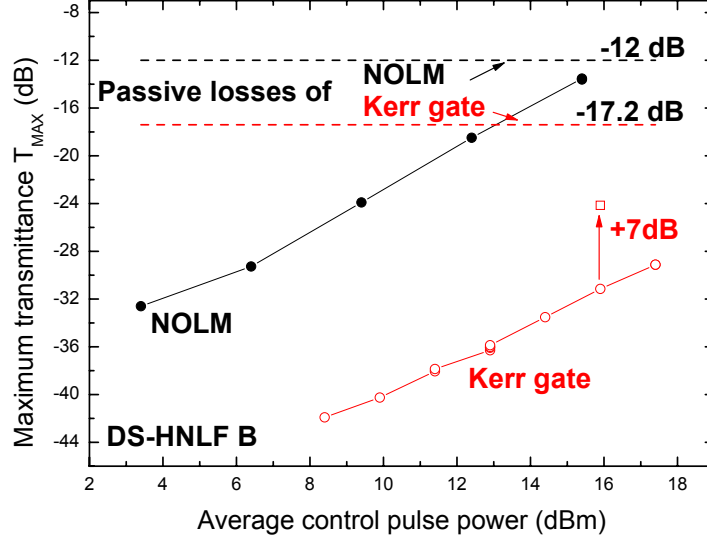


Figure 3.26: Maximum transmittance T_{MAX} measured for the NOLM and the Kerr gate with DS-HNLF B. Using a 3 dB coupler (instead of 10 dB) in the Kerr gate would result in an increase of T_{MAX} by 7 dB.

window, by using a shorter control pulse. Moreover, as in both gates the passive losses are in the same order of magnitude (comprising the loss of a 3 dB coupler, of the DS-HNLF and of fiber splices), an increased switching efficiency contributes to the reduction of the switching losses. In an experimental setup, where the gate would be followed by an EDFA or a detector (Receiver), the NOLM would guarantee a lower decrease of the OSNR than the Kerr gate. The maximum transmittance T_{MAX} measured for the NOLM and the Kerr gate where DS-HNLF B was utilized is shown in Fig. 3.26. On the same figure, the value of T_{MAX} interpolated for the case where a 3 dB coupler had been incorporated in the Kerr gate (instead of a 10 dB coupler) was plotted. The latter case corresponds to a decrease of the passive losses of the gate by 7 dB (and thus to an increase of the transmittance by the same amount). Even in this case, the NOLM took advantage of its inherent better switching efficiency and showed larger values for T_{MAX} . However, this solution was not preferred, as the switching performance of the Kerr gate would have severely suffered from the loss of control power.

The following tables 3.3 and 3.4 recapitulate the results obtained for the NOLM and for the Kerr gate, respectively:

NOLM	DS-HNLF A	DS-HNLF B	DS-HNLF C
Shortest FWHM (ps)	1.7	1.7	1.8
Highest ER (dB)	13.9	18.7	19.6
Highest T_{MAX} (dB)	-20.4	-13.5	-15.7

Table 3.3: Best parameters measured for the switching windows of the NOLM.

Kerr gate	DS-HNLF A	DS-HNLF B	DS-HNLF C
Shortest FWHM (ps)	1.8	2.0	2.5
Highest ER (dB)	9.4	13.2	18.9
Highest T_{MAX} (dB)	-31 (-24)	-29.1 (-22.1)	-22.7 (-15.7)

Table 3.4: Best parameters measured for the switching windows of the Kerr gate (10 dB coupler). The values of T_{MAX} that could be reached in the case of a 3 dB coupler are indicated in ().

Parametric amplification

The parametric amplification was investigated for the Kerr gate, and only a low parametric gain was measured (< 1.3 dB). Though parametric gain can reach high values when the wavelength allocation and the polarization states of data and control signals are properly adjusted (see Subsection 2.4), the influence of parametric amplification in the operating principle of the NOLM and of the Kerr gate could be neglected in the following chapter, where applications for the NOLM and the Kerr gate are presented. For the gates used in this work, the control and data polarization states were adjusted to enable maximum ER and high T_{MAX} , and the condition $\Delta k = -2\gamma P_C$, allowing maximum parametric gain, was not preferentially met.

Chapter 4

Applications in High Speed OTDM-Systems

The NOLM gate including DS-HNLF B was utilized as demultiplexer of a 640 Gbaud signal, as will be stated in Section 4.1. Section 4.2 presents an Add-Drop Multiplexing (ADM) experiment at 160 Gbit/s, with transmission of the high-bit rate signal after the ADM process. The Add-Drop Multiplexer, which was based on a Kerr gate, could be used for data rates up to 320 Gbit/s. Though the performance of a Kerr gate for Add-Drop Multiplexing was not investigated in this work, feasibility was demonstrated at high bit rates.

4.1 Demultiplexing 640 Gbaud

In the experiment considered in this section, the symbol rate (number of optical pulses / time unit) was different from the associated data rate (still measured in *bit/s*), as a special modulation format was used. In a Differential Quadrature Phase Shift Keying (DQPSK) modulated signal, each symbol carries 1 out of 4 logical states instead of 1 out of 2 states in a system with OOK or DPSK modulation format. This results in a higher spectral efficiency, as stated in [37, 38]. In the following, the symbol rate and the data rate are mentioned in the unit *baud* and *bit/s*, respectively. Using the DQPSK modulation format offers the possibility of easily doubling the data rate without changing the symbol rate, or to reduce the symbol rate for a given data rate. However, the system sensitivity when switching to DQPSK typically worsen by 2-3 dB (for a data rate increased by a factor 2) [39].

The requirements on the switching windows for the demultiplexing of a 640 Gbaud single-polarization (SP) data signal include a short FWHM (below 1.7 ps), a high ER (typical values are near 18 dB for a 40 GHz control signal) and a low insertion loss, so that the power of the demultiplexed data signal remains above the receiver sensitivity. Moreover, the optical gate chosen should be driveable by the control power offered by a standard EDFA (offering up to 20 dBm output power) or a high-power EDFA (30 dBm maximum output power).

In the present experiment, we report on the demultiplexing of 1.28 Tbit/s and 2.56 Tbit/s data signals where the DQPSK modulation format and polar-

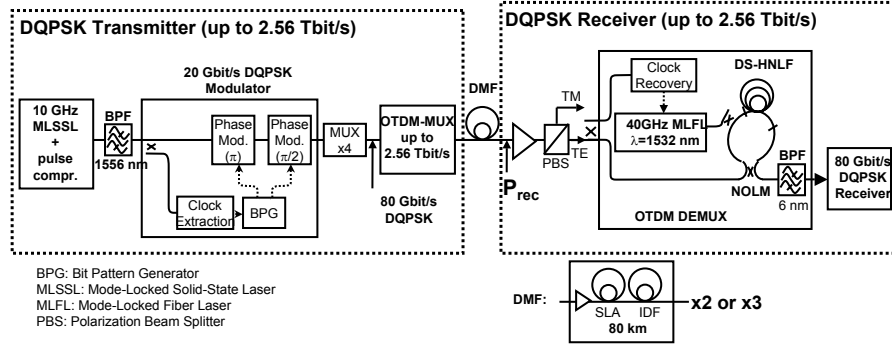


Figure 4.1: Experimental setup for DQPSK high bitrate experiment

ization multiplexing were used. The high bit rate signal was transmitted over one fiber span. The transmission influenced the FWHM of data pulses arriving to the demultiplexer, and will thus be briefly presented throughout the present Section.

The increase of the transmission speed up to 2.56 Tbit/s was a new record for single wavelength channel transmission, and a prerequisite was the proper operation of the demultiplexer for 640 Gbaud.

4.1.1 Experimental Setup

Fig. 4.1 shows the experimental setup comprising the DQPSK transmitter and receiver as well as the transmission link. In the transmitter, a 10 GHz mode-locked solid state laser (MLSSL, $\lambda=1550$ nm, FWHM=2.1 ps) and a pulse compression unit provided a 10 GHz optical pulse train with a pulse width of 0.42 ps. An optical bandpass filter (OBF) centered at $\lambda_D=1556$ nm defined the final pulsewidth for transmission. In the modulator unit, the 10 Gbaud signal was DQPSK modulated so that the 10 Gbaud signal had a data rate of 20 Gbit/s. Each pulse was coded in the phase with $n \times \pi/2$, $n \in 0, 1, 2, 3$. The 20 Gbit/s DQPSK signal was multiplexed to 80 Gbit/s (40 Gbaud) by passive optical PRBS-MUX stages, and the bit-rate was finally increased up to 1.28 Tbit/s or 2.56 Tbit/s. The last stage up to 2.56 Tbit/s was a bit-interleaved polarization multiplexing stage. The latter 2.56 Tbit/s signal thus consisted of two orthogonally polarized 640 Gbaud signal, each signal being modulated using DQPSK modulation.

The data signal was transmitted over up to three 80 km spans of dispersion managed UltrawaveTM Fiber (DMF) provided by OFS Denmark (53 km Super Large Area fiber SLA with $D = 20 \text{ ps nm}^{-1} \text{ km}^{-1}$, 27 km Inverse Dispersion Fiber IDF with $D = -40 \text{ ps nm}^{-1} \text{ km}^{-1}$, more details on these fibers can be found in Table A.2, p. 86). The dispersion was precisely matched by the insertion of short SMF or DCF pieces, while the dispersion slope was compensated by the SLA/IDF-combination and by choosing the different spans for opposite residual slope. The span input power was set to 12 dBm. The average DGD of the link was 0.7 ps for 3 spans (240 km). To mitigate the detrimental PMD-effects, the input polarization was adjusted to the principal states of polarization of the fiber.

In the receiver, a polarization demultiplexer (PBS, polarization beam splitter, ensuring the transition from the 2.56 Tbit/s signal with alternating polarization to the 1.28 Tbit/s signal with single polarization) was followed by a NOLM as optical gate for the single polarization (SP) 1.28 Tbit/s data signal.

In this experiment, the NOLM included the fiber DS-HNLF B ($L = 300 \text{ m}$, see Table 2.2, p. 14). The NOLM was preferred to the Kerr gate for this experiment due to its better switching efficiency, guaranteeing a lower attenuation, as discussed in Section 3.5. The choice of including DS-HNLF B in the NOLM was motivated by the considerations explained in Chapter 3. In particular, a shorter DS-HNLF would not have enabled sufficient switching efficiency (low $\Delta\varphi$), as the control laser emitted light at a wavelength where the gain of the available EDFA was limited. Consequently, the transmittance T of the gate would have been low, and the power level of the signal to be detected after the demultiplexer would have been under the receiver sensitivity. DS-HNLF C was not chosen, as the available control ($\approx 17 \text{ dBm}$ average power) power was high enough to enable $\Delta\varphi$ assuring good operation for the gate. Moreover, optical pulses would have experienced dispersive effects more significantly due to the length of the fiber.

A mode-locked fiber laser (MLFL, 40 GHz, $FWHM_C = 1.0 \text{ ps}$, $\lambda_C = 1535 \text{ nm}$) provided the control pulses for the NOLM, and was synchronized to the data signal by the clock recovery unit [40]. An optical delay line enabled precise control of the relative time delay between control and data pulses trains. The switching window characterizing the NOLM used for this experiment was measured and is shown in Fig. 4.2. This was characterized by a high ER (23.9 dB), a short FWHM (1.6 ps).

The maximum available power (17 dBm) was used for the data signal sent to the NOLM. Still, the data signal did not experience impairment due to nonlinear effects, as the energy per pulse was low due to the high bit-rate. The control pulse power used to gate the NOLM was $\approx 14 \text{ dBm}$.

In front of the 80 Gbit/s DQPSK receiver, the signal passed a 6 nm filter to separate the data signal from the control pulses. Within the 80 Gbit/s DQPSK receiver, a delay-line interferometer (DLI) with a differential delay of 100 ps operated as the phase decoder. A phase difference between the DLI-arms of $+\pi/4$ or $-\pi/4$ enabled the detection of the in-phase or quadrature component of the DQPSK signal by a balanced photodetector.

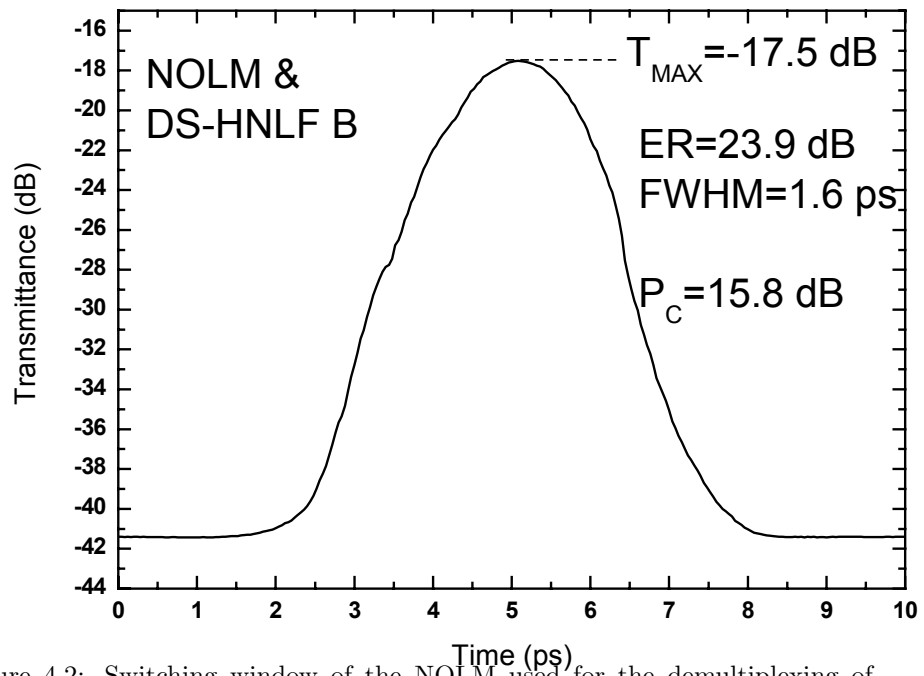


Figure 4.2: Switching window of the NOLM used for the demultiplexing of 1.28 Tbit/s. The control power sent to the DS-HNLF was *approx* 15.8 dBm.

4.1.2 Results

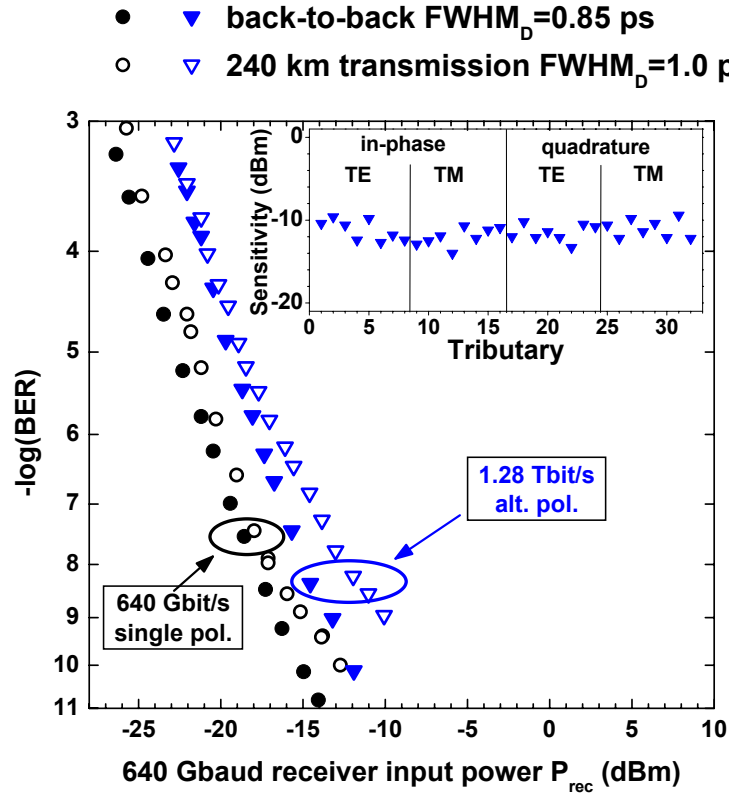


Figure 4.3: BER measurements up to 1.28 Tbit/s, with Data FWHM=1.0 ps and sensitivities for the 32 40 Gbit/s TDM channels.

Fig. 4.3 shows the BER measurements of 1.28 Tbit/s transmission together with 640 Gbit/s as reference over 240 km (3 spans) DMF and the corresponding back-to-back measurements versus the received signal power at the input of the

receiver (P_{rec} , as indicated in Fig. 4.1). The optical power was varied at the input of the 640 Gbaud receiver using an optical attenuator. When the input power is measured before the demultiplexer, a perfect demultiplexing operation reducing the symbol rate by a factor 2 results in the translation of the BER curve by 3 dB towards the lower receiver sensitivities. In these measurements we used a 5.4 nm filter after the pulse compression yielding a pulse width of 0.85 ps at the output of the transmitter. The pulse width after 240 km transmission was broadened to 1.0 ps due to residual higher order dispersion of the fiber link. The inset in Fig. 4.3 depicts the sensitivity at $BER=10^{-9}$ obtained for all tributaries of the 1.28 Tbit/s data signal. The latter 1.28 Tbit/s signal consisted of two orthogonally polarized 320 Gbaud signals, each signal being modulated using DQPSK modulation. Due to the broadened data pulse width after transmission, a further multiplexing operation (from 320 Gbaud to 640 Gbaud, leading to a 2.56 Gbit/s signal with DQPSK modulation) was not possible.

To evaluate the maximum bit rate of this system, the link length was reduced to 160 km with perfect dispersion slope compensation. In this case, the FWHM at the end of the link was such, that multiplexing and demultiplexing up to 2.56 Tbit/s could be done with an acceptable penalty. Fig. 4.4 shows the BER-measurements in this configuration for 2.56 Tbit/s and 1.28 Tbit/s transmission over 160 km DMF, plotted together with 80 Gbit/s and 640 Gbit/s back-to-back curves as reference. For these measurements we used a 8.0 nm filter after the pulse compression to adjust the pulse width to 0.65 ps at the output of the transmitter. The pulse width after 160 km transmission was 0.8 ps, as can be seen in Fig. 4.5.

For 2.56 Tbit/s transmission, it is desirable to shorten the pulses further. However, the reduction of the pulse width in the present setup was limited by the bandwidth of the cascaded non-gain-flattened EDFAs, fourth-order chromatic dispersion and higher order PMD. The coherence crosstalk due to the overlapping pulse tails resulted in variations of the performance as indicated by the dashed area in Fig. 4.4. At 2.56 Tbit/s the system performed error-free ($BER < 10^{-9}$) in the back-to-back configuration. Even at 160 km transmission distance, a best BER value of less than 10^{-5} was achieved which is sufficient to obtain a $BER < 10^{-12}$ when using standard Forward Error Coding (FEC).

In this experiment, the limit was clearly set by the width of the data pulses after the transmission link. At the input of the fiber link, the FWHM of the pulse was 0.42 ps. After the link of length 240 km, the data pulses were broadened to 1.0 ps, which did not allow error-free demultiplexing. By shortening the link to 160 km, the data pulse FWHM was reduced to 0.8 ps, enabling the multiplexing and error-free demultiplexing up to 2.56 Tbit/s. The pulses broadened during propagation, due to imperfect dispersion compensation.

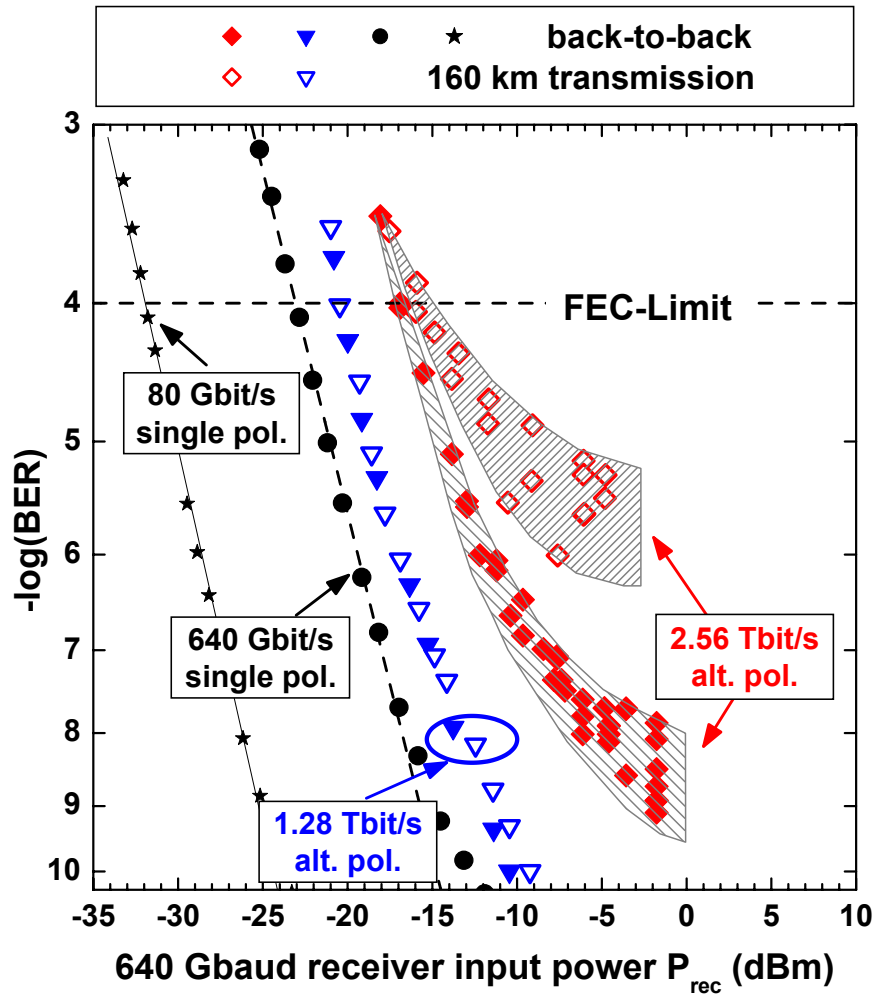


Figure 4.4: BER measurements up to 2.56 Tbit/s, with data FWHM=0.8 ps.

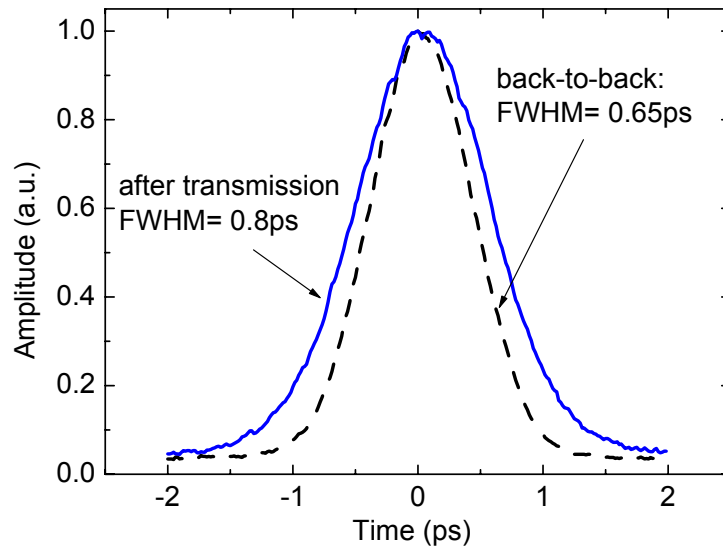


Figure 4.5: Autocorrelation for the data pulse arriving to the demultiplexer, with and without (dashed line) transmission over the 160 km link.

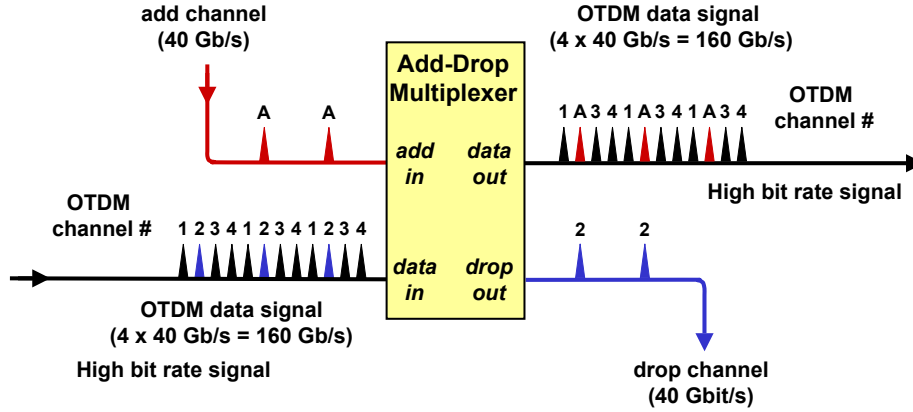


Figure 4.6: Principle of Add-Drop Multiplexing

4.2 Add-Drop Multiplexing at 160 Gbit/s and 320 Gbit/s

Add-Drop Multiplexing is a complicated operation, as two processes have to be simultaneously done on a high bit-rate channel: demultiplexing of one low bit-rate channel and replacing it with a new channel to re-establish the modified high bit-rate signal. The principle of an ADM can be seen in Fig. 4.6.

In this example, four 40 Gbit/s channel are multiplexed to a 160 Gbit/s data signal, which is sent to the ADM (*data in*). One channel (channel 2 in Fig. 4.6) is demultiplexed (*drop out*). A new 40 Gbit/s signal (the "add" **channel A**) is added into the empty time slot via the *add-in* port of the ADM. The signal leaving the ADM at its output *data out* has **channel A** replacing **channel 2**.

In addition to the difficulty of demultiplexing operation, great attention has to be paid to the following steps:

- the insertion of the new channel implies precise control of the arrival time of the two signals coming to the ADM.
- the new channel should be added with the same properties as the "dropped" channel (same wavelength, same FWHM, same power), and the ADM should treat the channel to be added in a transparent manner. In particular, wavelength conversion may be required, in the case where the wavelength of the channel to be added is different from the wavelength of the high bit-rate signal coming to the ADM.

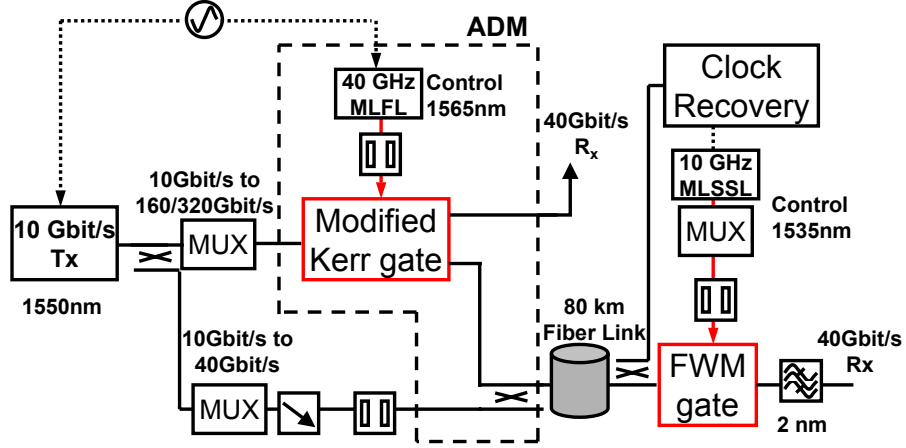


Figure 4.7: Overlook setup for 160/320 Gbit/s ADD-DROP Multiplexing experiment

- the demultiplexing ("drop") of one channel results in the attenuation of this particular channel in the high bit-rate signal. To avoid cross talk, this attenuation should be as good as possible.

4.2.1 Experimental Setup

Fig. 4.7 depicts the ADM experiment carried out in this work.

A 10 Gbit/s transmitter (T_x) was used to produce short optical pulses. The 10 Gbit/s signal was split by an optical coupler. One part of the signal was multiplexed to 160 Gbit/s or 320 Gbit/s, while the other part was multiplexed to 40 Gbit/s.

The 10 Gbit/s transmitter consisted of a 10 GHz pulse source, a 10 Gbit/s modulator driven by a 2^7-1 PRBS word and a pulse compression stage. The data pulse source was a 10 GHz solid-state mode-locked pulse source (SSMLL) emitting 1.8 ps (FWHM) sech pulses at 1550 nm. After standard OOK modulation, pulses were compressed in a DS-HNLF ($L=94$ m, $\lambda_0=1560.4$ nm) to 0.7 ps, using super-continuum generation [41]. The average power sent to the HNLF was ≈ 20 dBm at the input of the DS-HNLF. Though a pulse width of 1.5 ps would also have been short enough for ADM at 160 Gbit/s, pulse compression was used to investigate the feasibility of ADM at the higher bit rate of 320 Gbit/s.

The ADM used in this experiment was based on a Kerr gate (including a 3 dB coupler), as described in Section 3.2, and is depicted in Fig. 4.8. Moreover,

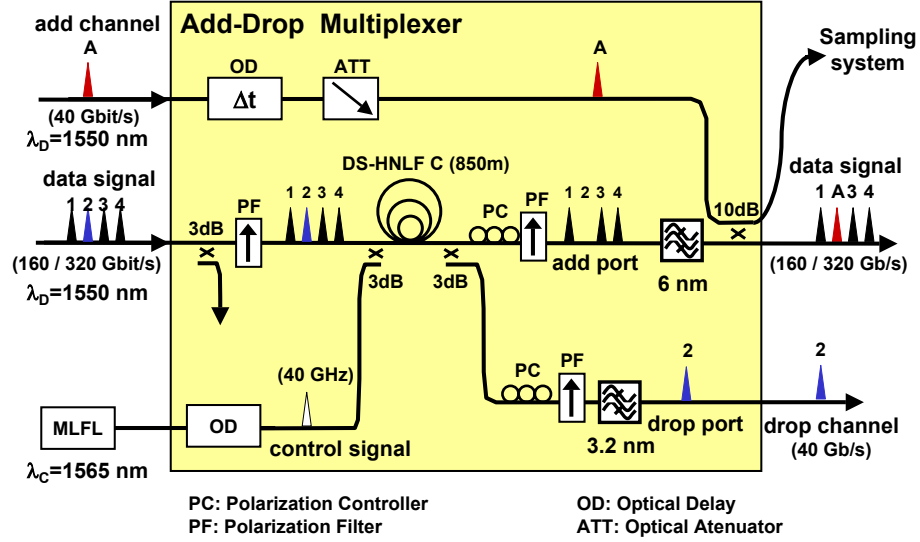


Figure 4.8: Add-Drop Multiplexer based on a Kerr gate.

a 3 dB optical coupler was built behind the DS-HNLF included in the gate, and the two outputs of the coupler - corresponding to the ADD and the DROP outputs of the ADM - were followed by polarization controllers and polarization filters. In this configuration, the ADD and DROP outputs could be optimized independently [42], which would not have been possible with a NOLM, where the polarization settings in the loop fully determine the amplitude of the transmitted data signal and of the reflected signal at the input of the gate. In the DROP port of the Kerr gate, the SOP of the data signal was adjusted in such a way that only the dropped channel was transmitted through the polarization filter when a control pulse induced a transmittance change, thus realizing the demultiplexing operation. In the ADD port, the SOP was adjusted for maximal suppression of the dropped channel after the polarization filter when control and data pulses overlapped during propagation inside the DS-HNLF. The ADM was gated by a 2.0 ps control pulse at 1565 nm, that was emitted by a mode-locked fiber laser (MLFL) at the repetition rate 40 GHz. An optical delay line (OD) enabled precise adjustment of the time delay between the data signal coming to the ADM and the control pulse.

The signal coming at the DROP output was directly sent to a 40 Gbit/s receiver for BER evaluation. The bandwidth (3.2 nm) of the filter used at the DROP output of the ADM was not critical, as the demultiplexed signal does not need to meet the requirements (especially short pulse width) for high bit-rates.

On the contrary, the bandwidth of the filter used at the Add output had to be carefully chosen (6 nm), making sure that the remaining three multiplexed 40 Gbit/s channels still can be transmitted. A filter with a narrow bandwidth

would broaden the pulses in time domain, making the adding of the new channel after the ADM impossible.

As depicted in Fig. 4.8, a 3 dB coupler was built right after the ADD output, and allowed the coupling of the "dropped" signal with the new 40 Gbit/s channel, thus reconstituting a complete 160/320 Gbit/s data signal.

Before being recoupled together, the autocorrelation trace was measured for the modified 160 Gbit/s signal as well as for the 40 Gbit/s signal coming from the pulse compression stage. Dispersion compensation was adjusted using additional DCF/SMF, so that both signals entered the transmission fiber with the same pulse width. An optical delay line (OD) and an optical attenuator (ATT) enabled fine adjustment for the amplitude and relative time position of both signals, which was checked using an optical sampling system (also based on a Kerr gate [43]) connected at the second output of the 10 dB optical coupler (see Fig. 4.8). Eye diagrams of the ADD signal (160 Gbit/s with a missing 40 Gbit/s channel) and of the 40 Gbit/s channel are shown in Fig. 4.9. In a practical ADM, synchronization of the new 40 Gbit/s channel with the modified 160 Gbit/s would be required. The practical realization of such a synchronization could involve an optical gate placed on the path of the "add" channel and gated by the control signal also driving the ADM: a control pulse causes a 40 Gbit/s channel to be attenuated in the 160 Gbit/s signal, and simultaneously gates the second optical gate to enable high transmittance for the new 40 Gbit/s channel, which should recombine with the modified 160 Gbit/s signal. As the gate used for synchronization would be used to control the transmittance of a low bit-rate signal, high speed processing ability would not be necessary for the latter gate.

The complete 160 Gbit/s signal was fed into a 80 km span of dispersion managed UltrawaveTM Fiber (DMF), consisting of 53 km of Super Large Area fiber (SLA) and 27 km of Inverse Dispersion Fiber (IDF) (see Table A.2 for detailed information on these fibers). After transmission, the data pulses were slightly broadened (FWHM=0.8 ps).

The signal was split in an optical coupler. The first output of the coupler led the signal to a FWM-based demultiplexer, which enabled the evaluation of the bit-error rate (BER) for the different 40 Gbit/s channels. The setup of the FWM-based demultiplexer is depicted in Fig. 4.10, and its operating principle is described later in this Section. The decision to use a FWM-based demultiplexer was motivated by the ability of such a scheme to demultiplex data rates over 160 Gbit/s, which is not possible with Electroabsorption Modulator-based demultiplexers. A drawback of using FWM to demultiplex is the resulting wavelength change for the data signal.

The second output of the coupler led the signal to an optical clock recovery [40], which recovered the 40 GHz clock signal necessary to drive the demultiplexer at the receiver side. A second solid state mode-locked laser emitted a 40 GHz pulse train (FWHM= 2.0 ps) at 1535 nm, used to gate the FWM-demultiplexer. The autocorrelation of the control pulse driving the FWM-based demultiplexer is depicted as inset in Fig. 4.10.

The control and data waves were fed into a DS-HNLF (DS-HNLF E, see Table 2.2) using a 3 dB coupler. As both signals have to propagate copolarized inside the fiber, polarization controllers (PC) were included, allowing optimization of their relative polarization states. An optical delay line was included, so that the relative delay between the control and the data pulses could be controlled. Given that control and data pulse overlap during propagation inside the

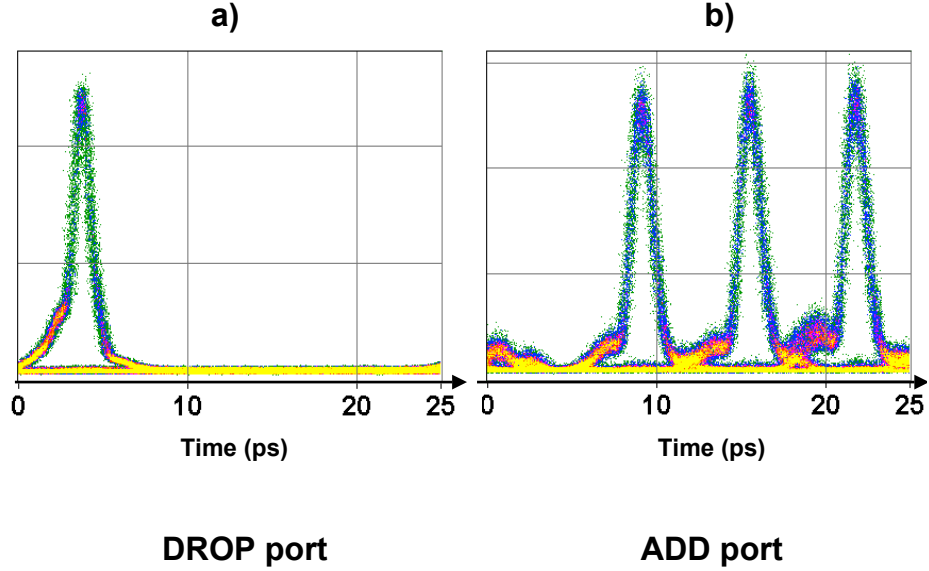


Figure 4.9: Eye diagrams measured at the DROP (a) and ADD (b) ports of the ADM, at 160 Gbit/s.

DS-HNLF, a FWM-product at the wavelength $\lambda_{FWM}=1565$ nm could be measured at the output of the fiber. As stated in Section 2.4, the FWM-wavelength λ_{FWM} corresponds to the optical frequency $\omega_{FWM} = \omega_C - \Delta\omega$. An optical filter was placed after DS-HNLF E, and the 40 Gbit/s demultiplexed signal at λ_{FWM} was sent to a 40 Gbit/s receiver.

Fig. 4.10 shows also an autocorrelation trace of the control pulse used to gate the demultiplexer and a switching window. A transmittance larger than 1 ($T > 0dB$ for the switching window in Fig. 4.10) was measured, which is due to the fact that no signal could be measured at λ_{FWM} at the input of the gate. Thus, the generation of the new wave led to high transmittance value, which does not correspond to a gain.

The FWM-demultiplexer used was first tested by bypassing the ADM and the transmission link, so that the demultiplexing ability of the gate could be investigated, for incoming signals of 160 Gbit/s and 320 Gbit/s. Very low penalties were observed when demultiplexing 160 Gbit/s and error-free operation was also achieved for 320 Gbit/s.

However, the 40 Gbit/s receiver was not wavelength dependent and the gate could demultiplex 160 Gbit/s with no additional penalty due to the demux operation or to the wavelength conversion process.

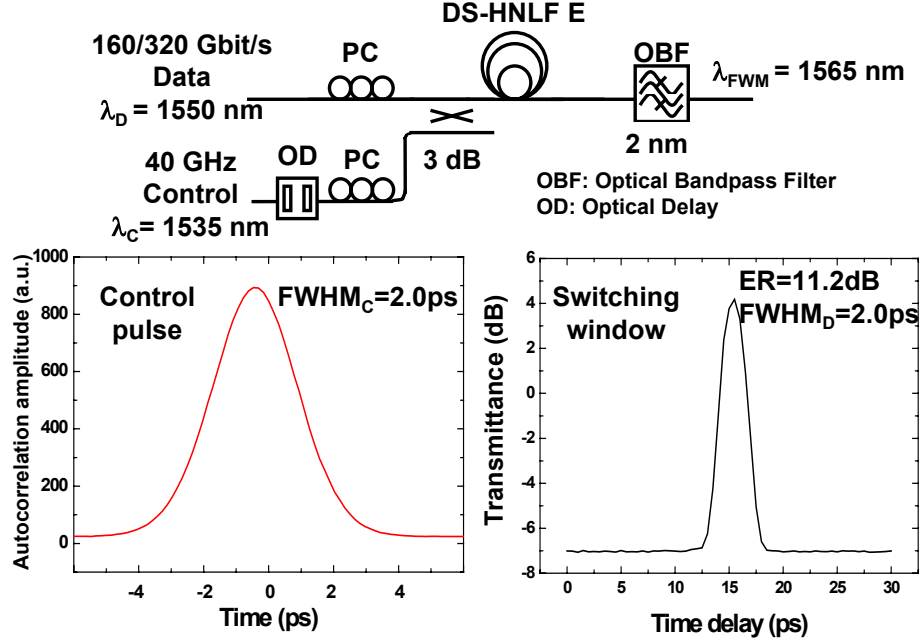


Figure 4.10: Setup for the FWM-based demultiplexer, autocorrelation of the control pulse gating the demultiplexer and switching window.

4.2.2 Results

DROP operation

The BER was measured at the DROP output of the ADM for 160 Gbit/s and 320 Gbit/s, and was investigated as a function of the optical power sent to the 40 Gbit/s receiver. An optical attenuator was used to vary the optical power going to the receiver. The results are presented in Fig. 4.11. Error-free demultiplexing was achieved in both cases. At 320 Gbit/s, no significant additional penalty was observed compared with 160 Gbit/s, asserting that the data pulse FWHM was chosen short enough for higher bit-rate. The reference measurement is referred to as "40 Gbit/s back-to-back" in Fig. 4.11, as it corresponds to the BER detected when the 40 Gbit/s signal went through the gate set on maximum transmission.

ADD operation

The BER was measured at 160 Gbit/s, for the four 40 Gbit/s channels, after transmission through the 80 km link. The optical power was varied before the 40 Gbit/s Receiver using an optical attenuator. The 40 Gbit/s channel to be measured was selected by varying the optical delay between the 160 Gbit/s data signal and the 40 GHz control pulse train at the FWM-based demultiplexer. The results are presented in Fig. 4.12. The average penalty was 2.0 dB compared with the back-to-back (b2b) measurement. The transmission characteristic used for the ADD-operation in the Kerr-gate is depicted in Fig. 4.13. The high ER

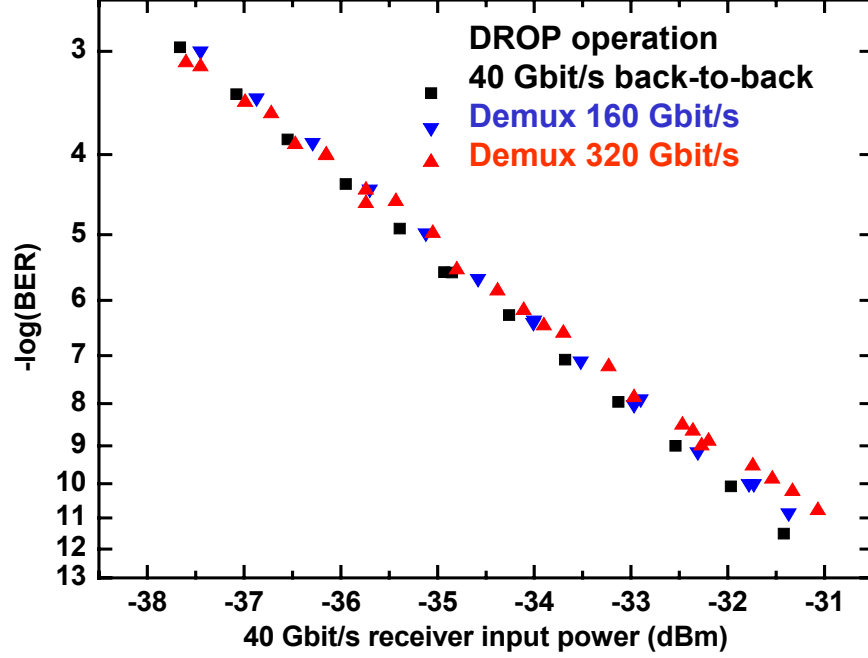


Figure 4.11: BER measurements for 160 Gbit/s and 320 Gbit/s, for the DROP operation.

(15 dB measured for a characteristic measured with 40 Gbit/s) as well as a FWHM of 4 ps enabled stable operation at 160 Gbit/s. The dashed lines in Fig. 4.13 represent the bit distribution over the switching characteristic, for 160 Gbit/s. Even at 320 Gbit/s, where the bit-slot is 3.125 ps, such a switching window could have been used when pulses are as short as 0.8 ps. However, the "ADD" characteristic showed a high attenuation of $T_{ADD\ MAX} = -41.8$ dB (see Fig. 4.13), which causes the SNR of the data signal to decrease after the ADM, and explains the penalties measured. The high attenuation of the Kerr gate is due to the extra passive loss caused by the additional 3 dB coupler needed for ADD-DROP operation, as well as to the low switching efficiency of the Kerr gate.

The requirements on the pulse widths and jitter for a 320 Gbit/s ADM experiment were met throughout this experiment. Still, no proper measurement could not be done over 160 Gbit/s, due to insufficient stability in the setup, involving three pulses sources, one ADM and a demultiplexer. Taken separately, the ADM-operation could be successfully done at 320 Gbit/s, as can be seen in Fig. 4.14, and as suggested by Fig. 4.13. Fig. 4.14 a) shows an eye diagram representing the extraction of a 40 Gbit/s channel out of a 320 Gbit/s signal, and Fig. 4.14 b) shows the same signal after the re-adding of a new 40 Gbit/s channel. These eye diagrams were taken at the input of the FWM-demultiplexer. In particular, the amplitude of the neighbour channels of the channel to be dropped in Fig. 4.14a) were not attenuated by the ADD-transmittance function shown in Fig. 4.13. The 320 Gbit/s signal experienced high attenuation in the Kerr

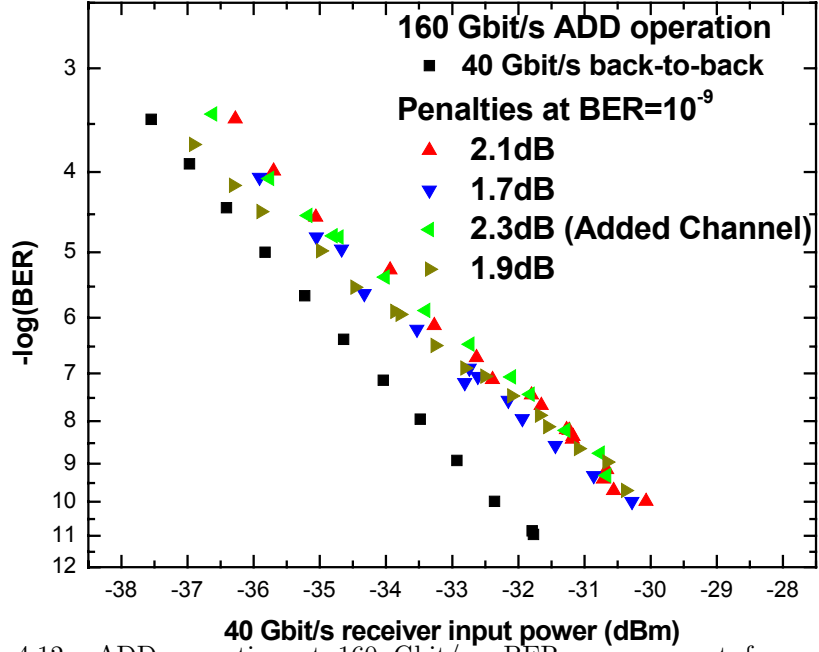


Figure 4.12: ADD operation at 160 Gbit/s: BER measurement for each 40 Gbit/s channel after the FMW-based demultiplexer.

ADM, which is responsible for the low resolution of the eye diagrams measured. Though the Kerr ADM fulfills the speed requirements for ADM over 160 Gbit/s, regeneration of the signal at the ADD output is required, due to the high attenuation of the ADM.

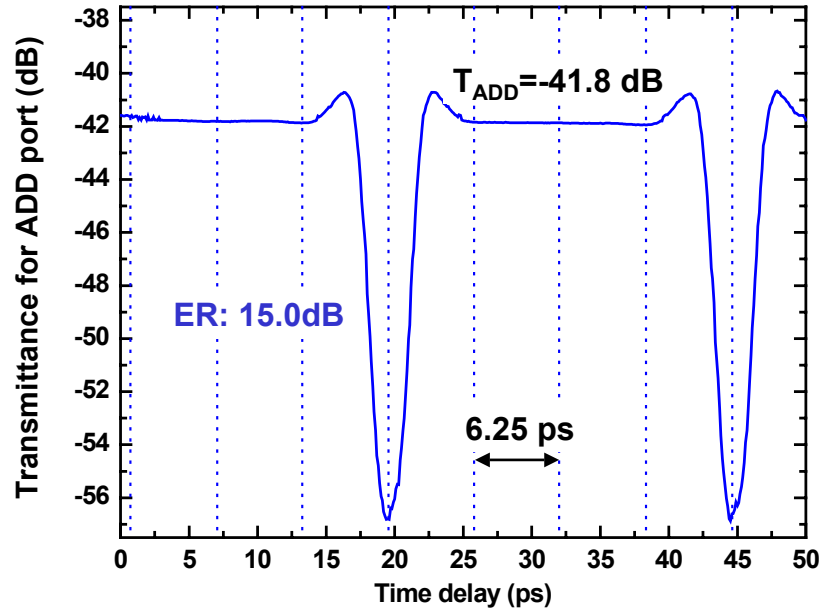


Figure 4.13: ADD operation at 160 Gbit/s: switching characteristic T_{ADD} for the ADD operation of the ADM.

Chapter 5

Conclusion

The NOLM and the Kerr gate were investigated experimentally. The phase shift induced through Cross-Phase Modulation was measured and offered an argument for comparing the two gates. Switching windows were also investigated, and the DS-HNLFs used were varied, which allowed to determine the influence of the parameters of the fibers on the performance of each gate. Low parametric amplification could be observed, and was not further investigated in this work. Both gates are capable of demultiplexing a 320 Gbit/s TDM data signal to 40 Gbit/s, and low penalties were measured. The NOLM was also successfully used to demultiplex a 640 Gbaud data signal. The fiber used was chosen in accordance with investigations presented in Chapter 3.

An Add-Drop Multiplexer took advantage of the principle of operation of the Kerr gate, as was presented in Chapter 4. The feasibility of ADM at bit-rates higher than 160 Gbit/s was demonstrated.

Experimental investigations allowed to improve insight on the advantage of using the NOLM or the Kerr gate, and illustrated the necessity of choosing the right fiber to be included in the gate.

Choice of the gate

Though boths gates basically have the same switching characteristics (same dependence of the transmittance T on the XPM-induced phase shift $\Delta\varphi$), practical considerations give an advantage to the NOLM when the demultiplexing functionality is needed. It is expected that for a given control pulse power, the XPM-induced phase shift is 1.5 times larger in the NOLM than in the Kerr gate. This was also observed in experimental investigations of the phase shift, and a factor 1.57 was measured between the slopes of the functions representing $\Delta\varphi_{NOLM}$ and $\Delta\varphi_{Kerr}$ versus the power of the control pulses for low powers. Considering a given control power budget, reaching a phase shift that will allow good operation ($\Delta\varphi > 0.6 \pi$, as suggested by experimental results) for the gate will be obtained easier with the NOLM. BER measurements proved that both gates are suitable for TDM demultiplexing, and no significant difference could be observed for the penalties measured. This is however consistent with the fact that both gates present a switching window with the same shape, and that the BER measurements carried out in Section 3.3 were not influenced by the additionnal insertion loss (passive loss associated to lower switching efficiency)

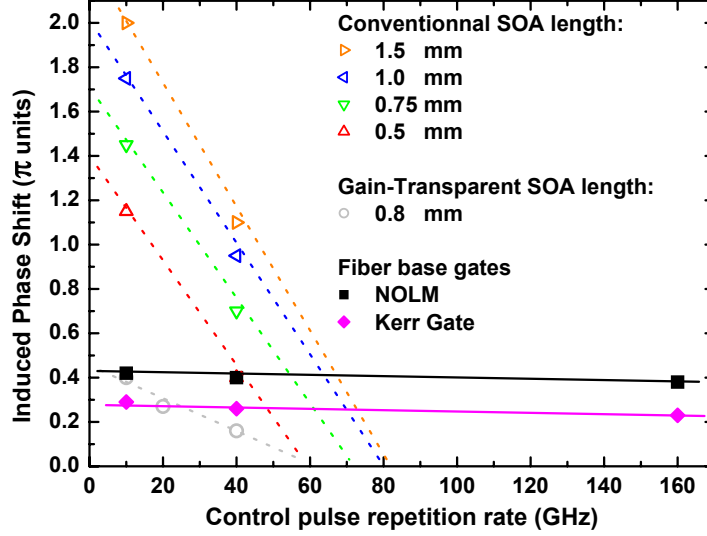


Figure 5.1: Comparison of phase shift measurements in fiber-based gates and in SOA based gates [1]

of the Kerr gate. In most of the cases the optical gate is followed by an amplifier (EDFA) which might add noise to the data signal if the signal power at its input is low. In such a configuration, the NOLM would be the gate of choice.

The base data rate considered in this work was 40 Gbit/s and is expected to increase in the future. Consequently, the repetition rate of the control pulse will double (when considering the upgrade from 40 Gbit/s to the 80 Gbit/s base rate). Assuming that the average control signal power remains constant, this results in a two times lower peak power for the control pulse. As this quantity is of high importance for switching (as observed in chapter 3), the NOLM is once again expected to outcompete the Kerr gate due to its better switching efficiency.

Fig. 5.1 presents a comparison of the phase shift measurements carried out in the NOLM and in the Kerr gate (see Chapter 3), as well as in interferometric gates incorporating SOAs, operated either conventionally or in the gain-transparent mode [1]. As can be seen, the phase shift that could be reached in a fiber is still much higher than this reachable in an SOA, as soon as the repetition rate of the control pulses exceeds 80 Gbit/s. The phase shift is also independent of the repetition rate of the control pulse.

This feature is a reason why the Kerr gate and the NOLM are predisposed gates for applications such as all-optical 3R-regenerators, where the transmittance of the gates is driven by a control signal with a high repetition rate [44].

Though this could not be observed at a bit-rate up to 640 Gbit/s, the NOLM is suspected to be limited through the bidirectional transmission of the data pulses in the HNLF. At high bit-rates, the time delay between two data pulses

is shortened, and the density of data pulses propagating Clockwise and counter-clockwise in the loop increases. Consequently, the relative phase shift difference induced on the clockwise propagating data pulses in the loop decreases, which may lead to a decrease of the performance of the NOLM. As in the case of the Kerr gate, data and control pulses propagate unidirectionally in the HNLF, the performance of the Kerr gate should not suffer from this limitation.

Choice of the DS-HNLF

The choice of the fiber to be incorporated in the interferometric gate is also an issue appointed in this work. Though the use of a long fiber ($L > 1\text{ km}$) might help to overcome the limitation for the available power of the control signal, the impairments due to dispersive and nonlinear effects (spectral broadening and shape change for the control pulse, mainly), scaling with L , were clearly shown to limit the performance of the gate. These impairments are however be reduced when using a DS-HNLF with a short length.

Throughout this work, the wavelengths of the pulse sources for data and control signals were mostly not tunable, so that the condition required to reduce the walk-off was not met. Still, short switching windows with high extinction ratios and low attenuation could be measured, and error-free operation was achieved for the experiments reported. Therefore, walk-off did not appear to be a strong limiting factor in this work.

The specifications given for DS-HNLFs (indications on λ_0 , γ , $S(\lambda_0)$, L) have to be taken with care, as they might lead to disagreement between experimental and simulated results. In particular, the zero-dispersion wavelength λ is rarely constant over the fiber length. Thus, the measured λ_0 should be considered as an "effective" zero-dispersion wavelength. The nonlinear parameter γ is also evaluated using different methods, and the estimation on γ may vary. In the near future, a better controlling of the manufacturing process of DS-HNLFs should provide more accuracy on these crucial parameters.

In the experiment of Nakazawa et al. [4], a very sophisticated setup was used for the demultiplexing of 640 Gbit/s. In the present work, various DS-HNLFs were used in two optical gates and demultiplexing could be done up to 640 Gbit/s with a much simplified setup.

Bibliography

- [1] Colja Schubert. *Interferometric Gates for All-Optical Signal Processing*. PhD thesis, Fakultät II (Mathematik und Naturwissenschaften), Technical University Berlin, 2004.
- [2] Marcel Kroh. *Semiconductor Mode-Locked Laser for High-Speed OTDM Transmission*. PhD thesis, Fakultät IV – Elektrotechnik und Informatik – der Technischen Universität Berlin, 2006.
- [3] J. Leuthold, C. H. Joyner, B. Mikkelsen, G. Raybon, J. L. Pleumeekers, B. I. Miller, K. Dreyer, and C. A. Burrus. 100 Gbit/ all-optical wavelength conversion with integrated SOA delayed-interference configuration. *Electron. Lett.*, 36(13):1129–1130, 2000.
- [4] M. Nakazawa, E. Yoshida, T. Yamamoto, E. Yamada, and A. Sahara. TDM Single Channel 640 Gbit/s Transmission Experiment over 60 km Using a 400 fs Pulse Train and a Walk-Off Free, Dispersion Flattened Nonlinear Optical Loop Mirror. *Proc. 23th Optical Fiber Commun.*, page PD14, march 1998.
- [5] N. J. Doran and D. Wood. Nonlinear-Optical Loop Mirror. *Optics Lett.*, 13(1):56–8, Jan. 1988.
- [6] M. A. Duguay. The ultrafast optical Kerr shutter, 1976.
- [7] M. Nakazawa, T. Yamamoto, and K.R. Tamura. 1.28Tbit/S-70km OTDM Transmission Using Third- and Fourth-Order Simultaneous Dispersion Compensation with a Phase Modulator. *Electron. Lett.*, 36(24):2027–9, Nov. 2000.
- [8] H.G. Weber, S. Ferber, M. Kroh, C. Schmidt-Langhorst, R. Ludwig, V. Marembert, C. Boerner, F. Futami, S. Watanabe, and C. Schubert. Single Channel 1.28 Tbit/S and 2.56 Tbit/S DQPSK Transmission. In *ecoc*, 2005. PD paper Th4.1.2.
- [9] S. Watanabe, R. Okabe, F. Futami, R. Hainberger, C. Schmidt-Langhorst, C. Schubert, and Hans-Georg Weber. Novel Fiber Kerr-Switch with Parametric Gain: Demonstration of Optical Demultiplexing and Sampling Up to 640 Gb/s. In *Proc. 30th Europ. Conf. on Opt. Comm. (ECOC'04)*, Stockholm, Sweden, 2004. postdeadline paper Th4.1.6.
- [10] Carsten Schmidt-Langhorst. *Optical Sampling of High Bit Rate Optical Data Signals*. PhD thesis, Fakultät II – Mathematik und Naturwissenschaften – der Technischen Universität Berlin, 2004.

- [11] A. M. Melo, V. Marembert, C. Schubert, C. Schmidt-Langhorst, and K. Petermann. Design optimization of ultra-high bit-rate NOLM-based OTDM demultiplexers. In *Lasers and Electro-Optics Society, IEEE Annual Meeting*, 2005.
- [12] B. Bakhshi, M. Manna, E. A. Golovchenko, P. Corbett, S. Jiang, H. Li, S.M. Abbott, M. Nissov, G. Harvey, R. Zhu, and Q. Zhong. 640 Gb/s (64 x 12.3 Gb/s) 12,700 km RZ-DPSK WDM Transmission with 75 km Repeater Spacing. In *ecoc05*, 2005.
- [13] N. Sugimoto, T. Nagashima, T. Hasegawa, and S. Ohara. Bismuth-based optical fiber with nonlinear coefficient of $1360 \text{ W}^{-1} \text{ km}^{-1}$. In *Proc. Optical Fiber Commun.*, volume 2, 2004.
- [14] G. Brambilla, F. Koizumi, V. Finazzi, and D.J. Richardson. Supercontinuum generation in tapered bismuth silicate fibres. In *Electron. Lett.*, volume 41, pages 795–797, July 2005.
- [15] J.T. Gopinath, H.M. Shen, H. Sotobayashf, and E.P. Ippen. Novel highly nonlinear bismuth oxide fiber for supercontinuum generation. In *Lasers and Electro-Optics Society, IEEE Annual Meeting*, 2004.
- [16] J.T. Gopinath, H.M. Shen, H. Sotobayashi, E.P. Ippen, T. Hasegawa, T. Nagashima, and N. Sugimoto. Highly nonlinear bismuth-oxide fiber for supercontinuum generation and femtosecond pulse compression. In *J. Lightwave Technol.*, volume 23, pages 3591–3596, 2005.
- [17] Ju Han Lee, S. Ohara, T. Nagashima, T. Hasegawa, N. Sugimoto, K. Igarashi, K. Katoh, and K. Kikuchi. Clock recovery and demultiplexing of high-speed OTDM signal through combined use of bismuth oxide nonlinear fiber and erbium-doped bismuth oxide fiber. In *IEEE Photon. Technol. Lett.*, volume 17, pages 2658–2660, 2005.
- [18] G. Meloni, M. Scaffardi, P. Ghelfi, A. Bogoni, L. Poti, and N. Calabretta. Ultrafast all-optical ADD-DROP multiplexer based on 1-m-long bismuth oxide-based highly nonlinear fiber. In *IEEE Photon. Technol. Lett.*, volume 17, pages 2661–2663, 2005.
- [19] H.G. Weber in E. Voges and K. Petermann. *Optische Kommunikationstechnik*. Springer Verlag, Berlin, 2002.
- [20] Govind P. Agrawal. *Nonlinear Fiber Optics*. Academic Press, London, UK, 3rd edition, 2001.
- [21] S. Bigo, O. Leclerc, and E. Desurvire. All-Optical Fiber Signal Processing and Regeneration for Soliton Communications. *IEEE J. Quantum Electron.*, 3:1208–1223, 1997.
- [22] A. T. Clausen, H. N. Poulsen, L.K. Oxenløwe, A.I. Siahlo, J. Seoane, and P. Jeppesen. Pulse Source Requirements For OTDM Systems. In *IEEE LEOS Annual Meeting Conference Proceedings, Tucson, AZ, USA*, 2003.

- [23] R. Ludwig, W. Pieper, Hans-Georg Weber, D. Breuer, K. Petermann, F. Küppers, and A. Mattheus. Unrepeated 40 Gbit/s RZ Single Channel Transmission over 150 Km of Standard Fiber at 1.55 μ M. *Electron. Lett.*, 36(16):1405–6, 2000.
- [24] G. Schiffner, W. R. Leeb, H. Krammer, and J. Wittmann. Reciprocity of birefringent single-mode fibers for optical gyros. *Appl. Optics*, 18(13):2096–2097, July 1979.
- [25] T. Yamamoto, E. Yoshida, and M. Nakazawa. Ultrafast Nonlinear Optical Loop Mirror for Demultiplexing 640 Gbit/s TDM Signals. *Electron. Lett.*, 34(10):1013–1014, may 1998.
- [26] Takahide Sakamoto, Fumio Futami, Kazuro Kikuchi, Shinichi Takeda, Yasushi Sugaya, and Shigeki Watanabe. All-Optical Wavelength Conversion of 500-fs Pulse Trains by Using a Nonlinear-Optical Loop Mirror Composed of a Highly Nonlinear DSF, 4 2001.
- [27] M. Jinno. Nonlinear Sagnac Interferometer Switch and its Applications. *IEEE J. Quantum Electron.*, 28:875–882, 1992.
- [28] E. Jahn, N. Agrawal, W. Pieper, H. J. Ehrke, D. Franke, W. Furst, and C. M. Weinert. Monolithically integrated nonlinear sagnac interferometer and its application as a 20 Gbit/s all-optical demultiplexer. *Electron. Lett.*, 32:782–784, 1996.
- [29] C. Schubert, L. Schares, C. Schmidt, G. Guekos, and Hans-Georg Weber. Phase Dynamics in Gain-Transparent Semiconductor Optical Amplifiers. In *Proc. 29th Europ. Conf. on Opt. Comm. (ECOC'03)*, pages 1062–1063, Rimini (Italy), September 2003. Paper Th3.5.2.
- [30] W.A. Atia and R.S. Bondurant. Demonstration of return-to-zero signaling in both OOK and DPSK formats to improve receiver sensitivity in an optically preamplified receiver. In *Lasers and Electro-Optics Society, IEEE Annual Meeting*, volume 1, pages 226 – 227, 1999.
- [31] A. H. Gnauck, S. Chandrasekhar, J. Leuthold, and L. Stulz. Demonstration of 42.7-Gb/s DPSK Receiver With 45 Photons/Bit Sensitivity. *IEEE Photon. Technol. Lett.*, 15(1):99–101, January 2003.
- [32] Govind P. Agrawal. *Fiber-Optic Communication Systems*. Wiley Series in Microwave and Optical Engineering. John Wiley and Sons, Inc., New York, 3rd edition, 2002.
- [33] Hans-Georg Weber, N. Agrawal, A. Ehrhardt, H. J. Ehrke, M. Eiselt, E. Jahn, R. Ludwig, W. Pieper, and R. Schnabel. Optical Time-Domain Demultiplexing Techniques Using Semiconductor Laser Amplifiers. In *Proc. 22nd Europ. Conf. Opt. Commun. (ECOC'96)*, Oslo, Norway, September 1996. Techn. Dig. invited Paper ThB.1.1.
- [34] Masahiko Jinno. Effects of Crosstalk and Timing Jitter on All-Optical Time-Division Demultiplexing Using a Nonlinear Fiber Sagnac Interferometer Switch. *IEEE J. Quantum Electron.*, 30(12):2842–2853, 1994.

- [35] S. Randel, J. K. Fischer, A. Marques de Melo, and K. Petermann. Equivalent Low-Pass Model for OTDM Receivers. *IEEE Photon. Technol. Lett.*, 17(5):1070–1072, may 2005.
- [36] M. M. Strasser, P. J. Winzer, and A. Napoli. Noise and Intersymbol-Interference Properties of OTDM and ETDM Receivers. In *IEEE Photon. Technol. Lett.*, 2004.
- [37] R.A. Griffin and A.C. Carter. Optical Differential Quadrature Phase-Shift Key (oDQPSK) for High Capacity Optical Transmission. In *OSA Trends in Optics and Photonics (TOPS) Vol. 55, Optical Fiber Commun. Conf., Technical Digest, Postconference Edition*, pages 367–368, Anaheim, CA (USA), March 2002. Paper WX6.
- [38] M. Daikoku, N. Yoshikane, and I. Morita. Performance comparison of modulation formats for 40 Gbit/s DWDM transmission systems. In *Proc. Optical Fiber Commun.*, 2005.
- [39] Sebastian Ferber, Colja Schubert, Reinhold Ludwig, Christof Boerner, Carsten Schmidt-Langhorst, and Hans-Georg Weber. 640 Gbit/s DQPSK Single-Channel Transmission over 480 km Fibre Link. In *ecoc05*, Glasgow, Scotland (U.K.), sep 2005. Paper We3.2.2.
- [40] C. Boerner, V. Marembert, S. Ferber, C. Schubert, R. Schmidt-Langhorst, C. Ludwig, and Hans-Georg Weber. 320 Gbit/s Clock Recovery with Electro-Optical PLL Using a Bidirectionally Operated Electroabsorption Modulator as Phase Comparator. In *Proc. 30th Opt. Fiber Commun. Conf. (OFC'05)*, Anaheim, CA (USA), mar 2005. Paper OTuO3.
- [41] M. Kroh, B. Hüttl, S. Ferber, and Hans-Georg Weber. Low Noise 400 Fs Pulse Generation by Monolithic Semiconductor Mode-Locked Laser and Soliton Pulse Compression. In *cleo-eu05*, Munich (Germany), jun 2005. Paper CB8-2-THU.
- [42] C. Schubert, C. Schmidt-Langhorst, K. Schulze, V. Marembert, and H.G. Weber. Time Division Add-Drop Multiplexing up to 320 Gbit/s. In *Proc. 30th Opt. Fiber Commun. Conf. (OFC'05)*, 2005.
- [43] C. Schmidt-Langhorst, C. Schubert, C. Boerner, V. Marembert, S. Ferber, R. Ludwig, and Hans-Georg Weber. Optical Sampling System Including Clock Recovery for 320 Gbit/s DPSK and OOK Data Signals. In *Proc. 30th Opt. Fiber Commun. Conf. (OFC'05)*, Washington, DC, mar 2005. Optical Society of America. Paper OWJ6.
- [44] Shigeki Watanabe, Reinhold Ludwig, Fumio Futami, Colja Schubert, Sebastian Ferber, Christof Boerner, Carsten Schmidt-Langhorst, Joern Berger, and Hans-Georg Weber. Ultrafast All-Optical 3R-Regeneration. *IEICE Trans. Electron.*, E87-C(7):1114–1118, July 2004.

Appendix A

Appendix

A.1 Fibers used

In the following, we present the fibers used throughout this work.

Fibers used as nonlinear medium

DS-HNLF	A	B	C	D	E	F
γ	21	10	21	21	20	21
L (m)	100	300	850	46	503	94
λ_0 (nm)	1536.7	1556.0	1550.3	1560.9	1550.0	1549.0
S ($\text{ps km}^{-1} \text{nm}^{-2}$)	0.02	0.02	0.02	0.016		0.016
PMD ($\text{ps km}^{-1/2}$)					0.053	0.053
Loss (dB)	0.6	1.4	1.6	1.4	1.5	1.1

Table A.1: Characteristic parameters for fibers used in this work

DS-HNLF A, B, and E and F were provided by OFS Denmark. DS-HNLF C and D were provided by Sumitomo Electric through Fujitsu Laboratories Ltd.

Fibers used for transmission

	SLA Fiber	ID Fiber
Length (km)	53	27
γ ($\text{W}^{-1} \text{km}^{-1}$)	0.87	3.05
$D@ 1550 \text{ nm}$ ($\text{ps km}^{-1} \text{nm}^{-1}$)	20	-40
A_{eff} (μm^2)	105	33
α (dB km^{-1})	0.187	0.234

Table A.2: Parameters of the Super Large Area (SLA) and Inverse Dispersion (ID) Fibers used for transmissions in Sections 4.2 and 4.1

A.2 Optical pulses

An optical pulse is commonly described by the indication on the Full-Width at Half-Maximum τ_{FWHM} of its intensity profile, on its shape (e.g. sech, Gaussian), and by its peak power P_{Peak} . The energy of a single pulse is given by

$$Energy_{Pulse}(P_{Peak}, \tau_{FWHM}) = P_{Peak} \int_{-\infty}^{+\infty} |A_{\tau_{FWHM}}^{norm.}(t)|^2 dt \quad (A.1)$$

where $A_{\tau_{FWHM}}^{norm.}(t)$ is the normalized amplitude of the pulse. In Eq. A.2, the pulse energy is expressed in Picojoule (pJ), P_{Peak} in Watt (W), and τ_{FWHM} in Picosecond (ps).

For a Sech pulse:

$$A_{sech \ \tau_{FWHM}}^{norm.}(t) = \frac{2}{\exp(\frac{1.7627 t}{\tau_{FWHM}}) + \exp(-\frac{1.7627 t}{\tau_{FWHM}})} \quad (A.2)$$

For a Gaussian pulse:

$$A_{gauss \ \tau_{FWHM}}^{norm.}(t) = \exp(-\frac{(1.6651 t)^2}{2\tau_{FWHM}^2}) \quad (A.3)$$

Consequently, the energy of a single pulse of width τ_{FWHM} can be expressed as a function of τ_{FWHM} :

$$Energy_{Pulse}(P_{Peak}, \tau_{FWHM}) = P_{Peak} \tau_{FWHM} \int_{-\infty}^{+\infty} |A_{FWHM=1}^{norm.}(t')|^2 dt' \quad (A.4)$$

where $t'=t/\tau_{FWHM}$ has no unit.

The factor $a_{sh.} = \int_{-\infty}^{+\infty} |A_{FWHM=1}^{norm.}(t)|^2 dt$ accounting for the pulse shape is $a_{sh.}=1.1346$ for a sech pulse, and $a_{sh.}=1.0645$ when considering a Gaussian pulse

The relations linking the pulse energy (in pJ), the average power $P_{avg.}$ (in mW) and the peak power P_{Peak} (in W) of a pulse emitted with the repetition frequency $\nu_{rep.}$ (in GHz) are [1]:

$$Energy_{Pulse} = P_{Peak} \tau_{FWHM} a_{sh.} \quad (A.5)$$

$$P_{Peak} = \frac{P_{avg.}}{\nu_{rep.} \ a_{sh.} \ \tau_{FWHM}} \quad (A.6)$$

$$Energy_{Pulse} = \frac{P_{avg.}}{\nu_{rep.}} \quad (A.7)$$

Appendix B

List of Symbols and Abbreviations

Abbreviations

In alphabetical order:

ADM: Add-Drop Multiplexing (Add-Drop Multiplexer)
AP: Alternating Polarization
BER: Bit Error Rate
DCF: Dispersion Compensating Fiber
DFF: Dispersion Flatened Fiber
DGD: Differential Group Delay
DILM: Dispersion Imbalanced Loop Mirror
DLI: Delay Line Interferometer
DOP: Degree of Polarization
DPSK: Differential Phase Shift Keying
DQPSK: Differential Quadrature Phase Shift Keying
DSF: Dispersion Shifted Fiber
DS-HNLF: Dispersion Shifted Highly Nonlinear Fiber
EAM: Electro-Absorption Modulator
EDFA: Erbium Doped Fiber Amplifier
ER: Extinction Ratio
FWHM: Full Width at Half Maximum
FWM: Four-Wave Mixing
FEC: Forward Error Coding
GVD: Group Velocity Dispersion
HNLF: Highly Nonlinear Fiber
IDF: Inverse Dispersion Fiber
IR: Infra Red
MLFL: Mode-Locked Fiber Laser
MLSSL: Mode-Locked Solid State Laser
NLSE: Nonlinear Schrödinger Equation
NOLM: Nonlinear Optical Loop Mirror
NRZ: Non Return-to-Zero
OBF: Optical Bandpass Filter
OD: Optical Delay

OSNR: Optical Signal-to-Noise Ratio
PA: parametric amplification
PBS: Polarization Beam Splitter
PF: Polarization Filter
PMD: Polarization Mode Dispersion
PMF: Polarization Maintaining Fiber
RZ: Return-to-Zero
SDH: Synchronous Digital Hierarchy
SLA: Super Large Area fiber
SLALOM: Semiconductor Laser Amplifier in a LOop Mirror
SONET: Synchronous Optical Network
SOA: Semiconductor Optical Amplifier
SOP: state of polarization
SP: Single Polarization
SPM: Self-Phase Modulation
SSMF: Standard Single Mode Fiber
SSMLL: Solid-State Mode Locked Laser
TSMLL: Tunable Semiconductor Mode-Locked Laser
WDM: Wavelength Division Multiplexing
OTDM: Optical Time Division Multiplexing
UV: Ultra Violet
XPM: Cross-Phase Modulation

Symbols

A_{eff} : effective area
 $A(z, t)$: slowly varying pulse envelope
 α : absorption coefficient
 β : propagation constant
 c : velocity of light
 D : Dispersion parameter
 ϵ_0 : vacuum permittivity
 $F(x, y)$: Electrical field modal distribution
 γ : nonlinear parameter
 g : parametric gain
 G_{MAX} : maximum parametric gain
 k : wave-vector
 Δk : wave-vector mismatch
 λ : Wavelength
 λ_0 : Zero Dispersion Wavelength
 λ_C : Control signal wavelength
 λ_D : Data signal wavelength
 $\lambda_{mid.}$: "Middle" Dispersion between λ_C and λ_D
 n_2 : nonlinear coefficient
 n_g : group index
 ρ_f : charge density
 \vec{B} : magnetic flux density vector
 \vec{D} : electric flux density vector
 \vec{E} : electric field vector
 \vec{H} : magnetic field vector
 \vec{P} : polarization vector
 P_{Peak} : Pulse peak power
 R_x : Receiver
 S : Dispersion-slope parameter
 T : Transmittance
 T' : 1- T
 T_x : Transmitter
 T_0 : Half-Width at (1/e)-Intensity point
 $T_{FWHM}, FWHM$: Full-Width at Half-Maximum
 μ_0 : vacuum permeability
 v_g : group velocity
 w : mode field radius
 ω : optical frequency

Appendix C

Publications by the Author

1. R. Ludwig, C. Schmidt, C. Schubert, J. Berger, E. Hilliger, M. Kroh, V. Marembert, C. Boerner, S. Ferber, H.-J. Ehrke, and Hans-Georg Weber. Technologies for 160 Gbit/S Transmission Systems. In *7th Optoelectronics and Commun. Conf. (OECC) Techn. Dig.*, pages 18–19, Yokohama (Japan), july 2002. paper 9B1-1.
2. Hans-Georg Weber, R. Ludwig, C. Schmidt, C. Schubert, J. Berger, E. Hilliger, M. Kroh, V. Marembert, C. Boerner, S. Ferber, and H.J. Ehrke. 160 Gbit/s TDM-Transmission Technology. In *Proc. 28th Europ. Conf. on Opt. Comm. (ECOC'02)*, 2002. invited paper 2.1.1.
3. C. Boerner, J. Berger, S. Ferber, E. Hilliger, V. Marembert, C. Schmidt, R. Ludwig, and Hans-Georg Weber. 160 Gb/s Clock Recovery and Demultiplexing Using One Single EAM. In *Proc. 29th Europ. Conf. on Opt. Comm. (ECOC'03)*, pages 988–989, Rimini, Italy, september 21-25 2003. Paper Th2.5.1.
4. C. Boerner, C. Schubert, C. Schmidt, E. Hilliger, V. Marembert, J. Berger, S. Ferber, E. Dietrich, R. Ludwig, B. Schmauss, and Hans-Georg Weber. 160 Gbit/s Clock Recovery with Electro-Optical PLL Using a Bidirectionally Operated Electroabsorption Modulator as Phase Comparator. In *OSA Trends in Optics and Photonics (TOPS) Vol. 86, Optical Fiber Commun. Conf., Technical Digest, Postconference Edition*, pages 670–671, Atlanta (USA), march 23-28 2003.
5. C. Boerner, C. Schubert, C. Schmidt, E. Hilliger, V. Marembert, J. Berger, S. Ferber, E. Dietrich, R. Ludwig, B. Schmauss, and Hans-Georg Weber. 160 Gbit/s Clock Recovery with Electro-Optical PLL Using a Bidirectionally Operated Electroabsorption Modulator as Phase Comparator. *Electron. Lett.*, 39(14):1071–1073, 10th july 2003.
6. E. Hilliger, V. Marembert, S. Ferber, M. Kroh, J. Berger, Hans-Georg Weber, and B. Schmauss. EAM with Improved Switching Performance by Self Cascading. In *OSA Trends in Optics and Photonics (TOPS) Vol. 86, Optical Fiber Commun. Conf., Technical Digest, Postconference Edition*, pages 268–269, Atlanta, Georgia (USA), March 2003.

7. A. Melo, S. Randel, V. Marembert, and K. Petermann. Novel scheme for all-optical XOR operation at 160Gbit/s. In *Proc. 29th Europ. Conf. on Opt. Comm. (ECOC'03)*, pages 388–389, Rimini (Italy), September 2003. Paper We1.5.3.
8. Carsten Schmidt-Langhorst, Colja Schubert, Christof Boerner, Sebastian Ferber, Reinhold Ludwig, Joern Berger, Enno Hilliger, Vincent Marembert, Marcel Kroh, Hans-Juergen Ehrke, and Hans-Georg Weber. Ultrafast Technologies in 160 Gbit/S Transmission Systems. In *SPIE International Symposium "IT COM", Pennsylvania, USA, 2004*.
9. Hans-Georg Weber, R. Ludwig, S. Ferber, C. Boerner, C. Schubert, C. Schmidt-Langhorst, E. Hilliger, M. Kroh, and V. Marembert. High-Speed Optical Signal Processing and Data Transmission. In *Proc. 6th Int. Conf. On Transparent Opt. Networks (ICTON 2004)*, pages 177–181, Wroclaw, Poland, 2004.
10. V. Marembert, C. Schubert, S. Ferber, K. Schulze, C. Schmidt-Langhorst, C. Boerner, M. Kroh, R. Ludwig, S. Watanabe, F. Futami, R. Okabe, and Hans-Georg Weber. Single-Channel 640 Gbit/s DPSK Transmission over a 160 km Fibre Link. In *Proc. 30th Europ. Conf. on Opt. Comm. (ECOC'04)*, Stockholm, Sweden, 2004. Post-deadline paper Th4.4.2.
11. R. Ludwig, S. Ferber, C. Boerner, C. Schubert, C. Schmidt, J. Berger, M. Kroh, E. Hilliger, V. Marembert, and Hans-Georg Weber. 160 Gb/s DPSK Transmission System with High Long-Term Stability. In *9th Optoelectron. and Commun. Conf. (OECC/COIN 2004), Technical Digest*, pages 472–473, Yokohama, Japan, jul 2004. Paper 14C4-2.
12. C. Schmidt-Langhorst, C. Schubert, C. Boerner, S. Ferber, R. Ludwig, J. Berger, E. Hilliger, V. Marembert, M. Kroh, H.-J. Ehrke, and Hans-Georg Weber. Ultrafast Technologies in 160 Gbit/s Transmission Systems. In Achyut K. Dutta, Abdul Ahad S. Awwal, Niloy K. Dutta, and Yasutake Ohishi, editors, *Active and Passive Optical Components for WDM Communications IV, Proc. of SPIE Vol. 5595*, pages 249–259, Bellingham, WA, 2004. The International Society for Optical Engineering (SPIE). OpticsEast Conf., Philadelphia (USA), October 2004, Invited Paper 5595-35.
13. R. Ludwig, S. Ferber, C. Boerner, C. Schmidt-Langhorst, E. Hilliger, M. Kroh, V. Marembert, and Hans-Georg Weber. 160 Gbit/s DPSK-Transmission - Technologies and System Impact. In *Proc. 30th Europ. Conf. on Opt. Comm. (ECOC'04)*, Stockholm, Sweden, 2004. invited paper Tu1.1.3.
14. Hans-Georg Weber, R. Ludwig, C. Schmidt, C. Schubert, J. Berger, E. Hilliger, M. Kroh, V. Marembert, C. Boerner, S. Ferber, and Hans-Jürgen Ehrke. Tecnologia de transmissao TDM de 160 Gbit/s. *Redes, Telecom e Instalações*, vi(60):78–82, may 2005.
15. S. Ferber, R. Ludwig, C. Boerner, C. Schubert, C. Schmidt-Langhorst, M. Kroh, V. Marembert, and H.G. Weber. 160 Gbit/S DPSK Transmission over 320 Km Fibre Link with High Long-Term Stability. *Electron. Lett.*, 41(4):200–2, 2005.

16. Sebastian Ferber, Carsten Schmidt-Langhorst, Reinhold Ludwig, Christof Boerner, Colja Schubert, Vincent Marembert, Marcel Kroh, and Hans-Georg Weber. 160 Gbit/s Transmission with Long-Term Stability. In *itg05*, pages 71–78, Berlin (Germany), may 2005. Informationstechnische Gesellschaft im VDE (ITG), VDE Verlag GmbH. ITG-Fachbericht 186.
17. Sebastian Ferber, Carsten Schmidt-Langhorst, Reinhold Ludwig, Christof Boerner, Colja Schubert, Vincent Marembert, Marcel Kroh, and Hans-Georg Weber. 160 Gbit/s OTDM Long-Haul Transmission with Long-Term Stability Using RZ-DPSK Modulation Format. *IEICE Trans. Electron.*, e88-b(5):1947–1954, may 2005. Invited Paper (Special Issue on Recent Progress in Optoelectronics and Communications).
18. V. Marembert, K. Schulze, C. Schubert, C. Weinert, F. Futami, S. Watanabe, and H. G. Weber. Investigations of Fiber Kerr Switch: Nonlinear Phase Shift Measurements and Optical Time-Division Demultiplexing of 320 Gbit/s DPSK signals. In *Conf. on Lasers and Electro-Optics (CLEO) Tech. Dig.*, 2005.
19. C. Boerner, V. Marembert, S. Ferber, C. Schubert, R. Schmidt-Langhorst, C. Ludwig, and Hans-Georg Weber. 320 Gbit/s Clock Recovery with Electro-Optical PLL Using a Bidirectionally Operated Electroabsorption Modulator as Phase Comparator. In *Proc. 30th Opt. Fiber Commun. Conf. (OFC'05)*, Anaheim, CA (USA), mar 2005. Paper OTuO3.
20. C. Schubert, C. Schmidt-Langhorst, K. Schulze, V. Marembert, and H.G. Weber. Time Division Add-Drop Multiplexing up to 320 Gbit/s. In *Proc. 30th Opt. Fiber Commun. Conf. (OFC'05)*, 2005.
21. C. Schmidt-Langhorst, C. Schubert, C. Boerner, V. Marembert, S. Ferber, R. Ludwig, and Hans-Georg Weber. Optical Sampling System Including Clock Recovery for 320 Gbit/s DPSK and OOK Data Signals. In *Proc. 30th Opt. Fiber Commun. Conf. (OFC'05)*, Washington, DC, mar 2005. Optical Society of America. Paper OWJ6.
22. R. Ludwig, S. Ferber, C. Boerner, C. Schubert, C. Schmidt-Langhorst, M. Kroh, V. Marembert, and Hans-Georg Weber. 160 Gbit/s Transmission Systems, Ready for Operation? In *oecc05*, pages 772–772, Seoul, Korea, jul 2005. Invited Paper 8B1-1.
23. V. Marembert, A. M. Melo, S. Randel, C. Schubert, K. Petermann, and H.G. Weber. Reduction of Pattern Effects in an SOA-based 40 Gb/s Wavelength Converter. In *Techn. Dig. of Optical Amplifiers and their Applications (OAA'05)*, Budapest, Hungary, August 2005.
24. R. Ludwig, S. Ferber, C. Boerner, C. Schubert, C. Schmidt-Langhorst, M. Kroh, V. Marembert, and Hans-Georg Weber. Technologies Enabling Ultrahigh Speed Transmission. In *oaa05*, Budapest, Hungary, aug 2005. Invited Paper SuB2.
25. Hans-Georg Weber, Sebastian Ferber, Marcel Kroh, Carsten Schmidt-Langhorst, Reinhold Ludwig, Vincent Marembert, Christof Boerner, Fumio Futami, Shigeki Watanabe, and Colja Schubert. Single Channel 1.28

- Tbit/s and 2.56 Tbit/s DQPSK Transmission. In *Proc. 31th Europ. Conf. on Opt. Comm. (ECOC'05)*, Glasgow, Scotland (U.K.), September 2005. Post-Deadline Paper Th4.1.2.
26. H.G. Weber, S. Ferber, M. Kroh, C. Schmidt-Langhorst, R. Ludwig, V. Marembert, C. Boerner, F. Futami, S. Watanabe, and C. Schubert. Single Channel 1.28 Tbit/S and 2.56 Tbit/S DQPSK Transmission. In *ecoc*, 2005. PD paper Th4.1.2.
 27. A. M. Melo, V. Marembert, C. Schubert, C. Schmidt-Langhorst, and K. Petermann. Design optimization of ultra-high bit-rate NOLM-based OTDM demultiplexers. In *Lasers and Electro-Optics Society, IEEE Annual Meeting*, 2005.
 28. Reinhold Ludwig, Carsten Schmidt-Langhorst, Colja Schubert, Sebastian Ferber, Vincent Marembert, Marcel Kroh, and Hans-Georg Weber. All Optical Signal Processing Technologies and Their Applications. In *cpt06*, Tokyo (Japan), jan 2006. Invited Paper G-1.
Brazilian Journal for Telecommunications.
 29. Hans-Georg Weber, Sebastian Ferber, Marcel Kroh, Carsten Schmidt-Langhorst, Reinhold Ludwig, Vincent Marembert, Christof Boerner, Fumio Futami, Shigeki Watanabe, and Colja Schubert. Single Channel 1.28 Tbit/s and 2.56 Tbit/s DQPSK Transmission. *Electron. Lett.*, 42(3):178–179, February 2006.
 30. M. Kroh, S. Ferber, C. Schmidt-Langhorst, V. Marembert And C. Schubert, R. Ludwig, and Hans-Georg Weber. Transmitter Enabling Ultra-High Speed Transmission of Phase Modulated Data Signals up to 640 Gbit/s. In *ofc06*, Anaheim, CA (USA), mar 2006. Invited Paper (upgraded) OWW1.
 31. V. Marembert, C. Schubert, C. Schmidt-Langhorst, M. Kroh, S. Ferber, and Hans-Georg Weber. Investigation of Fiber Based Gates for Time Division Demultiplexing up to 640 Gbit/s. In *Proc. Optical Fiber Commun.*, Anaheim, CA (USA), March 2006. Poster OWI12.

Appendix D

Acknowledgements

I am very grateful to a number of people who helped and supported me throughout this work. I particularly thank Professor H.G. Weber from the Fraunhofer Institute for Telecommunications, for giving me the opportunity to work in his group, for his kind supervision and patience throughout my time at the institute. Professor Weber made it possible for me as an exchange student to learn and profit a lot from his research group. My gratitude goes to my supervisor Professor K. Petermann from the Technical Universität Berlin, for his attention and guidance. I also would like to thank my present and former colleagues from the Fraunhofer Institute for Telecommunications (Heinrich-Hertz-Institut für Nachrichtentechnik), without whom I couldn't have successfully carried out this work. Dr. Enno Hilliger and Dr. Colja Schubert kindly introduced me to the field of OTDM, and I could learn a lot by assisting them. For their fruitful and pleasant collaboration, I thank Dr. Marcel Kroh, Sebastian Ferber, Dr. Carsten Schmidt-Langhorst, Dr. Jörn Berger, Erik Dietrich, Dr. Reinhold Ludwig, Herbert Knupke, Hans-Jürgen Ehrke.

I enjoyed working with my students colleagues Andre Grede, Alexandre Gual i Coca, Denis Plüschke, Martin Schubert, and Stefan Cortes.

I was fortunate to have the possibility of working with guest scientists and am very grateful to Karsten Schulze (Universidad Politecnica de Valencia, Spain), Quang Nghi Trong Le (COM Center, Denmark), with whom I shared uncountable interesting discussions during lab work and after. I appreciated sharing my knowledge with the exchange students who visited the institute and also supported my work: Romain Dhaluin and Xavier Conan (France), Lisa Garattini (Italy).

My work was greatly supported through the collaboration with Dr. Shigeki Watanabe and Dr. Fumio Futami from Fujitsu Laboratories, Japan. Their expertise and advices on the field of my thesis subject was very appreciated, and I enjoyed the time we successfully spend working for common experiments.

Alessandro Marques de Melo, Sebastian Randel (Technische Universität Berlin) and Dr. Carl-Michael Weinert greatly supported this thesis through computer simulation works and fruitful discussions.

I am very grateful for having an innumerable number of friends around the world, whose kind attentions were always important to me. I wish to warmly thank my brother Julien and my sister Emilie, as well as my parents for their unconditional support and encouragement.

My thesis work was supported by the Deutsche Forschungsgemeinschaft (DFG).

Appendix E

Curriculum Vitae

Personal Details

Name:	Vincent Marembert
Date of Birth:	29. August 1977
Place of Birth:	Bourges, France

Education

1988 - 1992	Collège Jean Valette in Saint-Amand Montrond, France.
1992 - 1995	Lycée Jean Moulin in Saint-Amand Montrond, France.
1995 - 1998	Preparatory classes ("classes préparatoires") at the Lycée Descartes in Tours, France.
1998 - 2001	Study of Physics at the "Ecole Nationale Supérieure de Physique de Marseille" (ENSPM, now "Ecole Généraliste d'Ingénieurs de Marseille" EGIM)

Professional Experience

03.2001	-	Heinrich-Hertz-Institut für Nachrichtentechnik Berlin GmbH (Germany), Student staff at the Department of Optical Signal Processing,
09.2001		
10.2001	-	Heinrich-Hertz-Institut für Nachrichtentechnik Berlin GmbH, then Fraunhofer
12.2005		Institute for Telecommunications
		Scientific staff at the Department of Optical Signal Processing,
		Research area: <i>Ultrafast fiber-based switches</i>
As from 04.2006		Patent-examiner at the European Patent Office in Munich (Germany).